

University of Alberta

**DESIGN AND OPTIMIZATION OF FRM FIR DIGITAL FILTERS USING GENETIC
ALGORITHMS OVER THE CSD AND DBNS MULTIPLIER COEFFICIENT SPACES**

by

Sai Mohan Kilambi



A thesis submitted to the Faculty of Graduate Studies and Research in partial fulfillment of the requirements for the degree of **Master of Science**.

Department of Electrical and Computer Engineering

Edmonton, Alberta
Fall 2007



Library and
Archives Canada

Bibliothèque et
Archives Canada

Published Heritage
Branch

Direction du
Patrimoine de l'édition

395 Wellington Street
Ottawa ON K1A 0N4
Canada

395, rue Wellington
Ottawa ON K1A 0N4
Canada

Your file *Votre référence*
ISBN: 978-0-494-33278-8
Our file *Notre référence*
ISBN: 978-0-494-33278-8

NOTICE:

The author has granted a non-exclusive license allowing Library and Archives Canada to reproduce, publish, archive, preserve, conserve, communicate to the public by telecommunication or on the Internet, loan, distribute and sell theses worldwide, for commercial or non-commercial purposes, in microform, paper, electronic and/or any other formats.

The author retains copyright ownership and moral rights in this thesis. Neither the thesis nor substantial extracts from it may be printed or otherwise reproduced without the author's permission.

AVIS:

L'auteur a accordé une licence non exclusive permettant à la Bibliothèque et Archives Canada de reproduire, publier, archiver, sauvegarder, conserver, transmettre au public par télécommunication ou par l'Internet, prêter, distribuer et vendre des thèses partout dans le monde, à des fins commerciales ou autres, sur support microforme, papier, électronique et/ou autres formats.

L'auteur conserve la propriété du droit d'auteur et des droits moraux qui protègent cette thèse. Ni la thèse ni des extraits substantiels de celle-ci ne doivent être imprimés ou autrement reproduits sans son autorisation.

In compliance with the Canadian Privacy Act some supporting forms may have been removed from this thesis.

Conformément à la loi canadienne sur la protection de la vie privée, quelques formulaires secondaires ont été enlevés de cette thèse.

While these forms may be included in the document page count, their removal does not represent any loss of content from the thesis.

Bien que ces formulaires aient inclus dans la pagination, il n'y aura aucun contenu manquant.


Canada

“My heart is a traitor, it doesn’t want me to go on” said the boy. “That makes sense,” the alchemist answered. “Naturally, it’s afraid that, in pursuing your dream, you might lose everything you’ve won.”

“Well then, why should I listen to my heart?”

To this the alchemist replied, “Because you will never again be able to keep it quiet.

Even if you pretend not to have heard what it tells you, it will always be there inside you,

repeating to you what you’re thinking about life, the world and it’s soul.”

- The Alchemist

To Amma and Nana - Two angels that watched over me.
To Shirdi Sai Baba - You are the beacon that guides my sail.

Abstract

It is well known that frequency response masking (FRM) finite impulse response (FIR) digital filters can be designed to exhibit very sharp-transition bands at the cost of slightly larger filter lengths as compared to the conventional FIR digital filters. The FRM FIR digital filters permit efficient hardware implementations due to an inherently large number of zero-valued multiplier coefficients in their transfer functions. The hardware complexity of FRM digital filters can be further reduced by employing computationally efficient number systems for the representation of the non-zero-valued multiplier coefficients. In this thesis, a novel look-up table (LUT)-based genetic algorithm is developed for the design and discrete optimization of FRM FIR digital filters over the conventional canonical signed-digit (CSD) as well as the emerging double base number system (DBNS) multiplier coefficient spaces. The underlying LUTs consist of permissible CSD/DBNS numbers, each identified by their unique indices such that the latter form a *closed set* under the genetic operations of crossover and mutation. The CSD/DBNS multiplier coefficient values themselves permit pre-specified wordlengths and pre-specified number of non-zero bits. The salient feature of the proposed genetic algorithm is that it automatically leads to legitimate CSD/DBNS multiplier coefficients without any recourse to gene repair. However, repeated computational investigations revealed that the aforementioned GA did not search the solution space robustly due to lack of mechanisms through which entrapment at local optima could be successfully avoided. Therefore, the proposed GA is modified to a diversity controlled genetic algorithm (DCGA). The advantage of the LUT-based DCGA over the conventional GA lies in the external control over population diversity and parent selection, giving rise to a rapid convergence to an optimal solution. The external control is achieved

through judicious choice of a pair of DCGA optimization parameters. An empirical investigation is undertaken for choosing appropriate values for these control parameters. The performance of the proposed LUT-based GA and DCGA are compared through their application to the optimization of FRM FIR digital filters with low-pass and bandpass magnitude responses. The resulting speed of convergence of the DCGA optimization is observed to be an order-of-magnitude higher as compared to that of conventional GAs.

Acknowledgements

I would like to thank Dr. Nowrouzian for his countless hours of advice, guidance and encouragement over the past two years. Without your help, Dr. Nowrouzian, I would never have been able to complete this work successfully. I would also like to thank NSERC for their financial support. My big thanks to all my friends at the HCDC lab, Chemical department and in Ottawa, who have been very kind, helpful and patient throughout my U. of Alberta days. Without you all, MSc would not have been half as fun as it was.

Most importantly, I would like to thank my parents, Aravinda and Rajagopalachari Kilambi for their fantastic upbringing, never-ending patience and rock-solid faith in my success. Thanks, mom and dad, for your belief in me. Without you both, I would not be as successful as I am today.

Table of Contents

1	Introduction	1
2	Design of Sharp-Transition Linear Phase FIR Digital Filters Using the Conventional FRM Approach	5
2.1	Digital Filters	5
2.2	Frequency Response Masking Approach	7
2.3	Design of Lowpass FRM FIR Digital Filters	8
2.3.1	Optimal value for the interpolation factor M	10
2.3.2	Bandedge design equations for digital sub-filters $H_a(z)$, $H_{ma}(z)$ and $H_{mb}(z)$	11
2.3.3	Passband ripples and stopband attenuation of digital sub-filters $H_a(z)$, $H_{ma}(z)$ and $H_{mb}(z)$	18
2.3.4	Design of the overall lowpass FRM FIR digital filter in terms of the digital sub-filters $H_a(z)$, $H_{ma}(z)$ and $H_{mb}(z)$	21
3	Design and Optimization of Finite-Precision FRM FIR Digital Filters Using Conventional Genetic Algorithms	22
3.1	CSD Multiplier Coefficient Representation	23
3.2	DBNS Multiplier Coefficient Representation	23
3.3	Genetic Algorithms: An overview	24
3.4	The Proposed GA Optimization for FRM FIR Digital Filters	25
3.4.1	Design of initial infinite-precision FRM digital filter	26
3.4.2	Generation of the CSD LUT	26
3.4.3	Generation of the DBNS LUT	27
3.4.4	Generation of seed CSD/DBNS FRM FIR digital filter	27
3.4.5	Generation of the initial population pool	27
3.4.6	Fitness evaluation	27
3.4.7	Generation of mating pool	28
3.4.8	Parent selection	28
3.4.9	The next-generation population pool	29
3.5	Application Examples	29
3.5.1	Design of lowpass FRM FIR digital filters	29
3.5.1.1	GA optimization of lowpass CSD FRM FIR digital filters	31

3.5.1.2	GA Optimization of lowpass DBNS FRM FIR digital filters	32
3.5.2	Design of bandpass FRM FIR digital filters	40
3.5.2.1	GA optimization of bandpass CSD FRM FIR digital filters	41
3.5.2.2	GA optimization of bandpass DBNS FRM FIR digital filters	42
4	Design and Optimization of Finite-Precision FRM FIR Digital Filters Using Diversity Controlled Genetic Algorithms	50
4.1	A Modified Technique for the Design of Bandpass and Bandstop FRM FIR Digital Filters with Arbitrary Lower and Upper Transition Bandwidths	50
4.1.1	Design of Bandpass FRM FIR Digital Filters with Arbitrary Lower and Upper Transition Bandwidth	51
4.1.2	Design of FRM Bandstop Digital Filters with Arbitrary Lower and Upper Transition Bandwidth	52
4.2	DCGA Optimization: An Overview	53
4.3	The Proposed DCGA Optimization of FRM FIR Digital Filters	56
4.3.1	Genetic Operations	57
4.3.2	Generation of the next-generation population pool	58
4.4	Application Examples	59
4.4.1	Design of lowpass FRM FIR digital filters	59
4.4.1.1	DCGA optimization of lowpass CSD FRM FIR digital filters	60
4.4.1.2	DCGA optimization of lowpass DBNS FRM FIR digital filters	61
4.4.2	Design of bandpass FRM FIR digital filters for the case $\Delta_l = \Delta_u$	70
4.4.2.1	DCGA optimization of bandpass CSD FRM FIR digital filters for the case $\Delta_l = \Delta_u$	71
4.4.2.2	DCGA optimization of bandpass DBNS FRM FIR digital filters for the case $\Delta_l = \Delta_u$	73
4.4.3	Design of bandpass FRM FIR digital filters for the case $\Delta_l \neq \Delta_u$	84
4.4.3.1	DCGA optimization of bandpass CSD FRM FIR digital filters for the case $\Delta_l \neq \Delta_u$	85
4.4.3.2	DCGA optimization of bandpass DBNS FRM FIR digital filters for the case $\Delta_l \neq \Delta_u$	86
5	Concluding Remarks	99
	Bibliography	101
A	Author's Contributions	105

B Filter Length Estimation	107
C CPU Processing Times for GA and DCGA	109

List of Tables

3.1	Filter Lengths for a Lowpass FRM FIR Digital Filter for Various Values of M	30
3.2	Bandedge Frequencies Associated with $H_a(z)$, $H_b(z)$, $H_{ma}(z)$ and $H_{mb}(z)$ Digital Sub-Filters for the Lowpass FRM FIR Digital Filter Case	31
3.3	Passband Ripples and Stopband Attenuations Associated with $H_a(z)$, $H_{ma}(z)$ and $H_{mb}(z)$ Digital Sub-filters for the Lowpass FRM FIR Digital Filter Case	31
3.4	Design Parameters for GA Optimization of Lowpass CSD FRM FIR Digital Filters	32
3.5	Lowpass CSD FRM FIR Digital Filter Magnitude Responses before and after GA Optimization	32
3.6	Design Parameters for GA Optimization of DBNS Lowpass FRM FIR Digital Filters	33
3.7	Lowpass DBNS FRM FIR Digital Filter Magnitude Responses before and after GA Optimization	33
3.8	Filter Lengths for Bandpass FRM FIR Digital Filter for Various Values of M	41
3.9	Bandedge Frequencies associated with $H_a(z)$, $H_b(z)$, $H_{ma}(z)$ and $H_{mb}(z)$ Digital Sub-Filters for the Bandpass FRM FIR Digital Filter Case	41
3.10	Passband Ripples and Stopband Attenuations Associated with $H_a(z)$, $H_{ma}(z)$ and $H_{mb}(z)$ Digital Sub-filters for the Bandpass FRM FIR Digital Filter Case	42
3.11	Design Parameters for GA Optimization of Bandpass CSD FRM FIR Digital Filter	42
3.12	Bandpass CSD FRM FIR Digital Filter Magnitude Responses before and after GA Optimization	42
3.13	Design Parameters for GA Optimization of Bandpass DBNS FRM FIR Digital Filter	43
3.14	Bandpass DBNS FRM FIR Digital Filter Magnitude Responses before and after GA Optimization	43
4.1	Filter Lengths for a Lowpass FRM FIR Digital Filter for Various Values of M	60

4.2	Bandedge Frequencies Associated with $H_{al}(z)$, $H_{mal}(z)$ and $H_{mbl}(z)$ Digital Sub-Filters for the Lowpass FRM FIR Digital Filter Case . . .	60
4.3	Passband Ripples and Stopband Attenuations for Digital Sub-filters $H_{al}(z)$, $H_{mal}(z)$ and $H_{mbl}(z)$ for the Lowpass FRM FIR Digital Filter Case	60
4.4	Design Parameters for DCGA Optimization of Lowpass CSD FRM FIR Digital Filters	61
4.5	Lowpass CSD FRM FIR Digital Filter Magnitude Responses before and after DCGA Optimization	61
4.6	Design Parameters for DCGA Optimization of Lowpass DBNS FRM FIR Digital Filters	62
4.7	Lowpass DBNS FRM FIR Digital Filter Magnitude Responses before and after DCGA Optimization	62
4.8	Filter Lengths for a Bandpass FRM FIR Digital Filter with $\Delta_l = \Delta_u$ for Various Values of M	71
4.9	Bandedge Frequencies for Associated with $H_{al(h)}(z)$, $H_{mal(h)}(z)$ and $H_{mbl(h)}(z)$ Digital Sub-Filters for the Bandpass FRM FIR Digital Filter Case with $\Delta_l = \Delta_u$	71
4.10	Passband Ripples and Stopband Attenuations for Associated with $H_{al(h)}(z)$, $H_{mal(h)}(z)$ and $H_{mbl(h)}(z)$ Digital Sub-Filters for the Bandpass FRM FIR Digital Filter Case with $\Delta_l = \Delta_u$	72
4.11	Design Parameters for DCGA Optimization of Bandpass CSD FRM FIR Digital Filter for the Case $\Delta_l = \Delta_u$	72
4.12	Bandpass CSD FRM FIR Digital Filter Magnitude Responses for the case $\Delta_l = \Delta_u$ before and after DCGA Optimization	73
4.13	Design Parameters for DCGA Optimization of Bandpass DBNS FRM FIR Digital Filter for the Case $\Delta_l = \Delta_u$	73
4.14	DBNS FRM FIR Bandpass Digital Filter Magnitude Responses before and after GA Optimization	74
4.15	Filter Lengths for the Constituent Lowpass FRM FIR Digital Filter for Various Values of M_{LP}	85
4.16	Filter Lengths for the Constituent Highpass FRM FIR Digital Filter for Various Values of M_{HP}	85
4.17	Bandedge Frequencies Associated with $H_{al(h)}(z)$, $H_{mal(h)}(z)$ and $H_{mbl(h)}(z)$ Digital Sub-Filters for the Bandpass FRM FIR Digital Filter Case with $\Delta_l \neq \Delta_u$	86
4.18	Passband Ripples and Stopband Attenuations Associated with $H_{al(h)}(z)$, $H_{mal(h)}(z)$ and $H_{mbl(h)}(z)$ Digital Sub-Filters for the Bandpass FRM FIR Digital Filter case with $\Delta_l \neq \Delta_u$	86
4.19	Design Parameters for DCGA Optimization of Bandpass CSD FRM FIR Digital Filter for the Case $\Delta_l \neq \Delta_u$	86
4.20	Bandpass CSD FRM FIR Digital Filter Magnitude Responses for the case $\Delta_l \neq \Delta_u$ before and after DCGA Optimization	87
4.21	Design Parameters for DCCA Optimization of Bandpass DBNS FRM FIR Digital Filter for the Case $\Delta_l \neq \Delta_u$	87

4.22	Bandpass DBNS FRM FIR Digital Filter Magnitude Responses for the Case $\Delta_l \neq \Delta_u$ before and after DCGA Optimization	88
C.1	CPU Processing Time for GA and DCGA Optimization of FRM FIR Digital filters	109

List of Figures

2.1	Synthesis structure of overall FRM FIR digital filter.	7
2.2	Realization of bandedge-shaping digital sub-filter $H_b(e^{j\omega})$	13
2.3	Realization of bandedge-shaping digital sub-filter $H_b(e^{j\omega})$ with sharing of delay elements.	13
2.4	Frequency Response of bandedge-shaping digital sub-filter $H_a(e^{j\omega})$	14
2.5	Frequency response of complementary bandedge-shaping digital sub-filter $H_b(e^{j\omega})$	14
2.6	M -interpolated complementary digital sub-filters $\hat{H}_a(e^{j\omega})$ and $\hat{H}_b(e^{j\omega})$	15
2.7	Frequency response of masking digital sub-filters $H_{ma}(e^{j\omega})$ and $H_{mb}(e^{j\omega})$	15
2.8	Frequency response of overall FRM digital filter $H_{LP}(e^{j\omega})$	16
2.9	Frequency response of masking digital sub-filters $H_{ma}(e^{j\omega})$ and $H_{mb}(e^{j\omega})$	16
2.10	Frequency response of overall FRM FIR digital filter $H_{LP}(e^{j\omega})$	17
2.11	Synthesis architecture of overall FRM FIR digital filter.	17
3.1	Magnitude response of sub-filter $H_a(z)$ for the lowpass FRM FIR digital filter case.	33
3.2	Magnitude response of complimentary sub-filter $H_b(z)$ for the lowpass FRM FIR digital filter case.	34
3.3	Magnitude response of M -interpolated version of $H_a(z)$ for the lowpass FRM FIR digital filter case.	34
3.4	Magnitude response of M -interpolated version of complementary sub-filter $H_b(z)$ for the lowpass FRM FIR digital filter case.	35
3.5	Magnitude response of masking digital sub-filter $H_{ma}(z)$ for the lowpass FRM FIR digital filter case.	35
3.6	Magnitude response of masking digital sub-filter $H_{mb}(z)$ for the lowpass FRM FIR digital filter case.	36
3.7	Infinite-precision lowpass FRM FIR digital filter.	36
3.8	Lowpass CSD FRM FIR digital filter before GA optimization.	37
3.9	Fitness evolution for lowpass CSD FRM FIR digital filter.	37
3.10	Lowpass CSD FRM FIR digital filter after GA optimization.	38
3.11	Lowpass DBSN FRM FIR Digital Filter before GA optimization.	38
3.12	Fitness evolution for lowpass DBNS FRM FIR digital filter.	39
3.13	Lowpass DBNS FRM FIR digital filter after GA optimization.	39

3.14	Magnitude response of digital sub-filter $H_a(z)$ for the bandpass FRM FIR digital filter case.	43
3.15	Magnitude Response of complimentary digital sub-filter $H_b(z)$ for the bandpass FRM FIR digital filter case.	44
3.16	Magnitude response of M -interpolated version of digital sub-filter $H_a(z)$ for the bandpass FRM FIR digital filter case.	44
3.17	Magnitude response of M -interpolated version of complementary digital sub-filter $H_b(z)$ for the bandpass FRM FIR digital filter case.	45
3.18	Magnitude response of masking digital sub-filter $H_{ma}(z)$ for the bandpass FRM FIR digital filter case.	45
3.19	Magnitude response of masking digital sub-filter $H_{mb}(z)$ for the bandpass FRM FIR digital filter case.	46
3.20	Infinite-precision bandpass FRM FIR digital filter $H_{BP}(z)$	46
3.21	Bandpass CSD FRM FIR digital filter before GA optimization.	47
3.22	Fitness evolution for bandpass CSD FRM FIR digital filter.	47
3.23	Bandpass CSD FRM FIR digital filter after GA optimization.	48
3.24	Bandpass DBNS FRM digital filter before GA optimization.	48
3.25	Fitness evolution for bandpass DBNS FRM FIR digital filter.	49
3.26	Bandpass DBNS FRM FIR digital filter after GA optimization.	49
4.1	Alternative realization of FRM approach for lowpass filters [21].	52
4.2	Alternative realization of FRM approach for highpass filters [21].	52
4.3	Synthesis structure for bandpass FRM FIR digital filters.	53
4.4	Synthesis structure for bandstop FRM FIR digital filters [21].	53
4.5	Magnitude response of digital sub-filter $H_{al}(z)$ for lowpass FRM FIR digital filter case.	63
4.6	Magnitude response of M -interpolated version of digital sub-filter $H_{al}(z)$ for lowpass FRM FIR digital filter case.	63
4.7	Magnitude response of masking digital sub-filter $H_{mal}(z)$ for lowpass FRM FIR digital filter case.	64
4.8	Magnitude response of masking digital sub-filter $H_{mbl}(z)$ for lowpass FRM FIR digital filter case.	64
4.9	Magnitude response of masking digital sub-filter $H_{dl}(z)$ for lowpass FRM FIR digital filter case.	65
4.10	Infinite-precision lowpass FRM FIR digital filter.	65
4.11	Lowpass CSD FRM FIR digital filter before DCGA optimization.	66
4.12	DCGA convergence speed for lowpass CSD FRM FIR digital filters for varying values of c and α	66
4.13	Average DCGA convergence speed for lowpass CSD FRM FIR digital filters for varying values of c	67
4.14	Lowpass CSD FRM FIR digital filter after DCGA optimization.	67
4.15	Lowpass DBNS FRM FIR digital filter before DCGA optimization.	68
4.16	DCGA convergence speed for lowpass DBNS FRM FIR digital filters for varying values of c and α	68

4.17	Average DCGA convergence speed for lowpass DBNS FRM FIR digital filters for varying values of c	69
4.18	Lowpass DBNS FRM FIR digital filter after DCGA optimization.	69
4.19	Magnitude response of digital sub-filter $H_{al}(z)$ for the bandpass FRM FIR digital filter case with $\Delta_l = \Delta_u$	74
4.20	Magnitude response of M_{LP} -interpolated version of digital sub-filter $H_{al}(z)$ for the bandpass FRM FIR digital filter case with $\Delta_l = \Delta_u$	75
4.21	Magnitude response of masking digital sub-filter $H_{mal}(z)$ for the bandpass FRM FIR digital filter case with $\Delta_l = \Delta_u$	75
4.22	Magnitude response of masking digital sub-filter $H_{mbl}(z)$ for the bandpass FRM FIR digital filter case with $\Delta_l = \Delta_u$	76
4.23	Magnitude response of masking digital sub-filter $H_{dl}(z)$ for the bandpass FRM FIR digital filter case with $\Delta_l = \Delta_u$	76
4.24	Magnitude response of digital sub-filter $H_{ah}(z)$ for the bandpass FRM FIR digital filter case with $\Delta_l = \Delta_u$	77
4.25	Magnitude response of M_{HP} -interpolated version of digital sub-filter $H_{ah}(z)$ for the bandpass FRM FIR digital filter case with $\Delta_l = \Delta_u$	77
4.26	Magnitude response of masking digital sub-filter $H_{mah}(z)$ for the bandpass FRM FIR digital filter case with $\Delta_l = \Delta_u$	78
4.27	Magnitude response of masking digital sub-filter $H_{mbh}(z)$ for the bandpass FRM FIR digital filter case with $\Delta_l = \Delta_u$	78
4.28	Magnitude response of masking digital sub-filter $H_{dh}(z)$ for the bandpass FRM FIR digital filter case with $\Delta_l = \Delta_u$	79
4.29	Infinite-precision bandpass FRM FIR digital filter with $\Delta_l = \Delta_u$	79
4.30	Bandpass CSD FRM FIR digital filter with $\Delta_l = \Delta_u$ before DCGA optimization.	80
4.31	DCGA convergence speed for bandpass FRM FIR digital filters for varying values of c and α	80
4.32	Average DCGA convergence speed for bandpass FRM FIR digital filters for varying values of c	81
4.33	Bandpass CSD FRM FIR digital filter with $\Delta_l = \Delta_u$ after DCGA Optimization.	81
4.34	Bandpass DBNS FRM FIR Digital Filter with $\Delta_l = \Delta_u$ before DCGA optimization.	82
4.35	DCGA convergence speed for bandpass DBNS FRM FIR digital filters for varying values of c and α	82
4.36	Average DCGA convergence speed for bandpass DBNS FRM FIR digital filters for varying values c	83
4.37	Bandpass DBNS FRM FIR digital filter $\Delta_l = \Delta_u$ after DCGA Optimization.	83
4.38	Magnitude response of digital sub-filter $H_{al}(z)$ for the bandpass FRM FIR digital filter case with $\Delta_l \neq \Delta_u$	88
4.39	Magnitude response of M_{LP} -interpolated version of digital sub-filter $H_{al}(z)$ for the bandpass FRM FIR digital filter case with $\Delta_l \neq \Delta_u$	89

4.40	Magnitude response of masking digital sub-filter $H_{mal}(z)$ for the bandpass FRM FIR digital filter case with $\Delta_l \neq \Delta_u$	89
4.41	Magnitude response of masking digital sub-filter $H_{mbl}(z)$ for the bandpass FRM FIR digital filter case with $\Delta_l \neq \Delta_u$	90
4.42	Magnitude response of masking digital sub-filter $H_{dl}(z)$ for the bandpass FRM FIR digital filter case with $\Delta_l \neq \Delta_u$	90
4.43	Magnitude response of digital sub-filter $H_{ah}(z)$ for the bandpass FRM FIR digital filter case with $\Delta_l \neq \Delta_u$	91
4.44	Magnitude response of M_{HP} -interpolated version of digital sub-filter $H_{ah}(z)$ for the bandpass FRM FIR digital filter case with $\Delta_l \neq \Delta_u$	91
4.45	Magnitude response of masking digital sub-filter $H_{mah}(z)$ for the bandpass FRM FIR digital filter case with $\Delta_l \neq \Delta_u$	92
4.46	Magnitude response of masking digital sub-filter $H_{mbh}(z)$ for the bandpass FRM FIR digital filter case with $\Delta_l \neq \Delta_u$	92
4.47	Magnitude response of masking digital sub-filter $H_{dh}(z)$ for the bandpass FRM FIR digital filter case with $\Delta_l \neq \Delta_u$	93
4.48	Infinite-precision bandpass FRM FIR digital filter with $\Delta_l \neq \Delta_u$	93
4.49	Bandpass CSD FRM FIR digital filter before DCGA optimization.	94
4.50	DCGA convergence speed for bandpass CSD FRM FIR digital filters for varying values of c and α	94
4.51	Average DCGA convergence speed for bandpass FRM FIR digital filters for varying values of c	95
4.52	Bandpass CSD FRM FIR digital filter after DCGA optimization.	95
4.53	Bandpass DBNS FRM FIR digital filter with $\Delta_l \neq \Delta_u$ before DCGA optimization.	96
4.54	DCGA convergence speed for bandpass DBNS FRM FIR digital filters for varying values of c and α	96
4.55	Average DCGA convergence speed for bandpass DBNS FRM FIR digital filters for varying values of c	97
4.56	Bandpass DBNS FRM FIR digital filter after DCGA optimization.	97

List of Symbols

Symbol	Definition
α	CPSS exponent
β	Weighting factor in DCGA
θ	Passband edge frequency of bandedge shaping digital sub-filter $H_a(e^{j\omega})$
ϕ	Stopband edge frequency of bandedge shaping digital sub-filter $H_a(e^{j\omega})$
ε_p	Maximum error in the passband
ε_s	Maximum error in the stopband
ω_p	Passband edge frequency of overall FRM FIR digital filter
ω_s	Stopband edge frequency of overall FRM FIR digital filter
Ω_p	Passband frequency points
Ω_s	Stopband frequency points
$\hat{\Omega}_s$	Stopband magnitude response points which fall in the range T_l and T_u
δ_p	Passband ripple of overall FRM FIR digital filter
δ_s	Stopband attenuation of overall FRM FIR digital filter
δ_{BS}	Deviation of bandstop FRM FIR digital filter
δ_{BP}	Deviation of bandpass FRM FIR digital filter
δ_{HP}	Deviation of highpass FRM FIR digital filter
δ_{LP}	Deviation of lowpass FRM FIR digital filter
$\delta_{mb}(\omega)$	Deviation of masking digital sub-filter $H_{mb}(e^{j\omega})$
$\delta_{ma}(\omega)$	Deviation of masking digital sub-filter $H_{ma}(e^{j\omega})$
$\delta_a(\omega)$	Deviation of bandedge shaping digital sub-filter $H_a(e^{j\omega})$
Δ_l	Lower transition bandwidth
Δ_u	Upper transition bandwidth
Δ	Transition bandwidth of overall FRM FIR digital filter
B	Wordlength of look-up table (LUT) index
c	CPSS shaping coefficient
c_p	Highest multiplier coefficient values
C	Constant chosen to render <i>fitness</i> value positive
$C(t)$	Pool of offspring
<i>fitness</i>	Fitness value of a chromosome
<i>fitness</i> ₁	Fitness value of a chromosome
<i>fitness</i> ₂	Fitness value of a chromosome with a <i>penalty</i> component
h	Hamming distance between a chromosome and the chromosome with the highest fitness value in the population pool

Symbol	Definition
$H_a(e^{j\omega})$	Bandedge shaping digital sub-filter
$\hat{H}_a(e^{j\omega})$	M -interpolation bandedge shaping digital sub-filter
$H_b(e^{j\omega})$	Complementary bandedge shaping digital sub-filter
$\hat{H}_b(e^{j\omega})$	M -interpolation complementary bandedge shaping digital sub-filter
$H_{ma}(e^{j\omega})$	Masking digital sub-filter
$H_{mb}(e^{j\omega})$	Masking digital sub-filter
$H_{al}(e^{j\omega})$	Lowpass bandedge shaping digital sub-filter
$H_{mal}(e^{j\omega})$	Lowpass masking digital sub-filter
$H_{mbl}(e^{j\omega})$	Lowpass masking digital sub-filter
$H_{dl}(e^{j\omega})$	Masking digital sub-filter for the lowpass FRM FIR digital filter case
$H_{ah}(e^{j\omega})$	Highpass bandedge shaping digital sub-filter
$H_{mah}(e^{j\omega})$	Highpass masking digital sub-filter
$H_{mbh}(e^{j\omega})$	Highpass masking digital sub-filter
$H_{dh}(e^{j\omega})$	Masking digital sub-filter for the highpass FRM FIR digital filter case
$H_{LP}(e^{j\omega})$	Lowpass FRM FIR digital filter
$H_{HP}(e^{j\omega})$	Highpass FRM FIR digital filter
$H_{BP}(e^{j\omega})$	Bandpass FRM FIR digital filter
$H_{BS}(e^{j\omega})$	Bandstop FRM FIR digital filter
L	Chromosome length
m_l	Integer less than M
m	Base 3 exponent
M	FRM FIR digital filter interpolation factor
M_{LP}	Lowpass FRM FIR digital filter interpolation factor
M_{HP}	Highpass FRM FIR digital filter interpolation factor
$M(t)$	A large pool consisting of parents and offspring
n	Base 2 exponent
N_{mating}	Number of chromosomes in the mating pool
N_p	Number of parent pairs
N	Number of chromosomes in a population pool
N_0	Length of overall FRM FIR digital filter
N_a	Length of bandedge shaping digital sub-filter $H_a(e^{j\omega})$
N_{ma}	Length of masking digital sub-filter $H_{ma}(e^{j\omega})$
N_{mb}	Length of masking digital sub-filter $H_{mb}(e^{j\omega})$
N_{al}	Length of lowpass bandedge shaping digital sub-filter $H_{al}(e^{j\omega})$
N_{mal}	Length of lowpass masking digital sub-filter $H_{mal}(e^{j\omega})$
N_{mbl}	Length of lowpass masking digital sub-filter $H_{mbl}(e^{j\omega})$
N_{ah}	Length of highpass bandedge shaping digital sub-filter $H_{ah}(e^{j\omega})$
N_{mah}	Length of highpass masking digital sub-filter $H_{mah}(e^{j\omega})$
N_{mbh}	Length of highpass masking digital sub-filter $H_{mbh}(e^{j\omega})$
N_{frm}	Number of multiplier required to realize an FRM FIR digital filter
p_F	Fixed probability factor for complementing a bit in the chromosome
p_s	Probability of selecting a chromosome
p_M	Probability of mutation

Symbol	Definition
P	Number of magnitude response points in the range T_l and T_u
$P(t - 1)$	Previous population
$P(t)$	Present population
R	Finite-precision radix-point in the range $0 < R < W$
t	Current generation number
$T_a(\omega)$	Magnitude response of bandedge shaping digital sub-filter $H_a(e^{j\omega})$
$T_{ma}(\omega)$	Magnitude response of masking digital sub-filter $H_{ma}(e^{j\omega})$
$T_{mb}(\omega)$	Magnitude response of masking digital sub-filter $H_{mb}(e^{j\omega})$
T_{LP}	Magnitude response of lowpass FRM FIR digital filter
T_{HP}	Magnitude response of highpass FRM FIR digital filter
T_{BP}	Magnitude response of bandpass FRM FIR digital filter
T_{BS}	Magnitude response of bandstop FRM FIR digital filter
T_l	Lower bound in the stopband. Used in calculating <i>penalty</i>
T_u	Upper bound in the stopband. Used in calculating <i>penalty</i>
U	LUT table size
w	Number of non-zero bits in CSD and DBNS number systems
W	Wordlength of CSD and DBNS numbers
W_I	Wordlength of the integer part in W
W_F	Wordlength of the fractional part in W
W_p	Passband weighting factor
W_s	Stopband weighting factor
x	Fitness rank of a particular chromosome
x_j	Infinite-precision multiplier coefficient values
\hat{x}_j	Finite-precision multiplier coefficient values
$X(z)$	Input signal
$Y(z)$	Output signal
Z	Probability of selecting a chromosome with a higher fitness value

List of Abbreviations

Abbreviation	Definition
FRM	Frequency response masking
FIR	Finite impulse response
GA	Genetic algorithms
DCGA	Diversity controlled genetic algorithms
DBNS	Double base number system
CSD	Canonical signed digit
CPSS	Cross-generational Probabilistic Survival Selection

Chapter 1

Introduction

A vast body of literature is available for the design and optimization of linear phase FIR digital filters. These digital filters exhibit guaranteed non-linear/linear stability features and low coefficient sensitivities, in addition to constant group delays [17]. Linear phase FIR digital filters with sharp-transition bands find many important practical applications, e.g. in digital audio systems [10]. However, the length of such filters is usually inversely proportional to the width of their transition bands, implying that their lengths become prohibitively large for narrow-transition bandwidths. Since the number of addition and multiplication operations carried out by the digital filter in each sampling interval is directly proportional to the filter length, FIR digital filters with large length entail high computational complexities. To this end, plenty of research has been directed towards developing new design techniques which reduce the computational complexity of linear phase FIR digital filters having sharp-transition bands (e.g. [6, 5, 26, 20, 3, 16, 24, 19, 31]).

The frequency response masking (FRM) approach is one of the most efficient techniques for the design of sharp-transition band FIR digital filters [11]. Given a set of design specifications, the length of a FRM FIR digital filter is only slightly longer than that of the corresponding conventional direct-form FIR digital filter. This is made possible by realizing a sharp-transition band FRM digital filter in terms of a combination of a pair of interpolated bandedge shaping and a corresponding pair of gradual-transition band masking FIR digital sub-filters. This causes a substantial reduction in the computational complexity of the overall FRM FIR digital filter mainly due to a relatively large number of zero-valued multiplier coefficients

in the constituent interpolated FIR digital sub-filters [11].

The non-zero valued multiplier coefficients in FRM FIR digital filters can be determined *in infinite-precision* by using the existing gradient-based optimization techniques such as the Parks-McClellan approach. More recent gradient-based optimization techniques for FRM digital filters include the weighted least-squares (WLS) approach [29], and the semi-definite [12] and second-order cone programming [13] approaches. However, in an actual hardware/software implementation of the FRM digital filter, these non-zero valued multiplier coefficients are quantized to their finite-precision counterparts, e.g. by using their signed-power-of-two (SPT) representations [28]. The SPT multiplier coefficient representation leads to a multiplier-free digital filter, achieved by replacing the required multiplication operations by a finite number of shift and add operations [30].

The SPT representation of a given number is non-unique, causing redundancy in the multiplier coefficient representation. This redundancy can potentially increase the corresponding computational complexity due to repetitive recourse to compare operations. In order to circumvent this problem, one may resort to special cases of the SPT number system, e.g. the canonical signed-digit (CSD) or the canonical double base number systems (CDBNS) [1, 2]. These number systems are capable of representing multiplier coefficient values uniquely by restricting the resulting number of non-zero bits.

After the quantization of the infinite-precision multiplier coefficient values, the frequency response of the FRM FIR digital filter may no longer satisfy the initial design specifications. As a result, optimization techniques have to be employed once again to obtain a finite-precision digital filter that satisfies the given design specifications.

In [27], it was demonstrated that by using integer programming over the SPT multiplier coefficient space, the frequency response of FIR digital filters can be optimized to meet very stringent design specifications. In the case of FRM digital filters, however, this optimization technique proves to be time consuming and results in sub-optimal solutions. This generally stems from a separate optimization of the constituent digital sub-filters.

Genetic algorithms (GAs) have emerged as an efficient alternative for the optimization of finite-precision FIR and IIR digital filters [1, 25]. These algorithms are based on an evolution of a population pool consisting of candidate solutions from one generation to the next in the process of arriving at the desired optimal solution. GAs are capable of automatically finding near-optimum solutions to discrete optimization problems while keeping the computational cost low [25].

In this thesis, a novel GA is developed for the design and optimization of low-pass and highpass FRM FIR digital filters with their application towards bandpass and bandstop FRM FIR digital filters¹. The optimization is performed over the fixed-radix point CSD and DBNS multiplier coefficient spaces, where the multiplier coefficients are permitted to have a pre-specified word-length W , and a pre-specified maximum number of non-zero bits w . In the course of this research it was observed that the conventional GAs do not search the solution space robustly due to lack of mechanisms through which entrapment at local optima can be successfully avoided, thereby prolonging the convergence to an optimal solution. In [22, 23], Shimodaira developed a diversity controlled (DC) GA that circumvents this problem by allowing external control over the diversity of the population pool. This external control prevents premature convergence to a local optimal solution, increasing the speed of convergence of the DCGA to a global optimum solution.

The performance of the proposed GA is further improved based on the concepts of diversity control for the design and optimization of FRM FIR digital filters. An empirical investigation is undertaken for the judicious choice of DCGA control parameters for rapid optimization of FRM digital filters. The optimization results obtained are compared against those of the conventional GAs. It is shown that by using DCGA for designing and optimizing FRM FIR digital filters, one may obtain approximately an order-of-magnitude increase in the speed of convergence to the desired optimal solution.

This thesis is divided into the following chapters: Chapter 2 presents the design of sharp-transition FIR digital filters using the conventional FRM approach.

¹The bandpass (bandstop) FRM FIR digital filter can be realized as a cascade (parallel) combination of corresponding lowpass and highpass FRM FIR digital filters.

Chapter 3 develops a novel GA for the optimization of FRM FIR digital filters and presents application examples involving the optimization of a lowpass and a bandpass FRM FIR digital filter over the CSD and DBNS multiplier coefficient spaces. Chapter 4 is concerned with a variation of the FRM approach for the design of bandpass and bandstop FRM FIR digital filters with arbitrary lower and upper transition bandwidths. Furthermore, the chapter modifies the proposed GA by employing diversity control mechanisms for the design and optimization of finite-precision FRM FIR digital filters. Application examples are presented for the design of a lowpass FRM FIR digital filter and a pair of bandpass FRM FIR digital filters with equal and unequal lower and upper transition bands over the CSD and DBNS multiplier coefficient spaces. Empirical results are also given for selecting the DCGA control parameters. Finally, Chapter 5 summarizes the main conclusions of the thesis.

Chapter 2

Design of Sharp-Transition Linear Phase FIR Digital Filters Using the Conventional FRM Approach

This chapter is concerned with the design of sharp-transition FIR digital filters using the conventional FRM approach [11]. Before delving into further details of the FRM approach, it is imperative to understand the basic definition of digital filters.

2.1 Digital Filters

Filtering is defined as a signal processing operation which alters the frequency spectrum in accordance with some given filter specifications [17]. The implementation of this operation (in hardware or software) is called a *filter*. A filter permits certain frequency components in a signal to pass through with negligible modifications, while attenuating other frequency components substantially. The frequencies of the signal components which pass through defines the *passband*, and the frequencies of the signal components which are attenuated defines the *stopband*. There are different types of filters depending on the nature of the filtering operation. These are as follows [17]:

1. *Lowpass Filter*: This filter allows all low-frequency components below a certain specified frequency ω_p called *passband edge frequency* to pass through and attenuates all high frequency components above the specified frequency ω_s called *stopband edge frequency*. Here $\omega_s > \omega_p$.

2. *Highpass Filter*: This filter passes all high-frequency components above a certain specified frequency ω_p and blocks all frequency components below ω_s . Here $\omega_s < \omega_p$.
3. *Bandpass Filter*: This filter allows all frequency components between two specified frequencies ω_{p1} and ω_{p2} and stops all those above and below ω_{s2} and ω_{s1} . Here $\omega_{s1} < \omega_{p1} < \omega_{p2} < \omega_{s2}$.
4. *Bandstop Filter*: This filter blocks all frequency components between two specified frequencies ω_{s1} and ω_{s2} and allows all those above and below ω_{p2} and ω_{p1} . Here $\omega_{p1} < \omega_{s1} < \omega_{s2} < \omega_{p2}$.

Other types of filters are also possible. For instance, a *notch filter* is a bandstop filter that blocks only one frequency and a *comb filter* is designed to block low-frequencies at integer multiples of a fundamental frequency [17].

Filters can be classified broadly into two categories, namely, analog filters and digital filters. Analog filters use electronic circuits such as capacitors, resistors, inductors and op-amps to achieve their filtering effects. The signal being filtered is a direct analogue of the physical quantity such as sound or voice.

Digital filters, on the other hand, use a digital signal processor (DSP) to perform numerical manipulations on sampled values of the signal. In order for digital filters to operate properly, the analog signal must be first sampled and quantized using an analog-to-digital converter (ADC). This sampled sequence is then processed by a DSP chip implementing the digital filter and then converted back to an analog signal using a digital-to-analog converter (DAC). Digital filters offer many advantages over their analog counterparts including programmability, adaptability, higher stability with respect to time (drift) and temperature and many others. As CMOS technology is scaling from one generation to the next, digital filters are being successfully implemented to higher frequency electronics owing to the increased speed of ICs.

Digital filters can be classified based on the length of the impulse response. If the impulse response is of finite length, then the digital filter is called finite impulse response (FIR) digital filters. On the other hand, if the impulse response is of infinite

length, then the filter is referred to as infinite impulse response digital (IIR) digital filters. This thesis deals with the design and optimization of FIR digital filters.

2.2 Frequency Response Masking Approach

Fig. 2.1 shows the FRM synthesis structure used for realizing sharp-transition FIR digital filters.

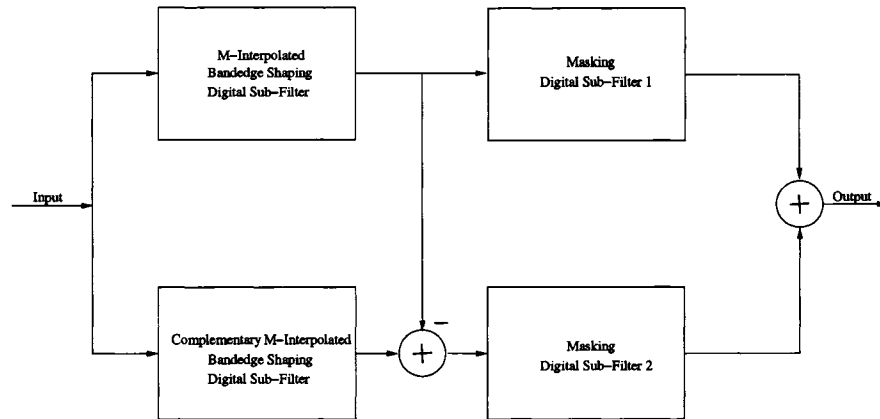


Figure 2.1: Synthesis structure of overall FRM FIR digital filter.

As can be observed, the FRM approach is based on an M -fold interpolation scheme. This technique begins with a gradual-transition linear phase FIR digital filter and replaces each delay element with M unit-delays. A multiple-band FIR digital filter is formed that has $(M + 1)$ frequency bands, with the passband and stopband of the original filter scaled by $1/M$. A complementary filter is obtained by subtracting the output of the $(M + 1)$ -band filter from a suitably delayed version of the input. When the frequency responses of the $(M + 1)$ -band filter and its complementary version are masked appropriately and recombined, a very sharp-transition FIR digital filter can be obtained [11]. This technique can be used to design very sharp-transition lowpass, highpass, bandpass and bandstop FIR digital filters.

The following sections presents the design of a lowpass FIR digital filter using the FRM approach.

2.3 Design of Lowpass FRM FIR Digital Filters

Consider the design of a lowpass FRM FIR digital filter having a transfer function $H_{LP}(z)$ and frequency response $H_{LP}(e^{j\omega})$, with passband edge frequency ω_p and stopband edge frequency ω_s . Moreover, consider a linear phase FIR bandedge shaping digital sub-filter $H_a(z)$ of odd length N_a , having passband and stopband edge frequencies θ and ϕ , respectively. Then, $H_b(z)$ can be defined as a complimentary version of $H_a(z)$ if,

$$|H_a(e^{j\omega}) + H_b(e^{j\omega})| = 1. \quad (2.1)$$

where $H_a(e^{j\omega})$ and $H_b(e^{j\omega})$ represent the corresponding frequency responses of $H_a(z)$ and $H_b(z)$ in the Fourier domain and are as shown in Figs. 2.4 and 2.5. This complementary filter pair can also be represented by the formulas,

$$\begin{aligned} H_a(e^{j\omega}) &= e^{-j((N_a-1)/2)\omega} \times T_a(\omega), \\ H_b(e^{j\omega}) &= e^{-j((N_a-1)/2)\omega} \times (1 - T_a(\omega)). \end{aligned} \quad (2.2)$$

Here $T_a(\omega)$ represents the magnitude response of the bandedge shaping digital sub-filter $H_a(z)$.

In the z -domain the complementary digital sub-filter $H_b(z)$ can be represented by the expression,

$$H_b(z) = z^{((N_a-1)/2)} - H_a(z). \quad (2.3)$$

In other words, the complementary transfer function $H_b(z)$ can be derived by subtracting the output of $H_a(z)$ from a delayed version of the input $X(z)$ as shown in Fig. 2.2. The delay elements need not be implemented separately for $H_b(z)$ since the delays in $H_a(z)$ can be reused for this purpose, resulting in some hardware savings (c.f. Fig. 2.3).

Let two filters $\acute{H}_a(e^{j\omega})$ and $\acute{H}_b(e^{j\omega})$ be derived from the complementary pair $H_a(e^{j\omega})$ and $H_b(e^{j\omega})$ by replacing each unit delay by M -unit delays such that $\acute{H}_a(e^{j\omega}) = H_a(e^{jM\omega})$ and $\acute{H}_b(e^{j\omega}) = H_b(e^{jM\omega})$. The respective frequency responses $\acute{H}_a(e^{j\omega})$ and $\acute{H}_b(e^{j\omega})$ are as illustrated in Fig. 2.6.

Two masking filters $H_{ma}(z)$ and $H_{mb}(z)$ with frequency responses $H_{ma}(e^{j\omega})$ and $H_{mb}(e^{j\omega})$ as shown in Fig. 2.7 may be used to mask $\hat{H}_a(e^{j\omega})$ and $\hat{H}_b(e^{j\omega})$ in order to realize the overall lowpass FRM FIR digital filter $H_{LP}(z)$. If the masked frequency responses of $\hat{H}_a(e^{j\omega})$ and $\hat{H}_b(e^{j\omega})$ are recombined as shown in Fig. 2.11, the desired frequency response, $H_{LP}(e^{j\omega})$ is obtained (as in Figs. 2.8 and 2.10). The frequency response of the overall FRM lowpass FIR digital filter can alternatively be described using the relation,

$$H_{LP}(e^{j\omega}) = \hat{H}_a(e^{j\omega}) \times H_{ma}(e^{j\omega}) + \hat{H}_b(e^{j\omega}) \times H_{mb}(e^{j\omega}). \quad (2.4)$$

It should be pointed out that for the above equation to be valid, the group delay of $H_{ma}(z)$ and $H_{mb}(z)$ must be equal, otherwise leading zeros must be added appropriately to fulfill this condition. Also, in order to avoid half sample delays, $(N_a - 1)M$ must be even.

In general, for a given set of design constraints, one must derive appropriate specifications for the constituent digital sub-filters $H_a(z)$, $H_{ma}(z)$ and $H_{mb}(z)$ such that the overall FRM FIR digital filter satisfies the given design specifications. This is achieved by first calculating an appropriate value for the interpolation factor M so that the overall complexity of FRM FIR digital filter is at a minimum. The passband edge θ and stopband edge ϕ of the bandedge shaping digital sub-filter $H_a(z)$ can then be calculated in terms of the interpolation factor M and the bandedge frequency specifications of the overall FRM FIR digital filter ω_p and ω_s . Having obtained the bandedge frequencies of $H_a(z)$, one can find appropriate bandedge frequencies of the masking digital sub-filters $H_{ma}(z)$ and $H_{mb}(z)$ in terms of θ , ϕ and M . It should be pointed out that a lowpass FRM FIR digital filter can be realized in two ways, in one of which the frequency response near the transition band of $H_{LP}(z)$ is determined mainly by $\hat{H}_a(z)$ (c.f. Fig. 2.8) and in the other of which the transition band of $H_{LP}(z)$ is determined by $\hat{H}_b(z)$ (c.f. Fig. 2.10). At any given time, only one of these cases will satisfy the constraint $0 < \theta < \phi < \pi$ and the bandedge equations pertaining to that case will result in valid digital sub-filters.

In addition to the bandedge frequency specifications, one also needs to find an appropriate set of passband ripples and stopband attenuations for the digital sub-

filters so that the passband ripple and the stopband attenuation of the overall FRM FIR digital filter satisfies the given design specifications. Once the appropriate design specifications for the digital sub-filters are derived, one can use standard optimization packages such as Parks-McClellan approach to design these digital sub-filters in infinite-precision.

The steps for realizing the desired lowpass FRM FIR digital filter in terms of the digital sub-filters is discussed below.

2.3.1 Optimal value for the interpolation factor M

A closed form expression for the interpolation factor M can be calculated using filter lengths of the digital sub-filters $H_a(z)$, $H_{ma}(z)$ and $H_{mb}(z)$ obtained from the Hermann's formulas in Eqns. B.3, B.4 and B.5 (c.f. Appendix B). Let the transition bandwidth $(\omega_s - \omega_p)$ be denoted by Δ . Hermann's equation can be written as:

$$N \approx \frac{D_\infty(\delta_p, \delta_s) - F(\delta_p, \delta_s)[(\Delta)/2\pi]^2}{(\Delta)}, \quad (2.5)$$

where N represents the length of the overall FRM FIR digital filter, δ_p represents the passband ripple and δ_s represents the stopband attenuation. It can be observed from Eqn. 2.5 that for $\Delta < 0.2$, the first term in the above equation becomes dominant, leading to

$$N \approx \frac{D_\infty(\delta_p, \delta_s)}{\Delta} \quad (2.6)$$

Since only an approximate solution is required for the calculation of the optimum value of M , the length of the bandedge shaping digital sub-filter $H_a(z)$ given by N_a can be expressed as [21]:

$$N_a \approx \frac{N}{M}. \quad (2.7)$$

Let N_{ma} and N_{mb} represent the lengths of the masking digital sub-filters $H_{ma}(z)$ and $H_{mb}(z)$. From Figs. 2.7 and 2.9, it can be concluded that the sum of the transition bandwidths of $H_{ma}(e^{j\omega})$ and $H_{mb}(e^{j\omega})$ is $2\pi/M$. Let the transition bandwidth of $H_{ma}(e^{j\omega})$ be represented by γ . Then,

$$N_{ma} + N_{mb} \propto \frac{1}{\gamma} + \frac{1}{\frac{2\pi}{M} - \gamma}. \quad (2.8)$$

By differentiating $(N_{ma} + N_{mb})$ with respect to γ and by setting the resulting equation to zero, the following relation is obtained:

$$\gamma = \frac{\pi}{M}. \quad (2.9)$$

Since the sum of the transition bandwidths of $H_{ma}(e^{j\omega})$ and $H_{mb}(e^{j\omega})$ is $2\pi/M$, then from Eqn. 2.9 it can be stated that the transition bandwidth of $H_{mb}(e^{j\omega})$ is equal to $\frac{2\pi}{M} - \frac{\pi}{M} = \frac{\pi}{M}$. Thus, for $(N_{ma} + N_{mb})$ to be at a minimum, the transition bandwidth of $H_{ma}(e^{j\omega})$ must be equal to that of $H_{mb}(e^{j\omega})$, or, equivalently,

$$N_{ma} = N_{mb}. \quad (2.10)$$

Therefore, for minimum hardware complexity, the length of the masking digital sub-filter $H_{ma}(e^{j\omega})$ must be equal to that of $H_{mb}(e^{j\omega})$. Moreover, the lengths of the masking digital sub-filters can be given by the relation [21]:

$$N_{ma} \approx N_{mb} \approx 0.32(MN)\Delta. \quad (2.11)$$

The total number of multipliers N_{frm} needed to implement the FRM FIR digital filter is thus,

$$N_{frm} = N_a + N_{ma} + N_{mb} \approx \left(\frac{1}{M} + 0.64M\Delta \right) N. \quad (2.12)$$

By differentiating N_{frm} with respect to M and setting the result to zero, the optimum value of M is obtained as

$$M_{opt} \approx \frac{1}{\sqrt{0.64\Delta}}, \quad (2.13)$$

where M_{opt} is the value of M at minimum complexity. At $M \approx M_{opt}$, the number of multipliers needed for the FRM FIR digital filter implementation is at its minimum.

The optimum value of M derived above can be used as a first approximation only. A better approximation can be obtained by tabulating the overall lowpass FRM FIR digital filter length as a function of M in the vicinity of the first approximation, and by selecting the M values which lead to a minimum overall FRM FIR digital filter length.

2.3.2 Bandedge design equations for digital sub-filters $H_a(z)$, $H_{ma}(z)$ and $H_{mb}(z)$

Case I: Transition band of $H_{LP}(z)$ is governed by $\hat{H}_a(z)$:

In this case, the passband and stopband edge frequencies ω_p and ω_s of the overall lowpass FRM FIR digital filter must fall in the range [11],

$$\frac{2m_l\pi}{M} < \omega_p, \omega_s < \frac{(2m_l+1)\pi}{M}. \quad (2.14)$$

It is clear from Figs. 2.7 and 2.8 that

$$\omega_p = \frac{2m_l\pi + \theta}{M}, \quad (2.15)$$

and

$$\omega_s = \frac{2m_l\pi + \phi}{M}. \quad (2.16)$$

In order for Eqns. 2.15 and 2.16 to yield correct solutions with $0 < \theta < \phi < \pi$ one must have

$$\theta = \omega_p M - 2m_l\pi, \quad (2.17)$$

$$\phi = \omega_s M - 2m_l\pi, \quad (2.18)$$

where $m_l = \left\lfloor \frac{\omega_p M}{2\pi} \right\rfloor$ is the largest integer less than $\frac{\omega_p M}{2\pi}$.

The bandedge frequencies for the masking digital sub-filters $H_{ma}(z)$ and $H_{mb}(z)$ can be calculated as shown in Fig. 2.7.

Case II: Transition band of $H_{LP}(z)$ is governed by $\hat{H}_b(z)$:

In this case, ω_p and ω_s must lie in the range, [11]

$$\frac{(2m_l-1)\pi}{M} < \omega_p, \omega_s < \frac{2m_l\pi}{M}. \quad (2.19)$$

It is clear from Figs. 2.9 and 2.10 that,

$$\omega_p = \frac{2m_l\pi - \phi}{M}, \quad (2.20)$$

and

$$\omega_s = \frac{2m_l\pi - \theta}{M}. \quad (2.21)$$

Again, in order for Eqns. 2.20 and 2.21 to yield correct solutions with $0 < \theta < \phi < \pi$ one must have

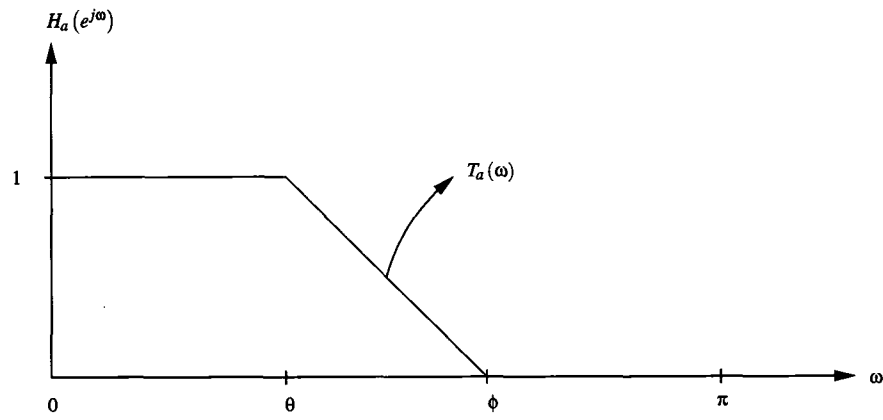


Figure 2.4: Frequency Response of bandedge-shaping digital sub-filter $H_a(e^{j\omega})$

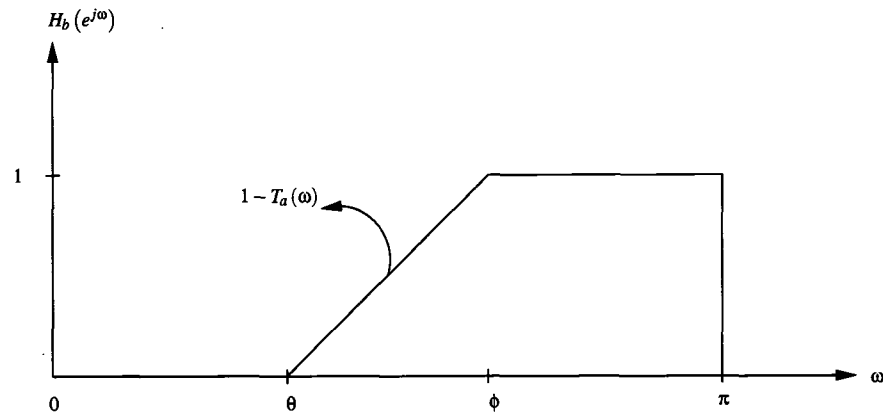


Figure 2.5: Frequency response of complementary bandedge-shaping digital sub-filter $H_b(e^{j\omega})$

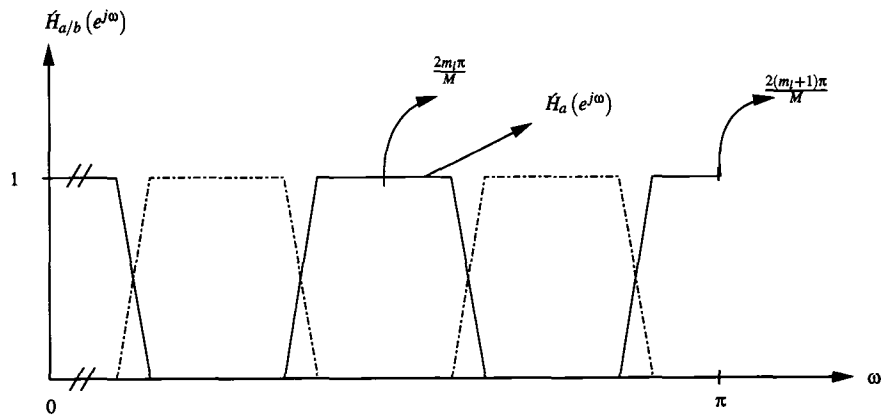


Figure 2.6: M -interpolated complementary digital sub-filters $H_a(e^{j\omega})$ and $H_b(e^{j\omega})$.

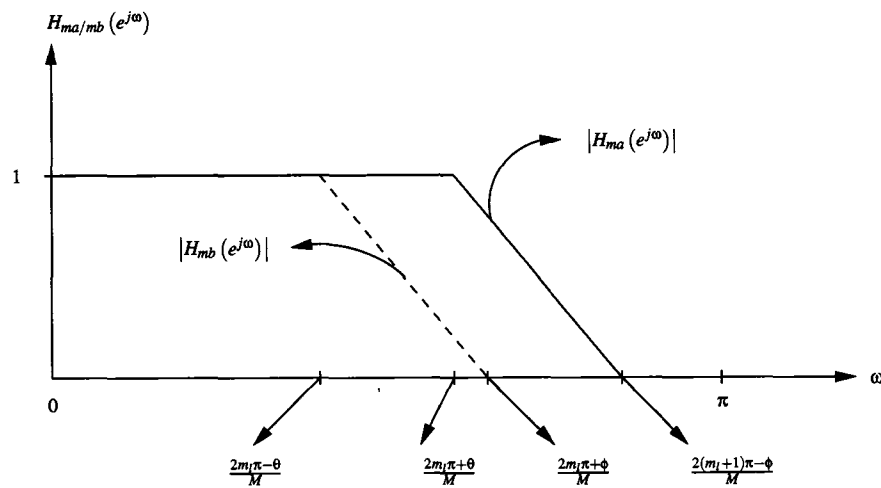


Figure 2.7: Frequency response of masking digital sub-filters $H_{ma}(e^{j\omega})$ and $H_{mb}(e^{j\omega})$

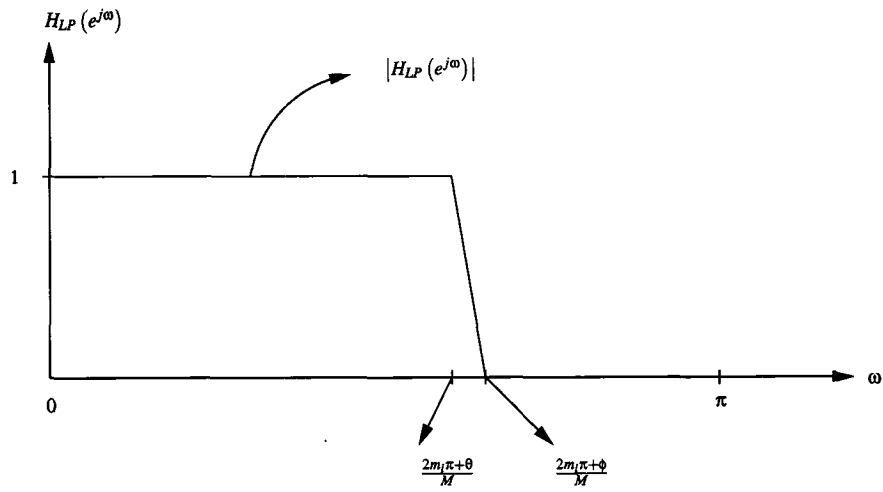


Figure 2.8: Frequency response of overall FRM digital filter $H_{LP}(e^{j\omega})$.

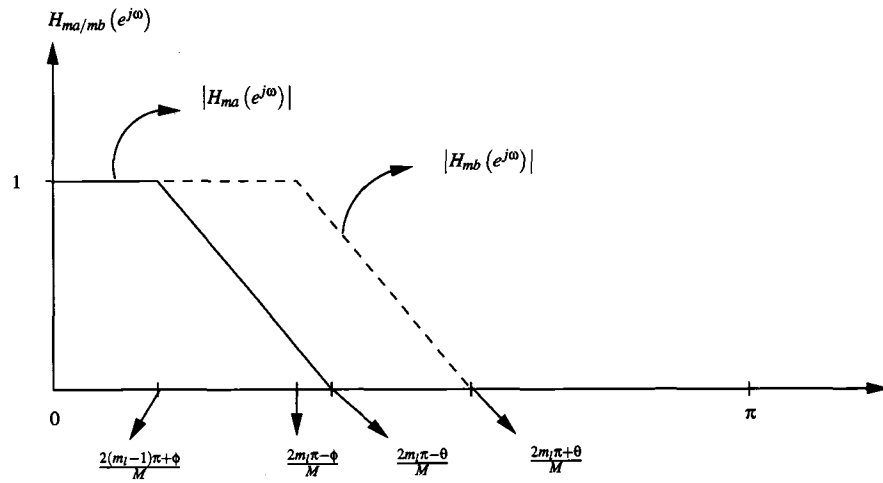


Figure 2.9: Frequency response of masking digital sub-filters $H_{ma}(e^{j\omega})$ and $H_{mb}(e^{j\omega})$

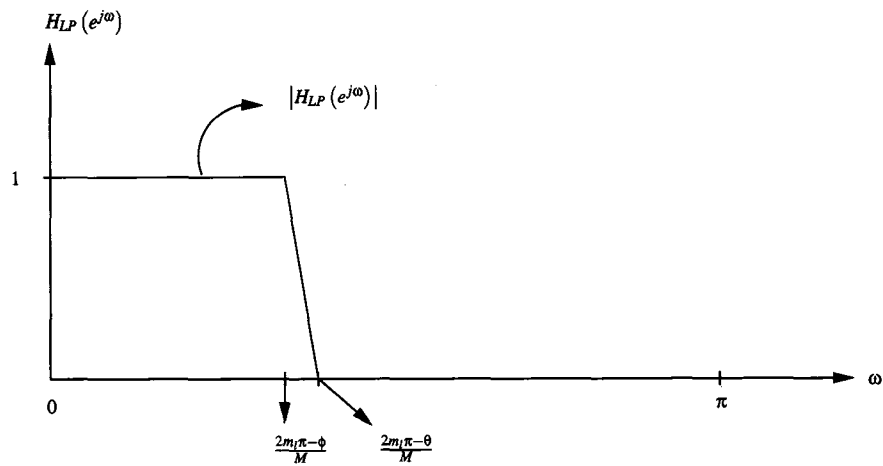


Figure 2.10: Frequency response of overall FRM FIR digital filter $H_{LP}(e^{j\omega})$.

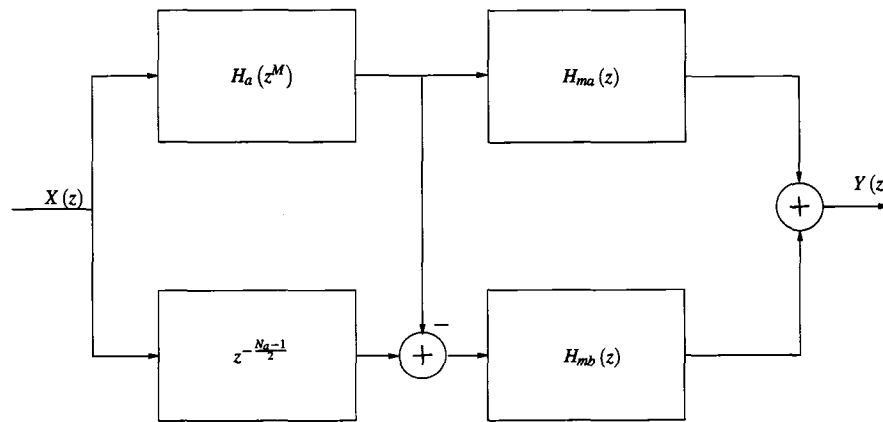


Figure 2.11: Synthesis architecture of overall FRM FIR digital filter.

2.3.3 Passband ripples and stopband attenuation of digital sub-filters $H_a(z)$, $H_{ma}(z)$ and $H_{mb}(z)$

Before discussing the calculation of appropriate values for the passband ripples and stopband attenuations for the digital sub-filters $H_a(e^{j\omega})$, $H_{ma}(e^{j\omega})$ and $H_{mb}(e^{j\omega})$, it is important to point out the effects of these ripples on those of the overall FRM FIR digital filter $H_{LP}(e^{j\omega})$. This is important as the passband ripples and stopband attenuations of the bandedge shaping digital sub-filter $H_a(e^{j\omega})$ can be designed to partially compensate for the effects of the masking digital sub-filter ripples in certain frequency ranges, thereby reducing their respective hardware complexities [11]. Let $T_{LP}(\omega)$ and $\delta_{LP}(\omega)$ represent the desired magnitude and deviation (i.e. passband ripple and stopband attenuation) of the overall FRM FIR digital filter $H_{LP}(e^{j\omega})$. Also, let $\hat{T}_a(\omega)$ and $\hat{\delta}_a(\omega)$ be the magnitude and deviation of the M -interpolated bandedge shaping digital sub-filter $\hat{H}_a(e^{j\omega})$. In this way, $\hat{T}_a(\omega)$ is 1 in the passband and is 0 in the stopband of $\hat{H}_a(e^{j\omega})$. In the transition band of $\hat{H}_a(e^{j\omega})$, one can define $\hat{T}_a(\omega)$ to be equal to $\hat{H}_a(e^{j\omega})$ with an error in the linear-phase term, i.e. $\hat{\delta}_a(\omega) = 0$. If $T_{ma}(\omega)$ and $T_{mb}(\omega)$, and $\delta_{ma}(\omega)$ and $\delta_{mb}(\omega)$ represent the respective magnitude response and deviation of the masking digital sub-filters $H_{ma}(e^{j\omega})$ and $H_{mb}(e^{j\omega})$, then, from Eqn. 2.4,

$$T_{LP}(\omega) + \delta_{LP}(\omega) = \{T_{ma}(\omega) + \delta_{ma}(\omega)\} \left\{ \hat{T}_a(\omega) + \hat{\delta}_a(\omega) \right\} + \{T_{mb}(\omega) + \delta_{mb}(\omega)\} \left\{ 1 - \hat{T}_a(\omega) + \hat{\delta}_a(\omega) \right\}. \quad (2.24)$$

In order to understand the effects of the digital sub-filters on the overall ripple, the frequency range $\{0, \pi\}$ is divided into three parts [11].

Frequency Range I where $T_{ma}(\omega) = T_{mb}(\omega) = 1$:

In this frequency range, the magnitude response $T_{LP}(\omega)$ of the overall lowpass FRM FIR digital filter is equal to 1. Thus, Eqn. 2.24 can be modified as

$$\delta_{LP}(\omega) = \hat{T}_a(\omega) \{ \delta_{ma}(\omega) - \delta_{mb}(\omega) \} + \delta_{mb}(\omega) + \hat{\delta}_a(\omega) \{ \delta_{ma}(\omega) - \delta_{mb}(\omega) \}. \quad (2.25)$$

Since the second order term $\hat{\delta}_a(\omega) \{ \delta_{ma}(\omega) - \delta_{mb}(\omega) \}$ is negligible, Eqn. 2.25 can be modified to,

$$\delta_{LP}(\omega) = \hat{T}_a(\omega) \{\delta_{ma}(\omega) - \delta_{mb}(\omega)\} + \delta_{mb}(\omega). \quad (2.26)$$

Eqn. 2.26 can be evaluated for various values of $\hat{T}_a(\omega)$, for instance, when $\hat{T}_a(\omega) = 1$,

$$\delta_{LP}(\omega) \approx \delta_{ma}(\omega). \quad (2.27)$$

When $\hat{T}_a(\omega) = 0$,

$$\delta_{LP}(\omega) \approx \delta_{mb}(\omega), \quad (2.28)$$

and when $0 < \hat{T}_a(\omega) < 1$,

$$\delta_{LP}(\omega) \leq \max\{|\delta_{ma}(\omega)|, |\delta_{mb}(\omega)|\}. \quad (2.29)$$

Frequency Range II where $T_{ma}(\omega) = T_{mb}(\omega) = 0$:

In this frequency range, the magnitude response $T_{LP}(\omega)$ of the overall FRM FIR digital filter is equal to 0. Thus, after ignoring the second order term Eqn. 2.24 can be modified as

$$\delta_{LP}(\omega) = \hat{T}_a(\omega) \{\delta_{ma}(\omega) - \delta_{mb}(\omega)\} + \delta_{mb}(\omega) \quad (2.30)$$

Again, Eqn. 2.30 can be evaluated for various values of $\hat{T}_a(\omega)$. For instance, when $\hat{T}_a(\omega) = 1$,

$$\delta_{LP}(\omega) \approx \delta_{ma}(\omega). \quad (2.31)$$

When $\hat{T}_a(\omega) = 0$,

$$\delta_{LP}(\omega) \approx \delta_{mb}(\omega), \quad (2.32)$$

and when $0 < \hat{T}_a(\omega) < 1$,

$$\delta_{LP}(\omega) \leq \max\{|\delta_{ma}(\omega)|, |\delta_{mb}(\omega)|\}. \quad (2.33)$$

Frequency Range III:

The frequency points not covered by the above two ranges fall in the range

$$\{(2m\pi - \theta)/M < \omega < (2(m+1)\pi - \phi)/M\} \quad (2.34)$$

for Fig. 2.7 and fall in the range

$$\{(2(m-1)\pi + \phi)/M < \omega < (2m\pi + \theta)/M\} \quad (2.35)$$

for Fig. 2.9.

Consider the case of Fig. 2.7 where for $\{(2m\pi - \theta)/M < \omega < \omega_p\}$, $T_{LP}(\omega) = \hat{T}_a(\omega) = G_{ma}(\omega) = 1$. Then after neglecting second order terms,

$$\delta_{LP}(\omega) \approx \delta_{ma}(\omega) + \delta'_a(\omega) \{1 - T_{mb}(\omega)\}. \quad (2.36)$$

As ω increases from $(2m\pi - \theta)/M$ to ω_p , $T_{mb}(\omega)$ decreases from 1 to 0. Therefore, in this frequency range,

$$|\delta_{LP}(\omega)| \leq |\delta'_a(\omega)| + |\delta_{ma}(\omega)|. \quad (2.37)$$

For $\{\omega_s < \omega < (2(m+1)\pi - \phi)/M\}$, $T_{LP}(\omega) = \hat{T}_a(\omega) = T_{mb}(\omega) = 0$, and thus,

$$\delta_{LP}(\omega) \approx T_{ma}(\omega) \delta'_a(\omega) + \delta_{mb}(\omega). \quad (2.38)$$

As ω increases from ω_s to $(2(m+1)\pi - \phi)/M$, $T_{ma}(\omega)$ decreases from 1 to 0 and thus,

$$|\delta_{LP}(\omega)| \leq |\delta'_a(\omega)| + |\delta_{mb}(\omega)|. \quad (2.39)$$

The bounds in Eqns. 2.37 and 2.39 are highly pessimistic and $T_a(\omega)$ can be designed such that its ripple can partially compensate for the ripples, $\delta_{ma}(\omega)$ and $\delta_{mb}(\omega)$.

From the above discussion it can be concluded that whenever $T_{ma}(\omega)$ and $T_{mb}(\omega)$ are both equal to 1 or 0, $\delta_{LP}(\omega)$ is determined mainly by $\delta_{ma}(\omega)$ and $\delta_{mb}(\omega)$ depending on whether $\hat{T}_a(\omega)$ is 0 or 1. Thus, both $H_{ma}(\omega)$ and $H_{mb}(\omega)$ have “dont care” bands within their respective frequency responses which can potentially be used to reduce the complexity of the masking digital sub-filters. Furthermore, $T_a(\omega)$ can be designed and optimized in such a way that $\delta'_a(\omega)$ can partially compensate for $\delta_{ma}(\omega)$ and $\delta_{mb}(\omega)$ near the transition bandedge frequencies.

In design problems, the magnitude of $\delta'_a(\omega)$, $\delta_{ma}(\omega)$ and $\delta_{mb}(\omega)$ is usually set to 10 – 15% below the maximum allowable $\delta(\omega)$ in order to compensate for the second order terms introduced by $\delta'_a(\omega)$.

2.3.4 Design of the overall lowpass FRM FIR digital filter in terms of the digital sub-filters $H_a(z)$, $H_{ma}(z)$ and $H_{mb}(z)$

In order to obtain an overall lowpass FRM FIR digital filter which satisfies the given design specifications, one must optimize $T_{LP}(\omega)$ based on the linear equation,

$$\delta_{LP}(\omega) = T_a(M\omega) \{T_{ma}(\omega) + \delta_{ma}(\omega) - T_{mb}(\omega) - \delta_{mb}(\omega)\} + T_{mb}(\omega) + \delta_{mb}(\omega) - T_{LP}(\omega) \quad (2.40)$$

Eqn 2.40 must be evaluated on a dense set of frequencies in the range $\left[\frac{2m\pi}{M}, \frac{(2m+1)\pi}{M}\right]$ for Fig. 2.8, and in the range $\left[\frac{(2m-1)\pi}{M}, \frac{2m\pi}{M}\right]$ for Fig. 2.10. The minimization of $|\delta_{LP}(\omega)|$ is a linear programming problem and one can use Parks-McClellan technique to obtain optimum magnitude responses of the digital sub-filters $H_a(z)$, $H_{ma}(z)$ and $H_{mb}(z)$ such that $|\delta_{LP}(\omega)|$ is minimum. Having obtained the optimum magnitude responses of the constituent FRM digital sub-filters, one can easily derive the corresponding infinite-precision multiplier coefficients for these digital sub-filters.

The above discussion can be easily extended to the design of highpass FRM FIR digital filters. The only difference being that the constituent digital sub-filters $H_a(e^{j\omega})$, $H_{ma}(e^{j\omega})$ and $H_{mb}(e^{j\omega})$ will have highpass magnitude response characteristics.

Chapter 3

Design and Optimization of Finite-Precision FRM FIR Digital Filters Using Conventional Genetic Algorithms

In chapter 2, it was discussed how FRM FIR digital filters with infinite-precision multiplier coefficient values can be realized using the conventional optimization techniques such as Parks-McClellan approach. In an actual hardware/software implementation, the constituent multiplier coefficient values are quantized to their finite-precision counterparts. These finite-precision filter coefficients can take only discrete values whose precision is limited by the register length of the hardware platform being used to implement the FRM FIR digital filter [17]. The quantization process leads to non-linear difference equations governing the FRM digital filters, which are hard and often impossible to analyze. In addition, by approximating the infinite-precision multiplier coefficients to their corresponding finite-precision counterparts, the frequency response of the FRM digital filter may no longer satisfy the given design specifications. However, one can use the resulting FRM FIR digital filter as a seed in GAs to obtain a corresponding finite-precision FRM FIR digital filter which meets the desired design specifications.

This chapter is concerned with computationally efficient finite-precision number systems, namely, the CSD and DBNS number representation schemes. These number systems are employed to quantize the infinite-precision multiplier coefficients values of the FRM FIR digital filter to their finite-precision counterparts.

The resulting FRM FIR digital filter is subsequently subjected to a novel GA for discrete optimization in order to search for an optimal finite-precision FRM FIR digital filter that satisfies the given design specifications. Two application examples are presented for the optimization of FRM FIR digital filters over the CSD/DBNS multiplier coefficient spaces, one having a lowpass magnitude response and the other having a bandpass magnitude response.

3.1 CSD Multiplier Coefficient Representation

The CSD number system is a special case of the SPT number system, where a given number has a unique CSD representation. In the case of FRM FIR digital filters, the infinite-precision multiplier coefficient values x_j can be quantized to their fixed radix-point CSD counterparts \hat{x}_j in accordance with,

$$\hat{x}_j = \sum_{i=1}^W D_{ji} \times 2^{R-i}, \quad (3.1)$$

where the integer R represents a radix-point in the range $0 < R < W$. As stated before, W and w represent the prespecified wordlength and prespecified non-zero bits. Due to the constraints

$$\begin{aligned} D_{ji} &\in \{1, -1, 0\}, \\ D_{ji} \times D_{j,i+1} &= 0, \\ \sum_{i=1}^W |D_{ji}| &\leq w, \end{aligned} \quad (3.2)$$

in the CSD number system, the finite-precision multiplier coefficient values \hat{x}_j may have very sparse representations, lending themselves to shift and add hardware implementations.

3.2 DBNS Multiplier Coefficient Representation

In the case of the DBNS number system, the infinite-precision multiplier coefficient values x_j can be approximated to their fixed-point DBNS counterparts \hat{x}_j in

accordance with

$$\hat{x}_j = \sum_{k,l} d_{kl} 2^k 3^l, \quad (3.3)$$

where $d_{kl} \in \{0, 1\}$, and where k and l are non-negative and independent integers [2]. In this way, when l is zero, the DBNS representation reduces to the binary representation. In general, a given number can have many DBNS representations, but not all of the representations are efficient in terms of the total number of non-zero bits. Thus, the objective is to find a DBNS representation that has the least number of non-zero bits. The resulting representation is referred to as the *canonical DBNS (CDBNS) representation*. By using the greedy algorithm in [2] one may or may not be able to find the CDBNS representation for a given number. However, this algorithm will find a representation that is close to the CDBNS system. This leads to a near-canonic DBNS (NCDBNS) representation [2]. In this thesis, the CDBNS numbers are assumed to have only one non-zero bit, bypassing the need for the aforementioned greedy algorithm altogether.

3.3 Genetic Algorithms: An overview

Since their inception in the 1970s, genetic algorithms have proved to be one of the most adroit techniques for finding solutions to discrete optimization problems. These algorithms simulate the process of biological evolution for finding optimal solutions by concurrently searching along all directions in the search space. Genetic algorithms begin with a seed bit sequence called the seed chromosome. An initial population pool of potential solutions is constructed from this seed chromosome by randomly complementing bits in the sequence. These chromosomes are then evaluated against a fitness function and are ranked accordingly. The population pool for the next generation is constructed by randomly selecting chromosomes to form a mating pool. Pairs of chromosomes (parents) are then exposed to genetic operations such as crossover and mutation to form offspring. These offspring become members of the next-generation population pool. It should be noted that non-elite (i.e. low fitness value) chromosomes are also added to the mating pool in order to increase diversity. The aforementioned genetic operations are repeated until a pre-specified

stopping criterion is reached.

The main differences [25, 4] between GAs and the conventional optimization techniques are:

- GAs do not require any gradient information to perform the optimization.
- GAs manipulate the design variables at the bit level rather than a direct manipulation of the variables themselves.
- GAs can perform a parallel search using a population of potential candidate chromosomes (derived by perturbing bits in a seed chromosome), making them very effective in finding optimum solutions to complex, multi-modal optimization problems.

Due to their inherent parallel search nature, GAs allow evaluation of many local optima, and can potentially find the global optimum. The parallel search capabilities are made possible by crossover and mutation operations.

3.4 The Proposed GA Optimization for FRM FIR Digital Filters

In the conventional optimization of FIR digital filters using GAs, the constituent multiplier coefficient values are replaced by their binary representations, and the resulting representations are concatenated to form a seed chromosome. The remaining members of the population pool are generated by complementing randomly selected bits in the seed chromosome. However, in the cases of CSD/DBNS multiplier coefficient representations, complementing the selected bits in the seed chromosome may result in a chromosome which may no longer conform to the CSD/DBNS number systems¹. In this thesis, this problem is avoided altogether by generating a pair of indexed look-up tables (LUTs) of permissible CSD/DBNS multiplier coefficient values in such a manner that the respective set of indices are closed under any genetic operation (including the operation of complementing bits). In this way,

¹The same problem arises under the operations of crossover and mutation in the course of optimization by the underlying GA.

the seed chromosome is formed by concatenating the binary representation of the CSD/DBNS multiplier coefficient value indices (as opposed to the multiplier coefficient values themselves). Consequently, the seed chromosome will always result in chromosomes which conform to the original CSD/DBNS number systems.

The proposed GA for the optimization of FRM FIR digital filters over the CSD/DBNS multiplier coefficient spaces is presented in the following section.

3.4.1 Design of initial infinite-precision FRM digital filter

The Parks-McClellan approach is employed to design an initial infinite-precision FRM digital filter which satisfies the given design specifications. The design of these FRM FIR digital filters is carried out in terms of the corresponding digital sub-filters $H_a(z)$, $H_{ma}(z)$ and $H_{mb}(z)$ ².

3.4.2 Generation of the CSD LUT

The CSD LUT is formed as a two-column table, with one column including CSD multiplier coefficient values, and with the other including their respective ordered indices. Let the infinite-precision multiplier coefficient values lie in the range $\{-c_p, +c_p\}$. Moreover, let $W = W_I + W_F$, where W_I represents the wordlength of the integer part, and where W_F represents the wordlength of the fractional part of the CSD multiplier coefficient values. Then, W_I must be chosen such that the integer part of c_p can be represented in CSD without exceeding the wordlength W . W_F , on the other hand, must be chosen based on the precision requirements of the FRM FIR digital filter application. Having decided on the values of W and w , the required CSD LUT of size U is generated exhaustively. The LUT is subsequently trimmed to a size of 2^B , where B is the largest integer such that $2^B < U$, in order to be able to represent each CSD number uniquely by an ordered index ranging from 1 to 2^B . In this way, the length of the LUT may have to be enlarged initially so that after trimming, the CSD LUT would still be capable of representing the integer part of c_p in W_I bits.

²The proposed GA can be easily modified to begin with a CSD or DBNS FRM FIR digital filter at the outset.

3.4.3 Generation of the DBNS LUT

The DBNS LUT is generated in much the same way as the CSD LUT, except that the DBNS LUT consists of five columns, including the base 2 exponent, the base 3 exponent, the decimal equivalent of the DBNS multiplier coefficient value, and the sign bit, in addition to the index column. The permissible DBNS multiplier coefficient values are generated to lie in the range $\{-2^n 3^m, 2^n 3^m\}$, where the integer exponents n and m are chosen such that $2^n 3^m > c_p$. The length of the resulting DBNS LUT is $(2n + 1) \times m$, which is trimmed to a size of 2^B (again, in order to form a closed set of indices under the GA operations).

3.4.4 Generation of seed CSD/DBNS FRM FIR digital filter

Having obtained the above indexed CSD/DBNS LUT, the infinite-precision multiplier coefficient values are quantized to their nearest CSD/DBNS counterparts in the LUTs. Subsequently, the indices of the CSD/DBNS multiplier coefficient values are converted to B -bit strings and concatenated to form the desired seed CSD/DBNS FRM FIR digital filter chromosome.

3.4.5 Generation of the initial population pool

By manipulating the resulting seed FRM FIR digital filter chromosome, a population pool of N chromosomes is generated. This manipulation involves the scanning of the seed chromosome B bits (i.e. one index) at a time, and by complementing the b^{th} bit (with $1 \leq b \leq B$) randomly in accordance with the probabilistic relationship $p_F \times 0.5^{B+1-b}$, where p_F is a fixed probability factor.

3.4.6 Fitness evaluation

The fitness value of each of the N FRM FIR digital filter chromosomes is evaluated in accordance with

$$fitness = -20 \log [\max \{ \epsilon_p, \epsilon_s \}] + C, \quad (3.4)$$

where

$$\varepsilon_p = \underbrace{\max}_{\omega \in \Omega_p} [W_p |H(e^{j\omega}) - 1|], \quad (3.5)$$

with Ω_p representing the passband frequency region(s), and where

$$\varepsilon_s = \underbrace{\max}_{\omega \in \Omega_s} [W_s |H(e^{j\omega})|], \quad (3.6)$$

with Ω_s representing the stopband frequency region(s). Here, W_p and W_s are passband and stopband weighting factors, and C is a constant chosen so as to render the *fitness* value in Eqn. 3.4 non-negative. In this way, the chromosomes in the population pool are ranked and sorted based on their fitness values. In the event that the resulting population pool does not contain a chromosome that satisfies the given design magnitude response specifications, the algorithm proceeds to generate the next-generation population pool. Otherwise, the algorithm terminates with the highest ranked chromosome declared as optimum.

3.4.7 Generation of mating pool

Having ranked the chromosomes based on their fitness values, a mating pool of size $N_{mating} < N$ is constructed by selecting chromosomes from the population pool using the relationship

$$p(x) = r^{1-x} Z^x, \quad (3.7)$$

where

$$r = \left(\frac{Z^N}{0.001} \right)^{1/(N-1)}, \quad (3.8)$$

where Z represents the probability of selecting a chromosome with a higher fitness value, and where x represents the fitness rank of the particular chromosome. It should be pointed out that Eqn. 3.7 is biased to select chromosomes with higher fitness values. In order to improve diversity, some non-elite chromosomes (i.e. chromosomes with low fitness values) are also incorporated in the mating pool.

3.4.8 Parent selection

Parent chromosomes are selected from the mating pool by using the conventional Roulette Wheel or the Correlative Roulette selection method [9, 8]. This thesis

is concerned with general Roulette Wheel parent selection. Let $Total_{fit}$ represent the sum of the fitness values of the chromosomes in the entire mating pool. Then, a random number is generated to lie between 0 and $Total_{fit}$. Consequently, the parent candidate chromosome is identified as such a chromosome for which the sum of its fitness value and the fitness values of all the preceding chromosomes in the mating pool is greater than or equal to this random number. This method is repeated until $N_p = \frac{N}{2}$ pairs of parent chromosomes have been selected.

3.4.9 The next-generation population pool

The next-generation population pool of size N is formed as discussed next:

- *Crossover Operations:* The parent chromosome pairs formed in the parent selection step undergo two-point crossover, reproducing two offspring chromosomes per parent chromosome pair. This results in N offspring chromosomes which become members of the next-generation population pool.
- *Mutation Operations:* The chromosomes in the resulting next-generation population pool undergo mutation operations in accordance with the probabilistic relationship $p_M \times 0.5^{B+1-b}$ to enhance diversity, where p_M represents the probability of mutation.

3.5 Application Examples

This section is concerned with the application of the proposed GA to the design and optimization of a pair of FRM FIR digital filters, one exhibiting a lowpass and the other a bandpass magnitude frequency response.

3.5.1 Design of lowpass FRM FIR digital filters

Consider the design of a benchmark [11] lowpass FRM FIR digital filter satisfying the following magnitude response specifications

$$\begin{array}{ll}
\text{Passband region} & 0 \leq \omega \leq 0.6\pi \\
\text{Stopband region} & 0.61\pi \leq \omega \leq \pi \\
\text{Maximum passband ripple} & \pm 0.1 \text{ dB} \\
\text{Minimum stopband attenuation} & 40 \text{ dB}
\end{array} \tag{3.9}$$

over the CSD/DBNS multiplier coefficient spaces.

In order to obtain the corresponding infinite-precision lowpass FRM FIR digital filter, one has to select an appropriate value for the interpolation factor M such that the overall complexity of the FRM digital filter is at a minimum. An initial approximation for this interpolation factor $M = 7$ can be obtained by using Eqn. 2.13. A better empirical approximation is obtained by evaluating the computational complexity of the FRM FIR digital filter for a range of values of M in the vicinity of the first approximation $M = 7$ as shown in Table 3.1. From Table 3.1, it is observed that an interpolation factor of $M = 6$ gives rise to the smallest FRM FIR digital filter total length, yielding digital sub-filters $H_a(z)$, $H_{ma}(z)$ and $H_{mb}(z)$ of lengths 84, 24 and 42, respectively.

Table 3.1: Filter Lengths for a Lowpass FRM FIR Digital Filter for Various Values of M

M	H_a	H_{ma}	H_{mb}	Total Length
2	254	24	2	280
3	168	8	42	218
4	126	16	24	166
5	102	506	12	620
6	84	24	42	150
7	72	22	76	170
8	64	126	24	214

Having fixed the value of M at 6, the passband and stopband edge frequencies of the digital sub-filters $H_a(z)$, $H_{ma}(z)$ and $H_{mb}(z)$ are determined by using the design equations given in Section 2.3.2. These bandedge frequencies have been tabulated as shown in Table 3.2. Moreover, the passband ripple and stopband attenuations of these sub-filters are set at 85% of the corresponding values in the design specifications given in Eqn. 3.9 (in order to account for any second order effects when using the design equations as discussed in Section 2.3.3). These passband ripples and stopband attenuations have been shown in Table 3.3.

By using the Parks McClellan approach together with the design specifications in Tables 3.2 and 3.3, the digital sub-filters $H_a(z)$, $H_{ma}(z)$ and $H_{mb}(z)$ can be designed to have magnitude frequency responses as shown in Figs. 3.1 to 3.6. Consequently, the magnitude frequency response of the overall infinite-precision lowpass FRM FIR digital filter $H_{LP}(z)$ is obtained as shown in Fig. 3.7.

Table 3.2: Bandedge Frequencies Associated with $H_a(z)$, $H_b(z)$, $H_{ma}(z)$ and $H_{mb}(z)$ Digital Sub-Filters for the Lowpass FRM FIR Digital Filter Case

Sub-filter	Passband Edge Frequency	Stopband Edge Frequency
$H_a(e^{j\omega})$	0.34π	0.4π
$H_b(e^{j\omega})$	0.4π	0.34π
$H_{ma}(e^{j\omega})$	0.4π	0.61π
$H_{mb}(e^{j\omega})$	0.6π	0.72π

Table 3.3: Passband Ripples and Stopband Attenuations Associated with $H_a(z)$, $H_{ma}(z)$ and $H_{mb}(z)$ Digital Sub-filters for the Lowpass FRM FIR Digital Filter Case

Sub-filter	Passband Ripple	Stopband Attenuation
$H_a(e^{j\omega})$	0.085 dB	-46 dB
$H_b(e^{j\omega})$	0.085 dB	-46 dB
$H_{ma}(e^{j\omega})$	0.085 dB	-46 dB
$H_{mb}(e^{j\omega})$	0.085 dB	-46 dB

3.5.1.1 GA optimization of lowpass CSD FRM FIR digital filters

The design parameters for the genetic optimization of the lowpass CSD FRM FIR digital filter are as shown in Table 3.4. Based on the above infinite-precision lowpass FRM FIR digital filter, the corresponding seed CSD FRM digital filter is obtained to have a magnitude frequency response as shown in Fig. 3.8. It can be observed that the resulting seed digital filter violates the magnitude response specifications by almost 0.5 dB in the pass-band, and by almost 18 dB in the stop-band region (c.f. Table 3.5). By applying the proposed GA to the seed FRM digital filter, the GA evolves from one generation to the next with the average fitness of the population pool and the fitness of the top 50% individuals as shown in Fig. 3.9. It can be observed that the trend of the genetic optimization is towards individuals with increased fitness. After 953 generations, the GA optimization converges to

the optimal lowpass FRM FIR digital filter having a magnitude frequency response as shown in Fig. 3.10. It should be pointed out that the optimized lowpass CSD FRM FIR digital filter outperforms its infinite-precision counterpart by 0.01 dB in the pass-band, and by almost 2.5 dB in the stop-band region (c.f. Table 3.5).

Table 3.4: Design Parameters for GA Optimization of Lowpass CSD FRM FIR Digital Filters

Design Step	Design Parameters
1	$M = 6, N_a = 84, N_{ma} = 24, N_{mb} = 42$
2	$w = 3 \text{ bits}, W_I = 3 \text{ bits}, W_F = 14 \text{ bits}, B = 12 \text{ bits}$
3	$p_F = 0.8, N = 500$
4	$C = 30$
5	$N_{mating} = 150, Z = 0.8$
6	$N_p = 235$
7	$p_M = 0.03$

Table 3.5: Lowpass CSD FRM FIR Digital Filter Magnitude Responses before and after GA Optimization

Multiplier Coefficient Representation	Passband Ripple	Stopband Attenuation
Infinite-Precision	0.075 dB	-41 dB
CSD before GA optimization	0.65 dB	-22.05 dB
CSD after GA Optimization	0.05 dB	-43.62 dB

3.5.1.2 GA Optimization of lowpass DBNS FRM FIR digital filters

In the case of the GA optimization of lowpass DBNS FRM FIR digital filter, the design parameters are as shown in Table 3.6. The corresponding seed DBNS FRM digital filter is obtained to have a magnitude frequency response as shown in Fig. 3.11, violating the magnitude response specifications by almost 0.04 dB in the pass-band, and by almost 3 dB in the stopband region (c.f. Table 3.7). By applying the proposed GA to the seed DBNS FRM digital filter, the evolution of the GA from one generation to the next is as shown in Fig. 3.12. Fig. 3.13 shows the optimized lowpass DBNS FRM FIR digital filter obtained after 1000 generations, outperforming its infinite-precision counterpart by almost 0.01 dB in the passband, and by almost 1.5 dB in the stopband region (c.f. Table 3.7).

Table 3.6: Design Parameters for GA Optimization of DBNS Lowpass FRM FIR Digital Filters

Design Step	Design Parameters
1	$M = 6, N_a = 78, N_{ma} = 22, N_{mb} = 38$
2	$n = 96, m = 69, B = 12 \text{ bits}$
3	$p_F = 0.8, N = 500$
4	$C = 30$
5	$N_{mating} = 150, Z = 0.8$
6	$N_p = 235$
7	$p_M = 0.03$

Table 3.7: Lowpass DBNS FRM FIR Digital Filter Magnitude Responses before and after GA Optimization

Multiplier Coefficient Representation	Passband Ripple	Stopband Attenuation
Infinite-Precision	0.075 dB	-41 dB
DBNS before GA optimization	0.146 dB	-37.3 dB
DBNS after GA Optimization	0.06 dB	-42.62 dB

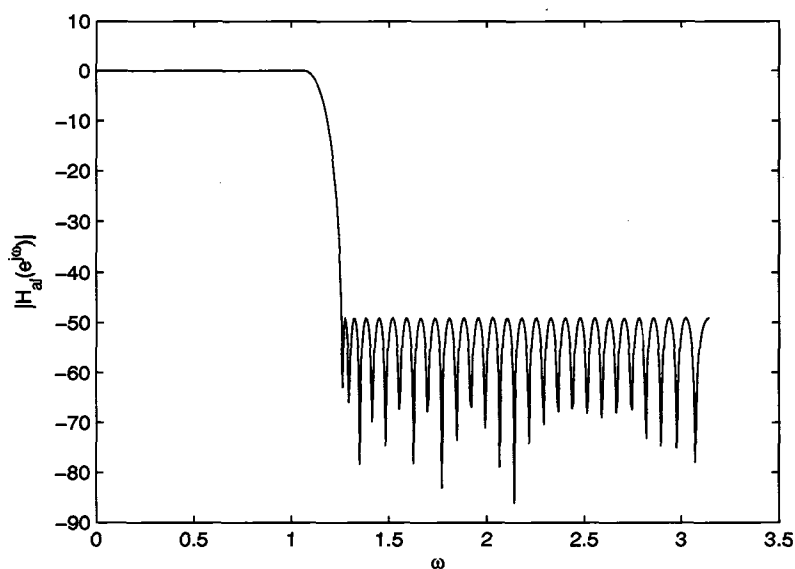


Figure 3.1: Magnitude response of sub-filter $H_a(z)$ for the lowpass FRM FIR digital filter case.

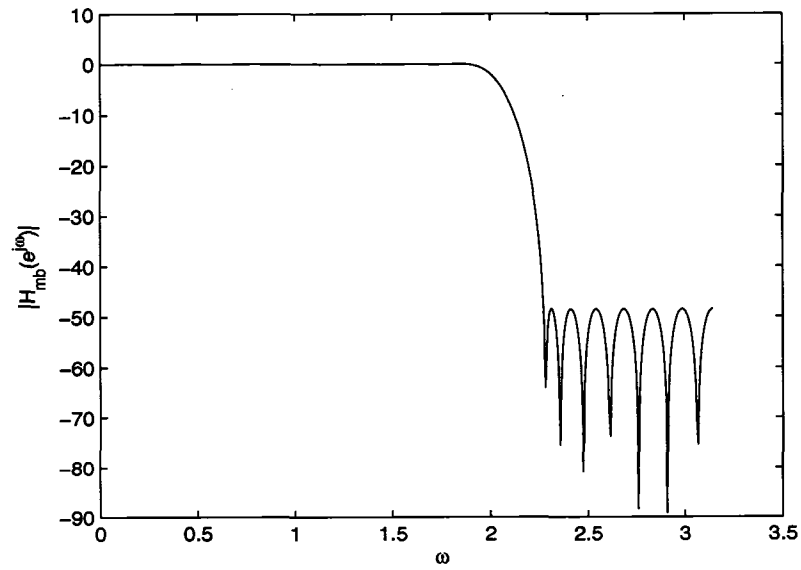


Figure 3.2: Magnitude response of complimentary sub-filter $H_b(z)$ for the lowpass FRM FIR digital filter case.

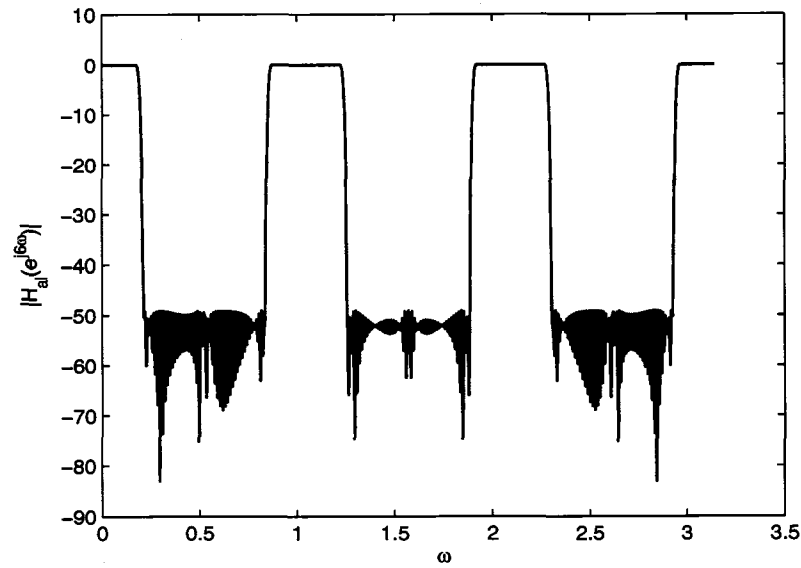


Figure 3.3: Magnitude response of M -interpolated version of $H_a(z)$ for the lowpass FRM FIR digital filter case.

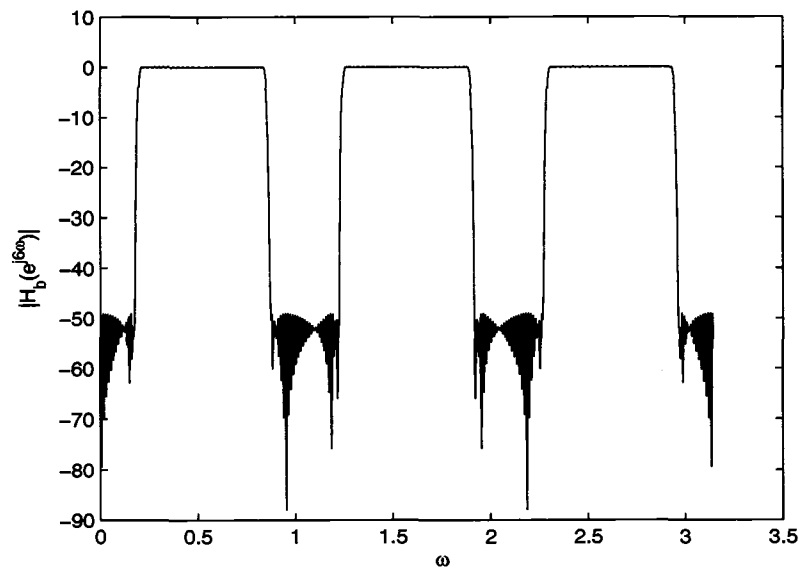


Figure 3.4: Magnitude response of M -interpolated version of complementary sub-filter $H_b(z)$ for the lowpass FRM FIR digital filter case.

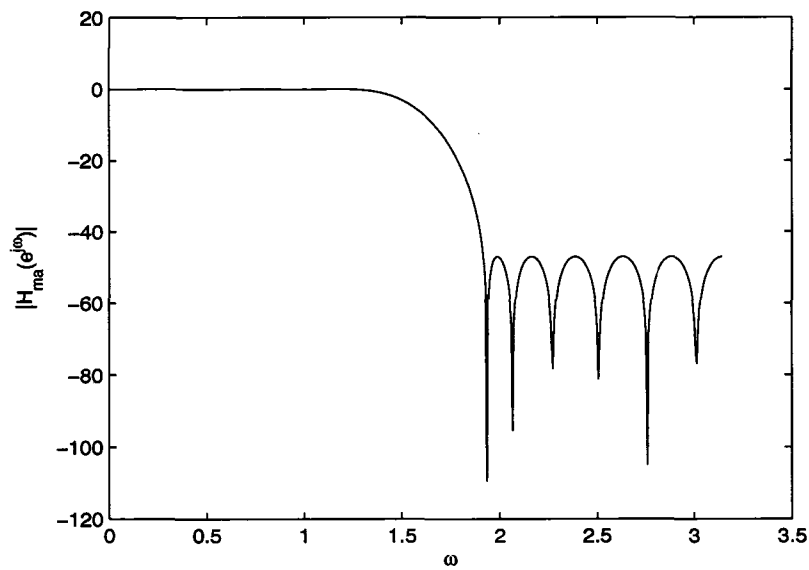


Figure 3.5: Magnitude response of masking digital sub-filter $H_{ma}(z)$ for the lowpass FRM FIR digital filter case.

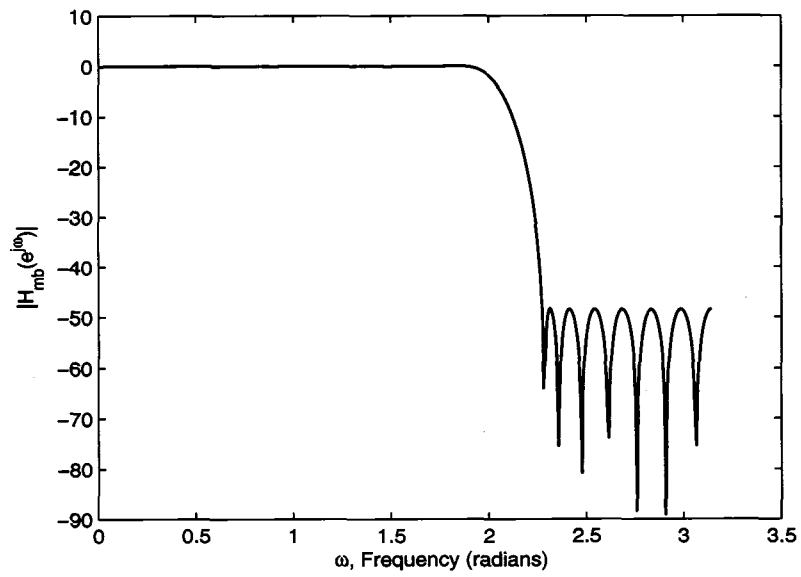


Figure 3.6: Magnitude response of masking digital sub-filter $H_{mb}(z)$ for the lowpass FRM FIR digital filter case.

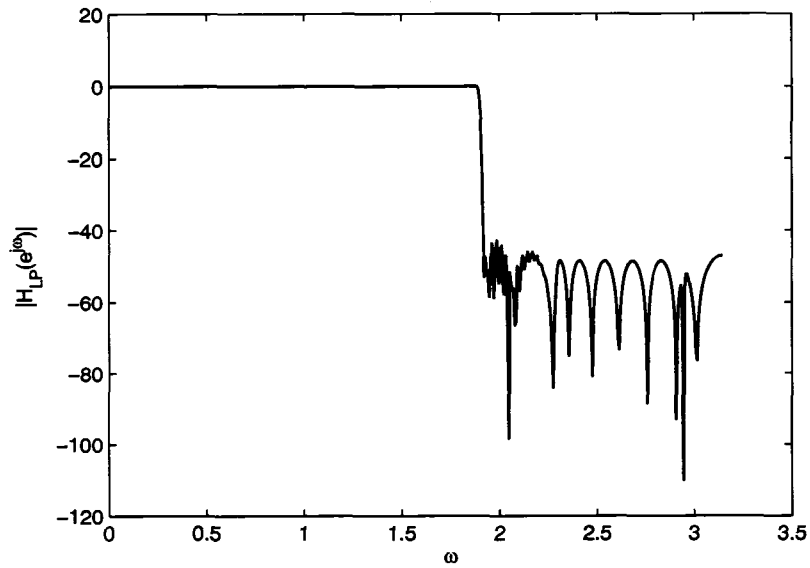


Figure 3.7: Infinite-precision lowpass FRM FIR digital filter.

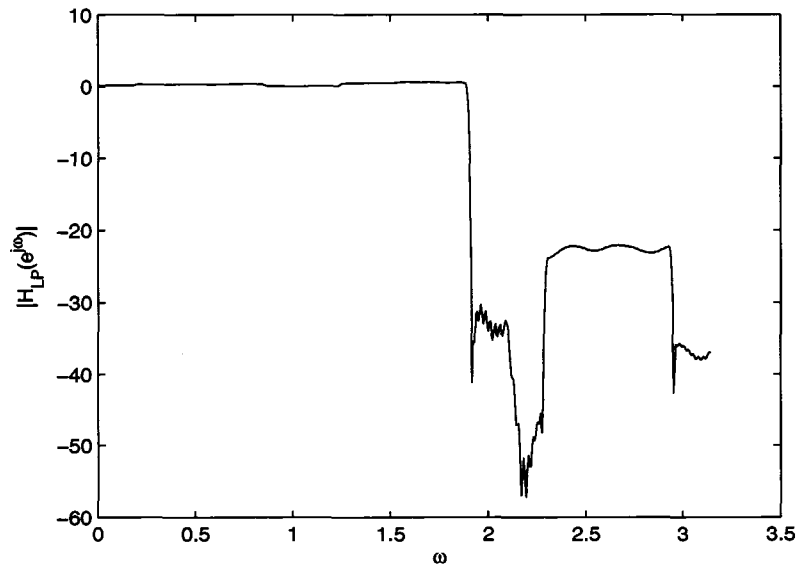


Figure 3.8: Lowpass CSD FRM FIR digital filter before GA optimization.

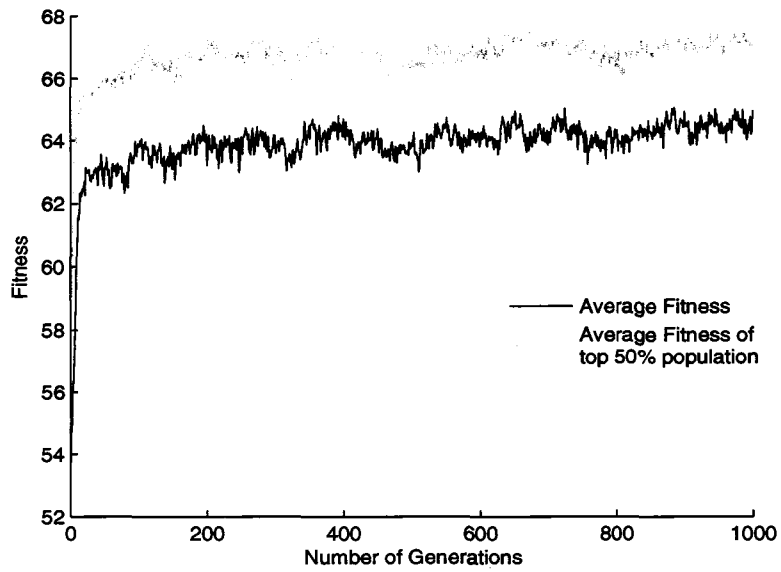


Figure 3.9: Fitness evolution for lowpass CSD FRM FIR digital filter.

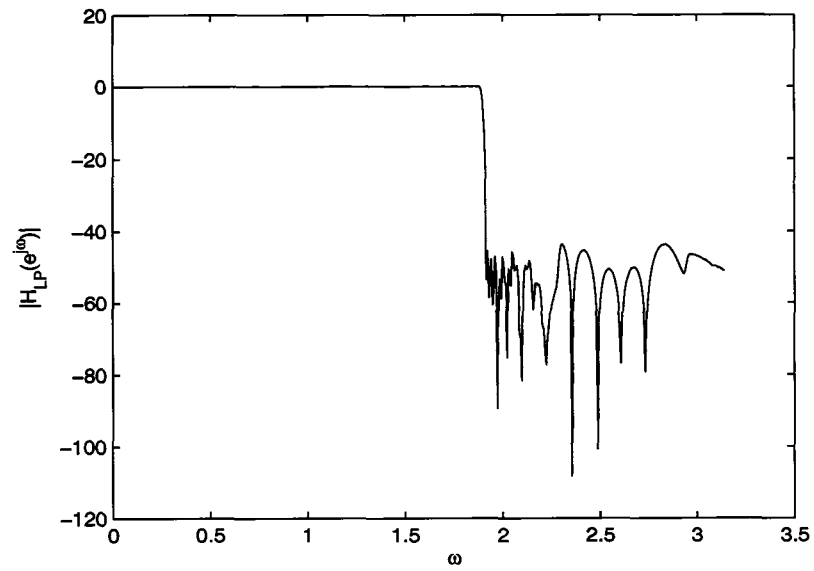


Figure 3.10: Lowpass CSD FRM FIR digital filter after GA optimization.

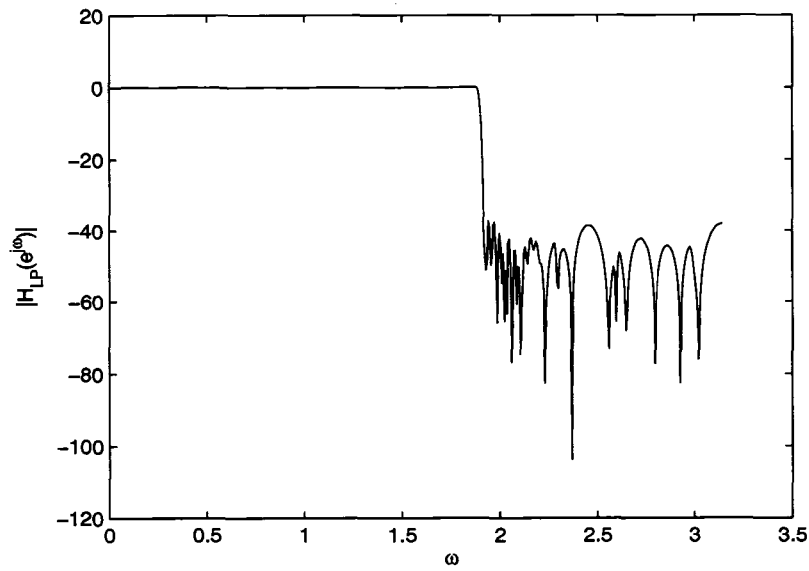


Figure 3.11: Lowpass DBSN FRM FIR Digital Filter before GA optimization.

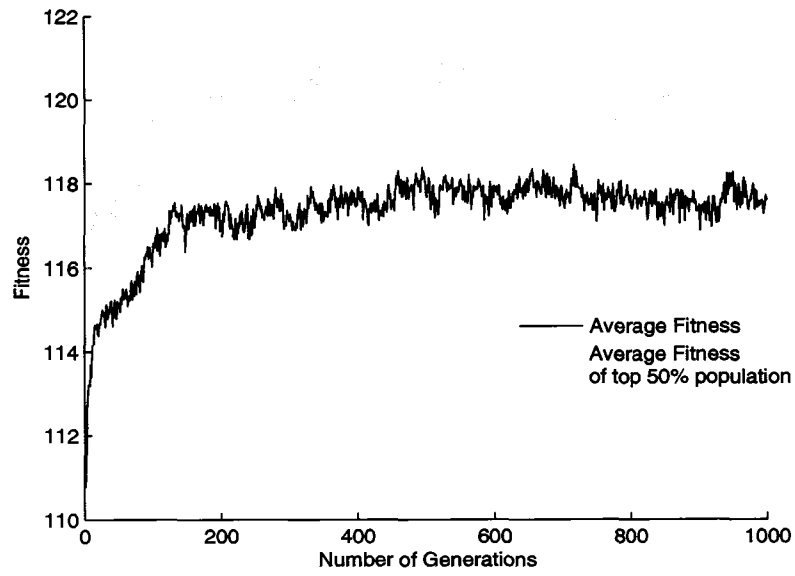


Figure 3.12: Fitness evolution for lowpass DBNS FRM FIR digital filter.

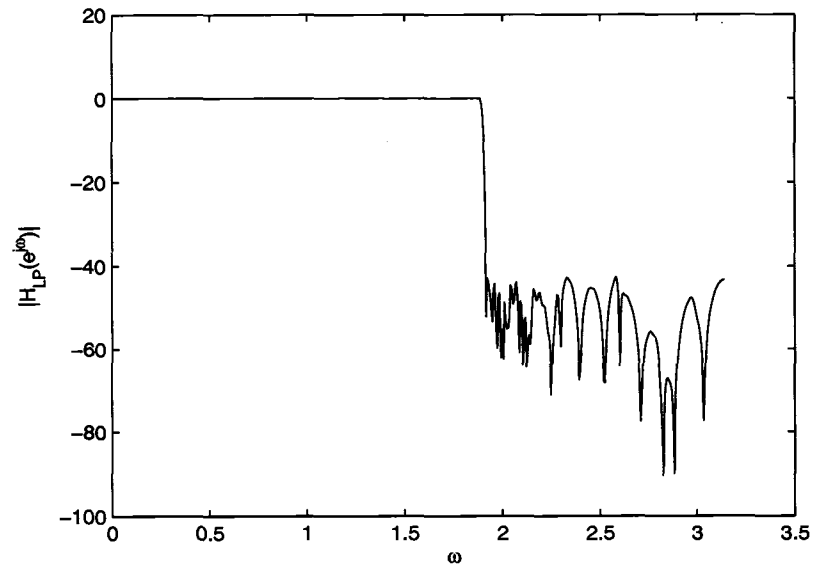


Figure 3.13: Lowpass DBNS FRM FIR digital filter after GA optimization.

3.5.2 Design of bandpass FRM FIR digital filters

Bandpass FRM FIR digital filters can be designed in much the same as the corresponding lowpass FRM FIR digital filters except that $H_{ma}(z)$ and $H_{mb}(z)$ become bandpass masking digital sub-filters. As stated before the design of this bandpass FRM FIR digital filter is limited by the interpolation factor M which causes the lower and upper transition bands to always have equal widths. In a later chapter it will be shown that in order to realize a bandpass (or a bandstop for that matter) FRM FIR digital filter with arbitrary lower and upper transition bandwidths, one must design the filter in terms of a cascade (or parallel) architecture consisting of lowpass and highpass FRM FIR digital filters. The constituent lowpass and highpass FRM filters are in turn designed to have different interpolation factors M in order to obtain unequal lower and upper transition bandwidths.

Let us consider the design of a FRM FIR bandpass digital filter satisfying the following magnitude response specifications over the CSD/DBNS multiplier coefficient spaces.

Passband region	$0.3\pi \leq \omega \leq 0.7\pi$	
Lower stopband region	$0 \leq \omega \leq 0.29\pi$	
Upper stopband region	$0.71\pi \leq \omega \leq \pi$	(3.10)
Maximum passband ripple	± 0.1 dB	
Minimum stopband attenuation	40 dB	

An initial approximation for the interpolation factor M is again calculated as 7 from Eqn. 2.13. A better approximation for M is obtained from Table 3.8 with $M = 8$, yielding $H_a(z)$, $H_{ma}(z)$ and $H_{mb}(z)$ of lengths 64, 32 and 56, respectively.

Tables 3.9 and 3.10 show the derived design specifications for the digital sub-filters $H_a(z)$, $H_{ma}(z)$ and $H_{mb}(z)$. By using the Parks-McClellan approach, the digital sub-filters $H_a(z)$, $H_{ma}(z)$ and $H_{mb}(z)$ can be designed to have magnitude frequency responses as shown in Figs. 3.14 to 3.19. Fig. 3.20 shows the magnitude frequency response of the overall infinite-precision bandpass FRM FIR digital filter $H_{BP}(z)$.

Table 3.8: Filter Lengths for Bandpass FRM FIR Digital Filter for Various Values of M

M	H_a	H_{ma}	H_{mb}	Total Length
2	254	10	6	270
3	168	6	66	240
4	126	56	10	192
5	102	24	26	152
6	84	20	66	170
7	72	272	18	362
8	64	32	56	152
9	56	34	66	156
10	50	506	26	582
11	46	36	114	196
12	42	56	66	164

Table 3.9: Bandedge Frequencies associated with $H_a(z)$, $H_b(z)$, $H_{ma}(z)$ and $H_{mb}(z)$ Digital Sub-Filters for the Bandpass FRM FIR Digital Filter Case

Sub-filter	Passband Edge Frequencies	Stopband Edge Frequencies
$H_a(e^{j\omega})$	0.32π	0.4π
$H_b(e^{j\omega})$	0.4π	0.32π
$H_{ma}(e^{j\omega})$	0.45π and 0.55π	0.29π and 0.71π
$H_{mb}(e^{j\omega})$	0.3π and 0.7π	0.21π and 0.79π

3.5.2.1 GA optimization of bandpass CSD FRM FIR digital filters

The design parameters for the genetic optimization of the bandpass CSD FRM FIR digital filter are shown in Table 3.11. Based on the above infinite-precision bandpass FRM FIR digital filter, the corresponding seed CSD FRM digital filter is obtained to have a magnitude frequency response as shown in Fig. 3.21. Consequently, the resulting seed digital filter violates the magnitude response specifications by almost 0.1 dB in the passband region and by almost 11 dB in the stopband region (c.f. Table 3.12). The progress of the proposed GA from one generation to the next is as shown in Fig. 3.22. After 1000 generations, the GA optimization converges to the optimal bandpass FRM FIR digital filter having a magnitude frequency response as shown in Fig. 3.23.

Table 3.10: Passband Ripples and Stopband Attenuations Associated with $H_a(z)$, $H_{ma}(z)$ and $H_{mb}(z)$ Digital Sub-filters for the Bandpass FRM FIR Digital Filter Case

Sub-filter	Passband Ripple	Stopband Attenuation
$H_a(e^{j\omega})$	0.085 dB	-46 dB
$H_b(e^{j\omega})$	0.085 dB	-46 dB
$H_{ma}(e^{j\omega})$	0.085 dB	-46 dB
$H_{mb}(e^{j\omega})$	0.085 dB	-46 dB

Table 3.11: Design Parameters for GA Optimization of Bandpass CSD FRM FIR Digital Filter

Design Step	Design Parameters
1	$M = 8, N_a = 64, N_{ma} = 32, N_{mb} = 56$
2	$w = 3 \text{ bits}, W_I = 3 \text{ bits}, W_F = 14 \text{ bits}, B = 12 \text{ bits}$
3	$p_F = 0.8, N = 500$
4	$C = 30$
5	$N_{mating} = 150, Z = 0.8$
6	$N_p = 235$
7	$p_M = 0.03$

Table 3.12: Bandpass CSD FRM FIR Digital Filter Magnitude Responses before and after GA Optimization

Multiplier Coefficient Values	Passband Ripple	Lower Stopband Attenuation	Upper Stopband Attenuation
Infinite-Precision	0.03 dB	-50 dB	dB
CSD before GA optimization	0.2 dB	-28.9 dB	dB
CSD after GA Optimization	0.045 dB	-41 dB	-41.9 dB

3.5.2.2 GA optimization of bandpass DBNS FRM FIR digital filters

Table 3.13 shows the design parameters for the GA optimization of the bandpass DBNS FRM FIR digital filter. The corresponding seed DBNS FRM FIR digital filter is obtained to have a magnitude frequency response as shown in Fig. 3.24, violating the magnitude response specifications by almost 0.1 dB in the passband, and by almost 2 dB in the stopband region (c.f. Table 3.14). Fig. 3.25 shows the the progress of the proposed GA from one generation to the next. After 976 generations, the GA optimization converges to the optimal bandpass FRM FIR digital filter having a magnitude frequency response as shown in Fig. 3.26.

Table 3.13: Design Parameters for GA Optimization of Bandpass DBNS FRM FIR Digital Filter

Design Step	Design Parameters
1	$M = 8, N_a = 64, N_{ma} = 32, N_{mb} = 56$
22	$n = 96, m = 69, B = 12 \text{ bits}$
3	$p_F = 0.8, N = 500$
4	$\omega_p = 0.6\pi, \omega_s = 0.61\pi, k = \frac{1.15}{0.85}, C = 30$
5	$N_{main} = 150, Z = 0.8$
6	$N_p = 235$
7	$p_M = 0.03$

Table 3.14: Bandpass DBNS FRM FIR Digital Filter Magnitude Responses before and after GA Optimization

Multiplier Coefficient Values	Passband Ripple	Lower Stopband Attenuation	Upper Stopband Attenuation
Infinite-Precision	0.03 dB	-50 dB	dB
DBNS before GA optimization	0.18 dB	-38.1 dB	-38.7 dB
DBNS after GA Optimization	0.038 dB	-47.2 dB	-47.2 dB

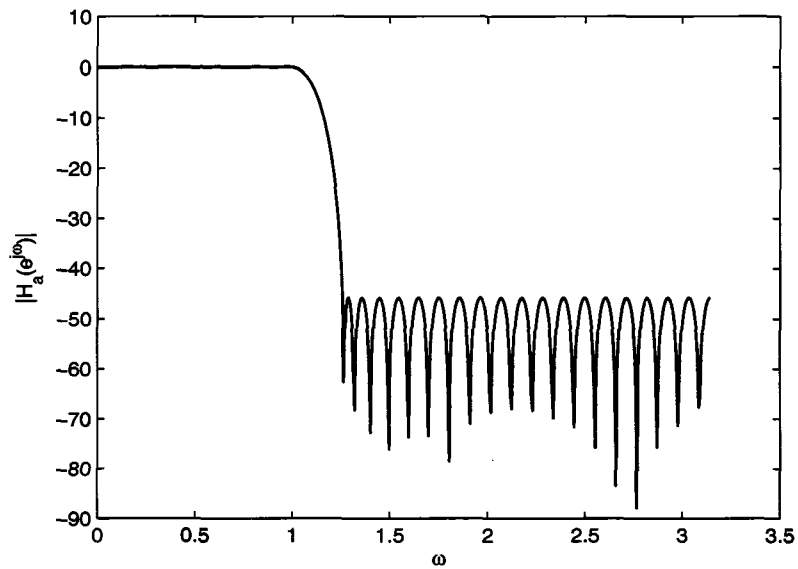


Figure 3.14: Magnitude response of digital sub-filter $H_a(z)$ for the bandpass FRM FIR digital filter case.

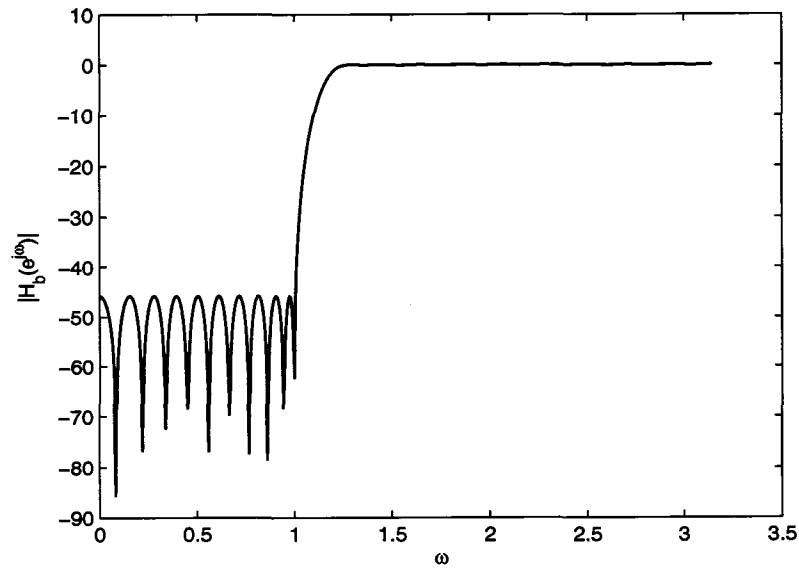


Figure 3.15: Magnitude Response of complimentary digital sub-filter $H_b(z)$ for the bandpass FRM FIR digital filter case.

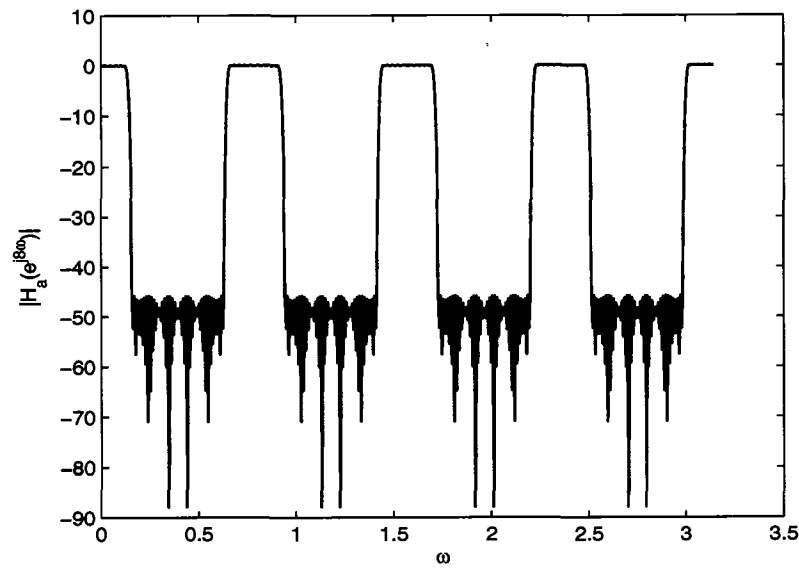


Figure 3.16: Magnitude response of M -interpolated version of digital sub-filter $H_a(z)$ for the bandpass FRM FIR digital filter case.

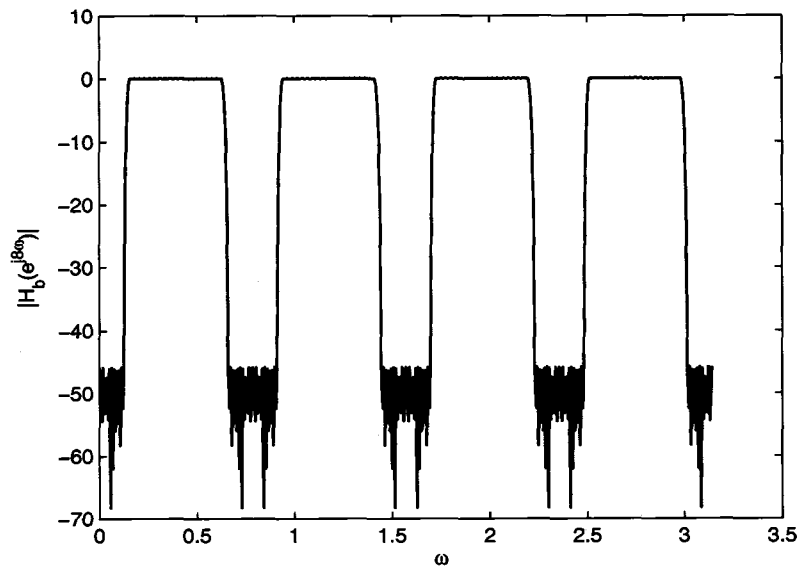


Figure 3.17: Magnitude response of M -interpolated version of complementary digital sub-filter $H_b(z)$ for the bandpass FRM FIR digital filter case.

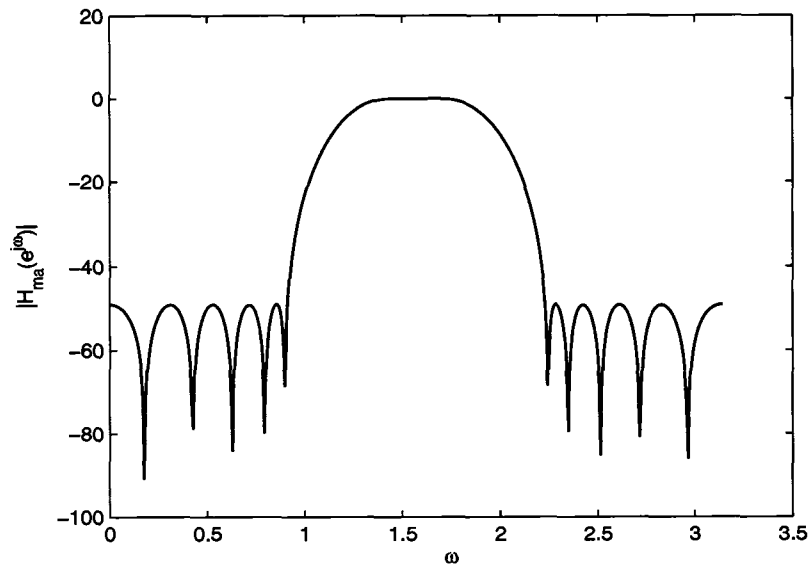


Figure 3.18: Magnitude response of masking digital sub-filter $H_{ma}(z)$ for the bandpass FRM FIR digital filter case.

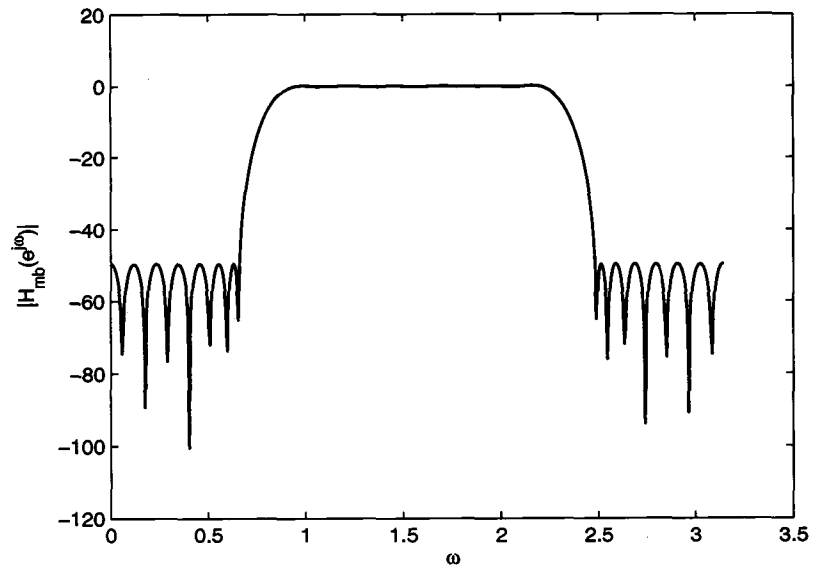


Figure 3.19: Magnitude response of masking digital sub-filter $H_{mb}(z)$ for the bandpass FRM FIR digital filter case.

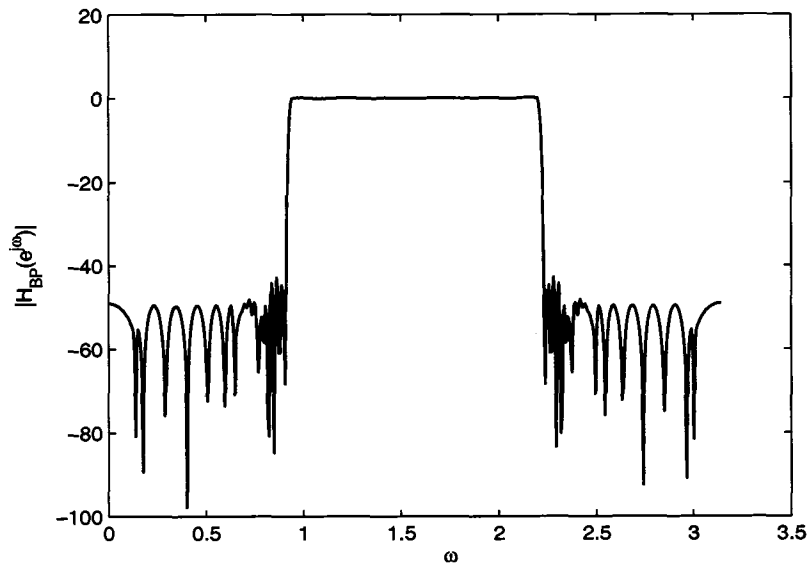


Figure 3.20: Infinite-precision bandpass FRM FIR digital filter $H_{BP}(z)$.

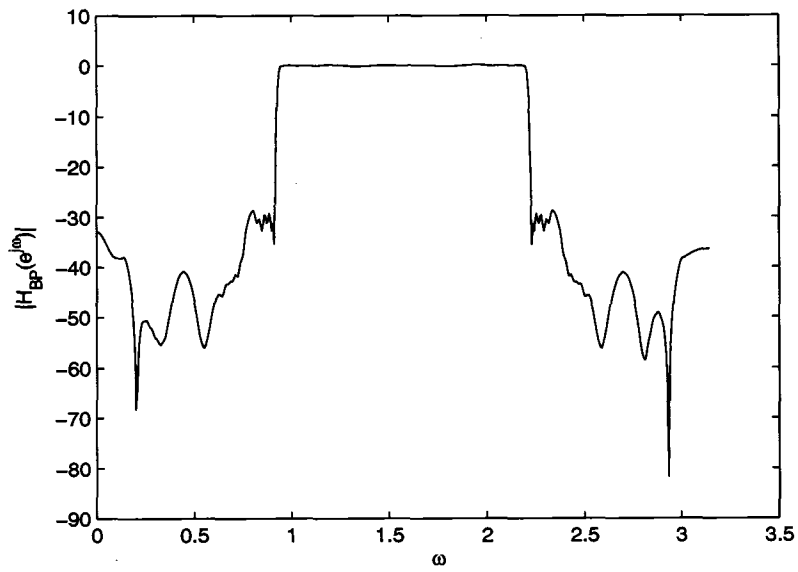


Figure 3.21: Bandpass CSD FRM FIR digital filter before GA optimization.

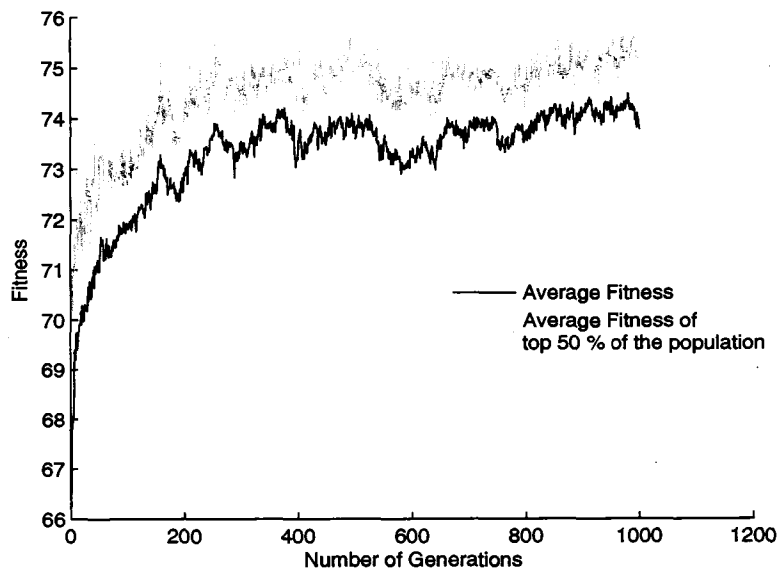


Figure 3.22: Fitness evolution for bandpass CSD FRM FIR digital filter.

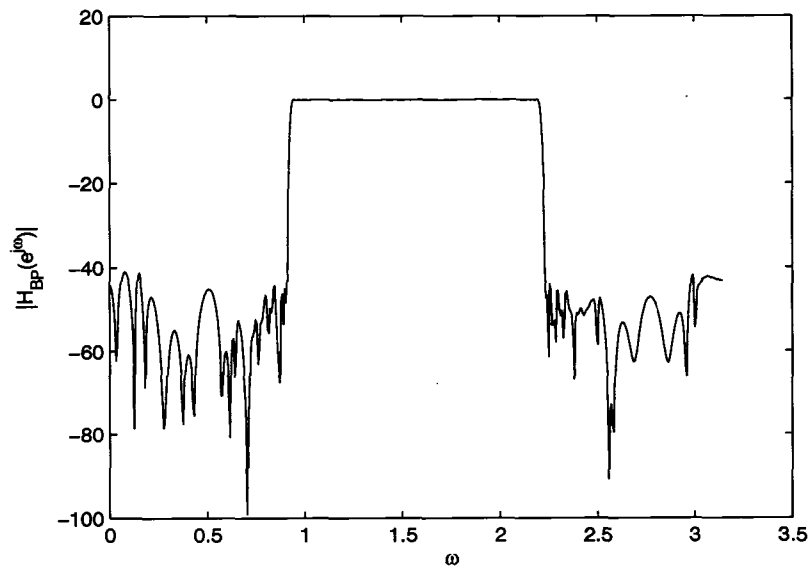


Figure 3.23: Bandpass CSD FRM FIR digital filter after GA optimization.

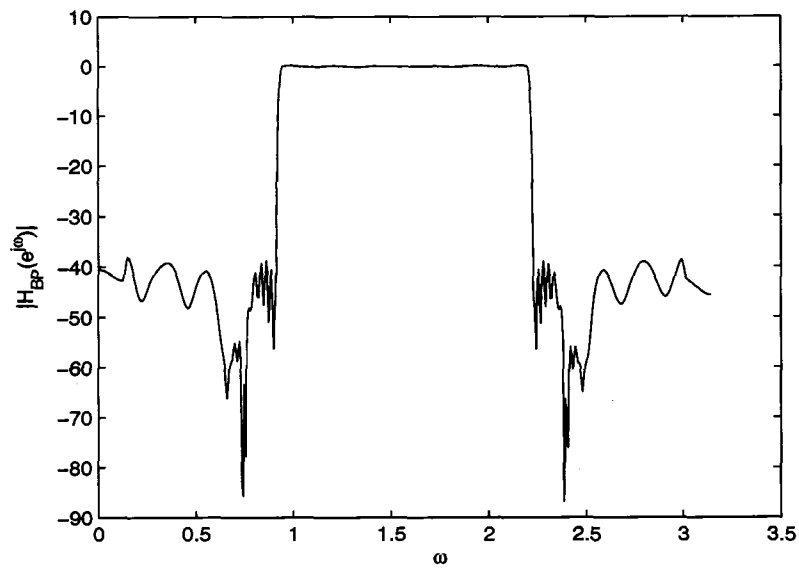


Figure 3.24: Bandpass DBNS FRM digital filter before GA optimization.

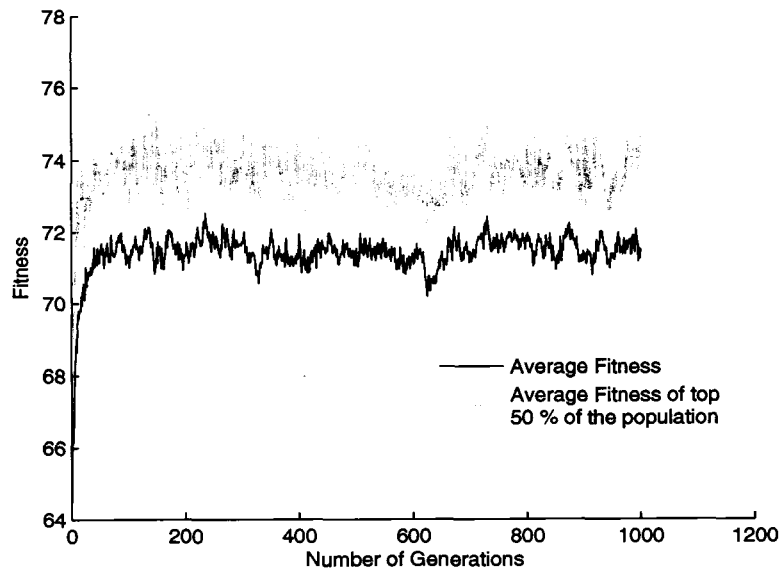


Figure 3.25: Fitness evolution for bandpass DBNS FRM FIR digital filter.

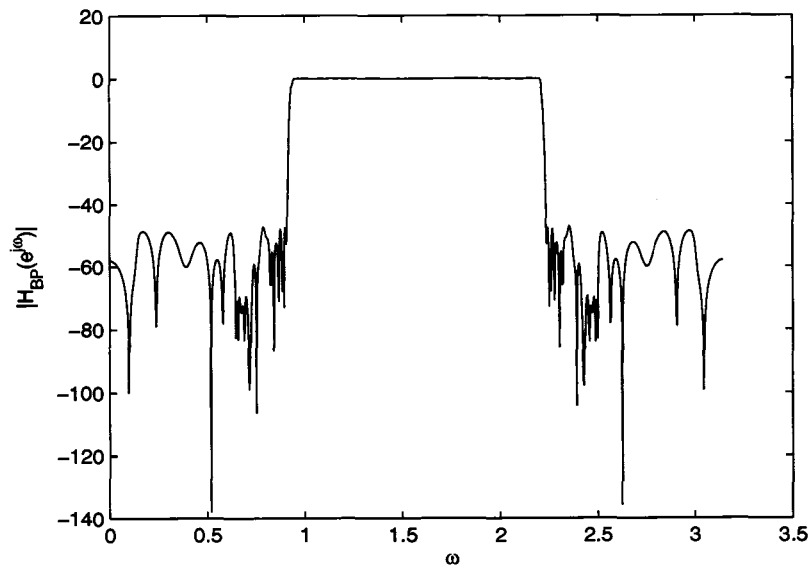


Figure 3.26: Bandpass DBNS FRM FIR digital filter after GA optimization.

Chapter 4

Design and Optimization of Finite-Precision FRM FIR Digital Filters Using Diversity Controlled Genetic Algorithms

This chapter is concerned with the application of an improved genetic algorithm called diversity controlled genetic algorithm to the design and optimization of FRM FIR digital filters. This improved GA provides speed of convergence advantages over the conventional GAs. Before proceeding with a discussion on DCGAs, it is imperative to modify the existing conventional FRM approach to allow the design of bandpass and bandstop FRM FIR digital filters with arbitrary lower and upper transition bandwidths.

4.1 A Modified Technique for the Design of Bandpass and Bandstop FRM FIR Digital Filters with Arbitrary Lower and Upper Transition Bandwidths

In general, it is possible to extend the conventional FRM approach (c.f. Chapter 2) for the design of bandpass and bandstop FRM FIR digital filters. However, the resulting FRM digital filters are constrained to have identical lower and upper transition bandwidths. In [21], this restriction was relaxed by realizing the bandstop FRM FIR digital filter as a parallel combination of a corresponding pair of lowpass and highpass FIR digital filters. The latter lowpass and highpass FRM digital filters

were obtained using a variation of the conventional FRM approach. This section presents a similar technique for the design of the corresponding bandpass FRM FIR digital filter having equal or unequal lower and upper transition bandwidths.

4.1.1 Design of Bandpass FRM FIR Digital Filters with Arbitrary Lower and Upper Transition Bandwidth

Let the desired bandpass FRM FIR digital filter $H_{BP}(z)$ have a lower transition bandwidth of Δ_l and an upper transition bandwidth of Δ_u . In order to permit $\Delta_u \neq \Delta_l$, $H_{BP}(z)$ is realized as a cascade combination of a pair of lowpass and highpass FRM FIR digital filters, so that

$$H_{BP}(z) = H_{LP}(z)H_{HP}(z), \quad (4.1)$$

where $H_{LP}(z)$ represents a lowpass and $H_{HP}(z)$ represents a highpass FRM FIR digital filter. In this way, $H_{LP}(z)$ can be obtained by rearranging Eqn. 2.4 as [21]

$$H_{LP}(z) = z^{\frac{M_{LP}(N_{al}-1)}{2}} H_{mbl}(z) + H_{dl}(z) H_{al}(z^{M_{LP}}) \quad (4.2)$$

where M_{LP} represents the interpolation factor of the constituent lowpass FRM FIR digital filter and

$$H_{dl}(z) = H_{mal}(z) - H_{mbl}(z). \quad (4.3)$$

In Eqn. 4.2, $H_{al}(z^{M_{LP}})$ represents the M_{LP} -interpolated version of the band-edge shaping digital sub-filter $H_{al}(z)$ of length N_{al} , and $H_{mal}(z)$ and $H_{mbl}(z)$ represent the corresponding lowpass masking digital sub-filters.

The highpass FRM FIR digital filter $H_{HP}(z)$ in Eqn. 4.1 can be represented in much the same way as [21]

$$H_{HP}(z) = z^{-M_{HP}(N_{ah}-1)/2} H_{mbh}(z) + H_{dh}(z) H_{ah}(z^{M_{HP}}) \quad (4.4)$$

where M_{HP} represents the interpolation factor of the constituent highpass FRM FIR digital filter and

$$H_{dh}(z) = H_{mah}(z) - H_{mbh}(z). \quad (4.5)$$

In Eqn. 4.4, $H_{ah}(z^{M_{HP}})$ represents the M_{HP} -interpolated version of the bandedge shaping digital sub-filter $H_{ah}(z)$ of length N_{ah} , and $H_{mah}(z)$ and $H_{mbh}(z)$ represent

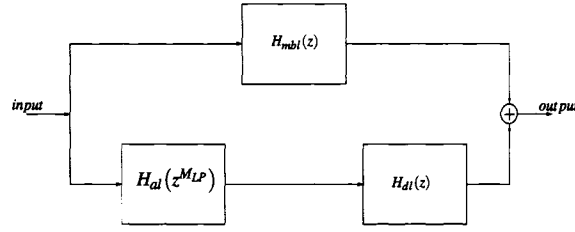


Figure 4.1: Alternative realization of FRM approach for lowpass filters [21].

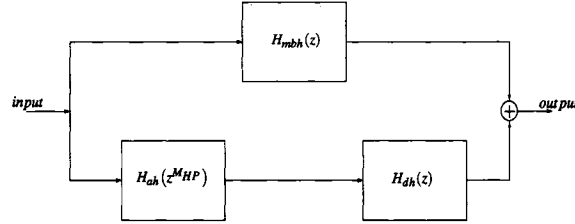


Figure 4.2: Alternative realization of FRM approach for highpass filters [21].

the corresponding highpass masking digital sub-filters. The lower (upper) transition bandwidth $\Delta_{l(u)}$ is governed by the constituent transition bandwidth of the highpass (lowpass) FRM FIR digital filter.

The realizations for $H_{LP}(z)$, $H_{HP}(z)$ and the desired $H_{BP}(z)$ are as shown in Figs. 4.1, 4.2 and 4.3.

4.1.2 Design of FRM Bandstop Digital Filters with Arbitrary Lower and Upper Transition Bandwidth

Bandstop FRM FIR digital filters may be designed in much the same way as bandpass FRM FIR digital filters [21]. The overall FRM bandstop FRM FIR digital filter $H_{BS}(z)$ can be represented by the relation (c.f. Fig. 4.4),

$$H_{BS}(z) = H_{LP}(z) + H_{HP}(z). \quad (4.6)$$

where $H_{LP}(z)$ and $H_{HP}(z)$ are given by Eqns. 4.2 and 4.4 respectively. In the bandstop FRM FIR digital filter, the lower transition bandwidth Δ_l is governed by the constituent lowpass FRM FIR digital filter whereas the upper transition bandwidth Δ_u is governed by the corresponding highpass FRM FIR digital filter. As in the bandpass FRM FIR digital filter case, one must design for different M_{LP} and M_{HP} to obtain $\Delta_l \neq \Delta_h$.

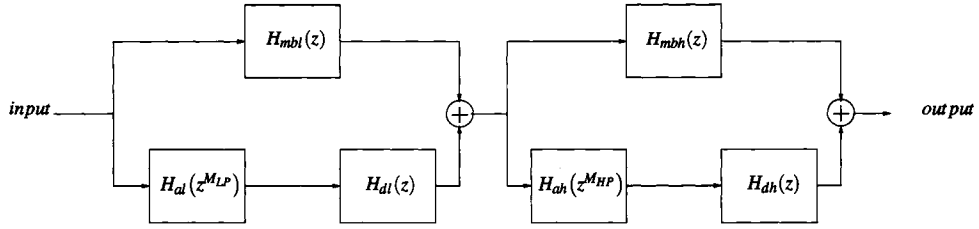


Figure 4.3: Synthesis structure for bandpass FRM FIR digital filters.

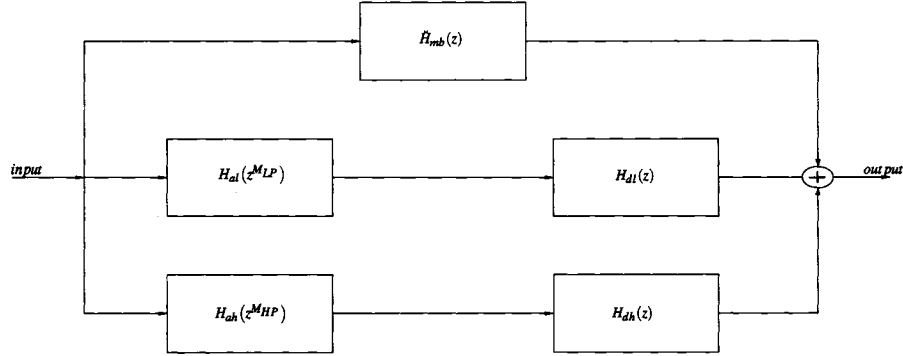


Figure 4.4: Synthesis structure for bandstop FRM FIR digital filters [21].

The constituent digital sub-filters $H_{al(h)}(z)$, $H_{dl(h)}(z)$ and $H_{mbl(h)}(z)$ can be designed in infinite-precision using the Parks-McClellan approach.

4.2 DCGA Optimization: An Overview

Despite the fact that GAs are excellent choices for discrete optimization problems, they do not search the solution space robustly due to lack of mechanisms through which entrapment at *local optima* could be successfully avoided. This leads to *premature convergence* which is usually the result of a quick decrease in population diversity.

To circumvent the above problem, Shimodaira [23] developed DCGA where, the search is made effective by keeping track of current chromosomes which have low-fitness values but which have the potential of evolving to individuals with high fitness values in future generations. In addition, the diversity of a population pool is controlled externally by removing duplicate chromosomes from the current population pool. In this way, chromosomes for the next-generation population pool are

selected probabilistically on the basis of their distances from the current chromosome having the highest fitness value. However, the latter chromosome itself is left intact from one generation to the next as it may indeed be in the vicinity of the global optimum. DCGA begins with an initial population of N chromosomes and can be summarized in the following steps [23].

- Let the population pool be denoted by $P(t - 1)$ where, t represents the current generation number (with $t - 1$ representing the previous generation). A seed chromosome is constructed by using the design variables specific to the optimization problem at hand. The remaining members of the initial population pool are constructed by randomly complementing bits in the seed chromosome.
- To select parents for reproduction, each chromosome in $P(t - 1)$ is chosen only once as a parent. In this way, $N/2$ parent pairs are formed to undergo the genetic operations of crossover and mutation. Two offspring are produced per parent pair, resulting in N offspring chromosomes. The resulting N offspring chromosomes are represented by a population pool $C(t)$.
- The chromosomes in $P(t - 1)$ and $C(t)$ are combined to form a large population pool $M(t)$ of size $2N$. The chromosomes in $M(t)$ are evaluated by using a fitness function, where the corresponding fitness value signifies how closely the design objectives and/or constraints are satisfied.
- In order to form the next-generation population pool, each chromosome is selected on the basis of a probabilistic selection scheme. The following sub-steps are performed to form the next-generation population pool:
 1. All chromosomes which have the same exact bit representation are replaced by one chromosome in $M(t)$ in order to avoid premature convergence in later generations. This maintains diversity in the population pool.

2. To form the next generation population pool $P(t)$, the chromosome with the highest fitness value in $P(t - 1)$ is selected at the outset. The remaining $N - 1$ chromosomes are selected from $M(t)$ by using a *cross-generational probabilistic survival scheme (CPSS)*. In CPSS, the probability of selection is given by

$$p_s = [(1 - c) * (h/L) + c]^\alpha, \quad (4.7)$$

where h represents the hamming distance between a chromosome and the chromosome with the highest fitness value in the population pool, where L represents the chromosome length, and where c and α represent control parameters with c representing the shape coefficient and α representing the exponent. The control parameters c and α are used to maintain an external control over the population diversity. In order to avoid premature convergence on the one hand, and to obtain an optimal solution as rapidly as possible on the other, an appropriate level of diversity must be maintained in the population pool. This is achieved by striking a balance between the number of candidate chromosomes which are quite similar or quite different to the chromosome with the highest fitness value. As there are no analytical solutions available for c and α , empirical investigations must be undertaken to find their appropriate values. In particular, if the fitness function has a few local optima only, then by using a high value of c and/or small value of α , one can achieve a rapid convergence to an optimal solution. On the other hand, when the fitness function is multimodal, lower values of c and/or higher values of α can be chosen to increase the probability of selecting chromosomes which are different from the chromosome with the highest fitness value. However, it should

be pointed out that the speed of convergence to an optimal solution is, in general, a function of both c and α values. This implies that one has to empirically find a range of values for c and α in order to achieve rapid convergence [23].

3. A uniform random number is generated between 0 and 1, and if p_s is greater than this random number, then the candidate chromosome is selected for the next-generation population pool up to a total of N chromosomes.

- The above algorithm is repeated until an appropriate termination condition is reached.

4.3 The Proposed DCGA Optimization of FRM FIR Digital Filters

The proposed DCGA optimization begins in the much the same way as the conventional GA discussed in Section 3.4 where Parks-McClellan approach is employed to design an initial infinite-precision FRM digital filter which satisfies the given design specifications. The design of bandpass and bandstop FRM FIR digital filters is carried out in terms of the corresponding lowpass and highpass FRM digital filters $H_{LP}(z)$ and $H_{HP}(z)$, where $H_{LP}(z)$ and $H_{HP}(z)$ are themselves designed in terms of the digital sub-filters $H_{al(h)}(z)$, $H_{mal(h)}(z)$ and $H_{mbl(h)}(z)$ ¹. In order to obtain an initial seed CSD/DBNS FRM FIR digital filter, a pair of indexed CSD and DBNS LUTs are constructed and the infinite-precision multiplier coefficient values are quantized to their nearest CSD/DBNS counterparts. The indices of the CSD/DBNS multiplier coefficients are then concatenated in binary format to obtain the seed CSD/DBNS FRM FIR digital filter chromosome. A population pool of N chromosomes is generated by randomly complementing bits in this seed chromosome.

The remaining steps in the proposed DCGA optimization are as follows:

¹The proposed DCGA can be easily modified to begin with a CSD/DBNS FRM FIR digital filter at the outset.

4.3.1 Genetic Operations

The size of the population pool is initially increased from N to $2 \times N$ by using the following genetic operations:

- *Crossover operations*: In the population pool of N chromosomes, $N/2$ pairs of chromosomes are selected as parents so that no chromosome becomes a parent more than once. These chromosome pairs undergo two-point crossover operations, reproducing two offspring chromosomes for each pair. The offspring are then combined with the initial population pool of N chromosomes, enlarging the current population pool to $2 \times N$ chromosomes.
- *Mutation operations*: Each member in the population pool of $2 \times N$ chromosomes undergoes mutation operations in accordance with the probabilistic relationship $p_M \times 0.5^{B+1-b}$ to enhance diversity, where p_M is the probability of mutation.
- *Fitness evaluation*: The fitness value of each of the $2 \times N$ FRM digital filter chromosomes is evaluated in accordance with

$$fitness_1 = -20 \log [\max \{\epsilon_p, \epsilon_s\}] + C, \quad (4.8)$$

where

$$\epsilon_p = \underbrace{\max}_{\omega \in \Omega_p} [W_p |H_{LP(HP)}(e^{j\omega}) - 1|] \quad (4.9)$$

with Ω_p representing the passband frequency region(s), and where

$$\epsilon_s = \underbrace{\max}_{\omega \in \Omega_s} [W_s |H_{LP(HP)}(e^{j\omega})|] \quad (4.10)$$

with Ω_s representing the stopband frequency region(s). Here, W_p and W_s are passband and stopband weighting factors, and C is a constant chosen so as to render the $fitness_1$ value in Eqn. 4.8 non-negative. Unfortunately, even the most-fit chromosome inferred by $fitness_1$ in Eqn. 4.8 may not necessarily satisfy all the magnitude response specifications.

This is mainly due to the over optimization of the magnitude response over certain frequency points which occurs at the expense of drastic under optimization of the magnitude response over other frequency points. In order to circumvent this problem, $fitness_1$ in Eqn. 4.8 is modified through the addition of a penalty function in accordance with

$$fitness_2 = fitness_1 - \beta \times penalty_{\omega \in \{\text{over-optimized frequency points}\}}, \quad (4.11)$$

where β is a weighting factor. The $penalty$ component in Eqn. 4.11 takes into account the frequency points where the response is over optimized by rendering the respective chromosome less fit. This is facilitated by penalizing all the stopband frequency points that fall within a lower bound T_l and upper bound T_u in the stopband, where the limits T_l and T_u are selected to be less than the specified stopband attenuation. The penalty function in Eqn. 4.11 is given by

$$penalty = \sum_{i=1}^P \frac{|H_{LP(HP)}(e^{j\omega})|_{\omega \in \hat{\Omega}_s}}{P} \quad (4.12)$$

where $\hat{\Omega}_s$ represents the stopband magnitude response points which fall in the range T_l and T_u , and where P represents the number of such magnitude response points. At the completion of fitness evaluation, the chromosomes are ranked and duplicate chromosomes are eliminated to avoid affecting diversity adversely. In the event that the resulting population pool does not contain a chromosome that satisfies the given design magnitude response specifications, the DCGA optimization proceeds to generate the next-generation population pool. Otherwise, it terminates with the highest ranked chromosome declared as optimum.

4.3.2 Generation of the next-generation population pool

The next generation population pool is formed by using CPSS in Eqn. 4.7, where the parameter L is given by

$$L = (N_{al(h)} + N_{mal(h)} + N_{mbl(h)}) \times B, \quad (4.13)$$

and where $N_{al(h)}$, $N_{mal(h)}$ and $N_{mbl(h)}$ are the number of multiplier coefficients in the sub-filters $H_{al(h)}(z)$, $H_{mal(h)}(z)$ and $H_{mbl(h)}(z)$, respectively. The selected chromosome is chosen as a candidate for the next generation population pool if p_s is greater than a locally generated uniform random number. This process is repeated until N chromosomes are identified for the next generation population pool.

4.4 Application Examples

In this section, the proposed DCGA is applied to the design and optimization of a lowpass FRM FIR digital filter and a pair of bandpass FRM FIR digital filters, one having equal and the other having arbitrary lower and upper transition bandwidths Δ_l and Δ_h . Empirical investigations are also undertaken to identify a range for the DCGA control parameters c and α .

4.4.1 Design of lowpass FRM FIR digital filters

Consider the design and optimization of the benchmark lowpass FRM FIR digital filter [11] over the CSD/DBNS multiplier coefficient spaces satisfying the following magnitude response specifications

Passband region	$0 \leq \omega \leq 0.6\pi$	(4.14)
Stopband region	$0.61\pi \leq \omega \leq \pi$	
Maximum passband ripple	± 0.1 dB	
Minimum stopband attenuation	-40 dB.	

By using Eqn. 2.13, the first approximation to the optimum value of the interpolation factor M is obtained as 7. Table 4.1 shows the overall lowpass FRM FIR digital filter length as a function of M in the vicinity of the first approximation. Through inspection of Table 4.1, the optimum value of M is found to be 6, yielding digital sub-filters $H_{al}(z)$, $H_{mal}(z)$ and $H_{mbl}(z)$ of lengths 84, 24 and 42, respectively.

Having determined the above digital sub-filter lengths, their bandedge frequencies can be determined as given in Table 4.2 using the design equations given in Section 2.3.2 [11, 21]. Moreover, the corresponding maximum passband ripple and minimum stopband attenuations are set as given in Table 4.3. As before, the values

of the passband ripples and stopband attenuations are set to 85% of their budgetted values as given in the design specifications (c.f. Eqn 4.14).

By using the Parks-McClellan approach together with the design specifications in Tables 4.2 and 4.3, the initial infinite-precision digital sub-filters $H_{al}(z)$, $H_{mal}(z)$, and $H_{mbl}(z)$ are designed to have the magnitude frequency responses as shown in Figs. 4.5 to 4.9, and the corresponding overall infinite-precision lowpass FRM FIR digital filter is designed to have a magnitude frequency response as shown in Fig. 4.10.

Table 4.1: Filter Lengths for a Lowpass FRM FIR Digital Filter for Various Values of M

M_{LP}	H_a	H_{ma}	H_{mb}	Total Length
2	254	24	2	280
3	168	8	42	218
4	126	16	24	166
5	102	506	12	620
6	84	24	42	150
7	72	22	76	170

Table 4.2: Bandedge Frequencies Associated with $H_{al}(z)$, $H_{mal}(z)$ and $H_{mbl}(z)$ Digital Sub-Filters for the Lowpass FRM FIR Digital Filter Case

Sub-filter	Passband Edge Frequency	Stopband Edge Frequency
$H_{al}(e^{j\omega})$	0.34π	0.4π
$H_{mal}(e^{j\omega})$	0.4π	0.61π
$H_{mbl}(e^{j\omega})$	0.6π	0.72π

Table 4.3: Passband Ripples and Stopband Attenuations for Digital Sub-filters $H_{al}(z)$, $H_{mal}(z)$ and $H_{mbl}(z)$ for the Lowpass FRM FIR Digital Filter Case

Sub-filter	Passband Ripple	Stopband Attenuation
$H_{al}(e^{j\omega})$	0.085 dB	-46 dB
$H_{mal}(e^{j\omega})$	0.085 dB	-46 dB
$H_{mbl}(e^{j\omega})$	0.085 dB	-46 dB

4.4.1.1 DCGA optimization of lowpass CSD FRM FIR digital filters

The design parameters for the proposed DCGA optimization of the lowpass CSD FRM FIR digital filter are as given in Table 4.4. Fig. 4.11 shows the magnitude

response of the seed lowpass FRM FIR digital filter after the the infinite-precision multiplier coefficient values are quantized to their CSD counterparts. The resulting magnitude response violates the design specifications by almost 0.5 dB in the pass-band, and by almost 18 dB in the stop-band region (c.f. Table 4.5).

Before proceeding with the application of the proposed DCGA to the optimization of the seed lowpass CSD FRM FIR digital filter, one must determine appropriate values for the control parameters c and α . Fig. 4.12 shows the convergence speed of the DCGA optimization for the parameter c ranging from 0.1 to 0.5 and parameter α ranging from 0.1 to 0.3. As can be observed, the fastest convergence speed is obtained for $c = 0.35$ and $\alpha = 0.1$ where the required optimum lowpass CSD FRM FIR digital filter is obtained within 61 generations. The magnitude frequency response of this lowpass CSD FRM FIR digital filter is as shown in Fig. 4.14. Fig. 4.13 shows the convergence speed for varying values of c averaged over the parameter α . It can be stated that, on average, one can obtain high convergence speeds for c ranging from 0.35 to 0.5.

Table 4.4: Design Parameters for DCGA Optimization of Lowpass CSD FRM FIR Digital Filters

Design Step	Design Parameters
1	$M_{LP} = 6, N_{al} = 84, N_{mal} = 24, N_{mbl} = 42$
2	$w = 3 \text{ bits}, W_I = 3 \text{ bits}, W_F = 14 \text{ bits}, B = 12 \text{ bits}$
3	$p_F = 0.8, N = 500$
4	$C = 30, W_p = 1.15, W_s = 0.85, \beta = 100, T_u = 0.0005, T_l = 0.008$
5	$L = 1800$

Table 4.5: Lowpass CSD FRM FIR Digital Filter Magnitude Responses before and after DCGA Optimization

Multiplier Coefficient Representation	Passband Ripple	Stopband Attenuation
Infinite-Precision	0.075 dB	-41 dB
CSD before DCGA optimization	0.65 dB	-22.05 dB
CSD after DCGA Optimization	0.08 dB	-40.4 dB

4.4.1.2 DCGA optimization of lowpass DBNS FRM FIR digital filters

In the case of the DCGA optimization of lowpass DBNS FRM FIR digital filter, the design parameters are as shown in Table 4.6. Fig. 4.15 shows the seed low-

pass FRM FIR digital filter after its infinite-precision multiplier coefficient values have been approximated to the nearest DBNS values. It can be observed that the magnitude response of the seed lowpass DBNS FRM digital filter violates the given design specifications by almost 0.04 dB in the passband, and by almost 3 dB in the stopband region (c.f. Table 4.7).

The fastest speed of convergence for the lowpass FRM FIR digital filter was obtained for parameter $c = 0.4$ and parameter $\alpha = 0.1$ as shown in Fig. 4.16. Fig. 4.17 shows the speed of convergence plotted against varying values of the parameter c and averaged over the parameter α . On average, higher convergence speeds were observed for values of c ranging from 0.25 to 0.5.

At $c = 0.4$ and $\alpha = 0.1$, the desired lowpass DBNS FRM FIR digital filter was obtained in 42 generations as shown in Fig. 4.18.

Table 4.6: Design Parameters for DCGA Optimization of Lowpass DBNS FRM FIR Digital Filters

Design Step	Design Parameters
1	$M = 6, N_a = 84, N_{ma} = 24, N_{mb} = 42$
2	$n = 96, m = 69, B = 12 \text{ bits}$
3	$p_F = 0.8, N = 500$
4	$C = 30, W_p = 1.15, W_s = 0.85, \beta = 100, T_u = 0.0005, T_l = 0.008$
5	$L = 1800$

Table 4.7: Lowpass DBNS FRM FIR Digital Filter Magnitude Responses before and after DCGA Optimization

Multiplier Coefficient Representation	Passband Ripple	Stopband Attenuation
Infinite-Precision	0.075 dB	-41 dB
DBNS before GA optimization	0.146 dB	-37.3 dB
DBNS after GA Optimization	0.08 dB	-40.98 dB

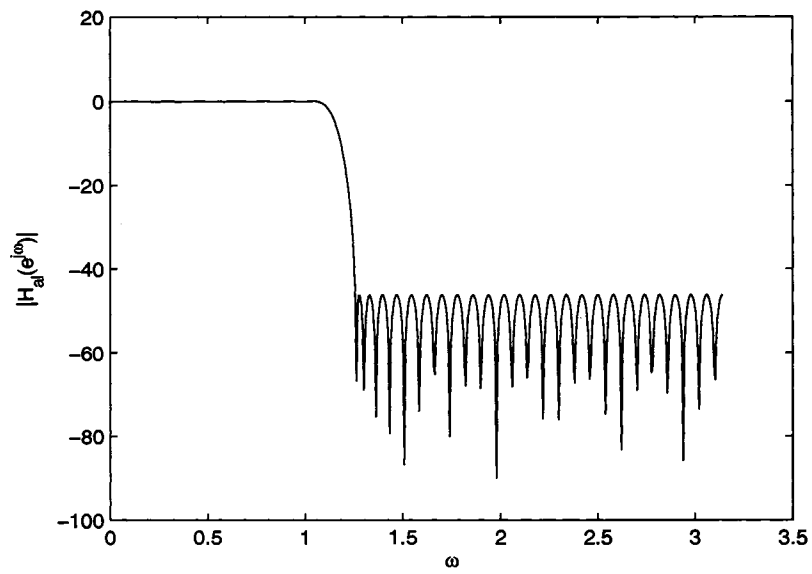


Figure 4.5: Magnitude response of digital sub-filter $H_{ai}(z)$ for lowpass FRM FIR digital filter case.

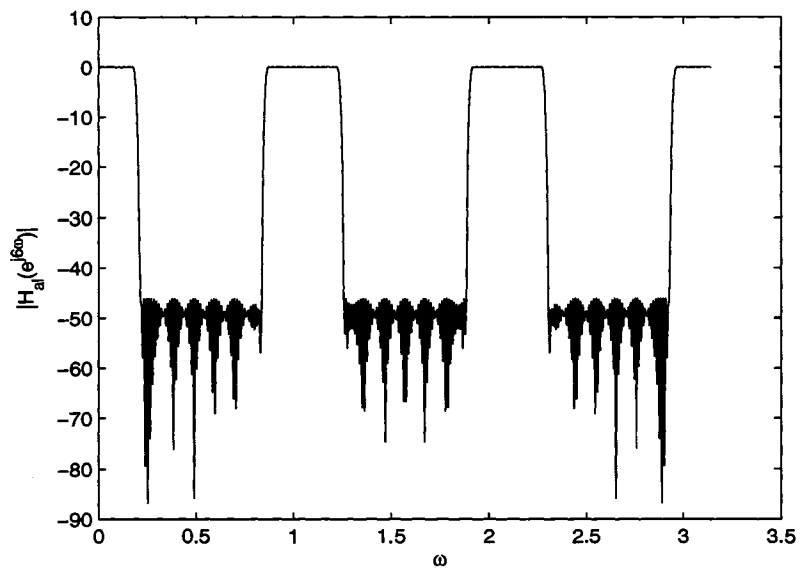


Figure 4.6: Magnitude response of M -interpolated version of digital sub-filter $H_{ai}(z)$ for lowpass FRM FIR digital filter case.

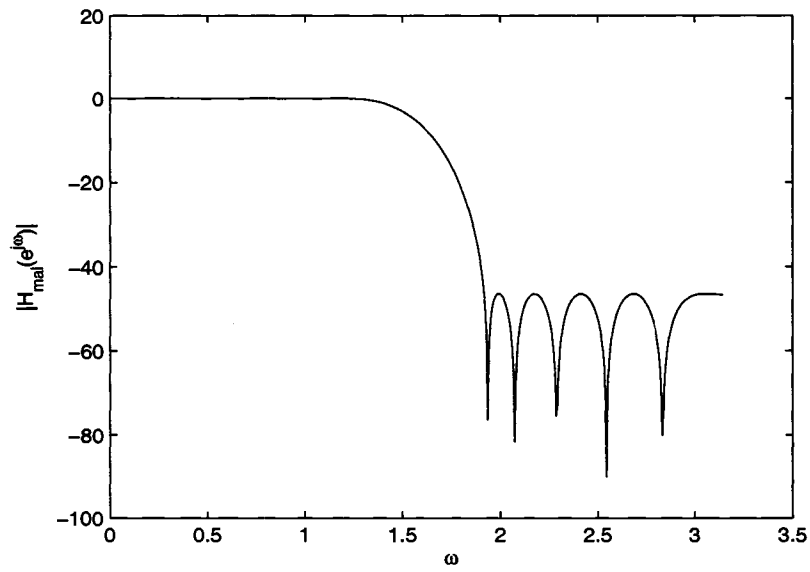


Figure 4.7: Magnitude response of masking digital sub-filter $H_{mal}(z)$ for lowpass FRM FIR digital filter case.

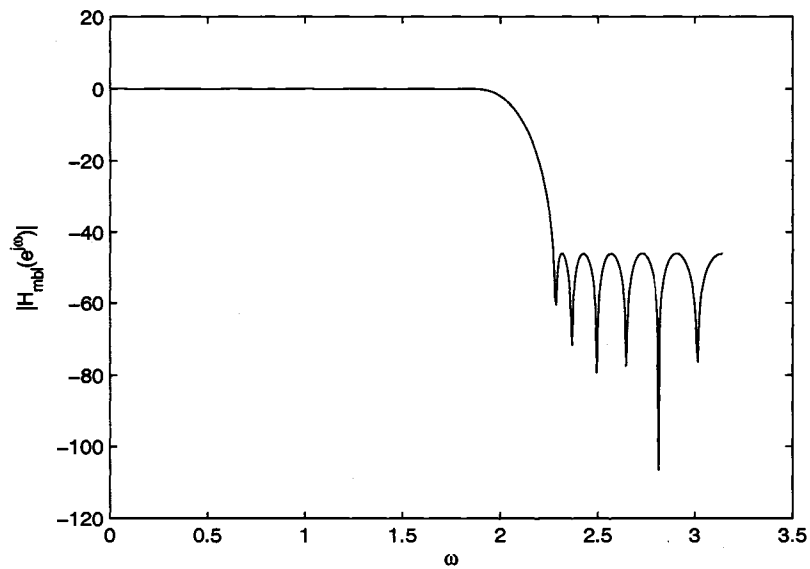


Figure 4.8: Magnitude response of masking digital sub-filter $H_{mbl}(z)$ for lowpass FRM FIR digital filter case.

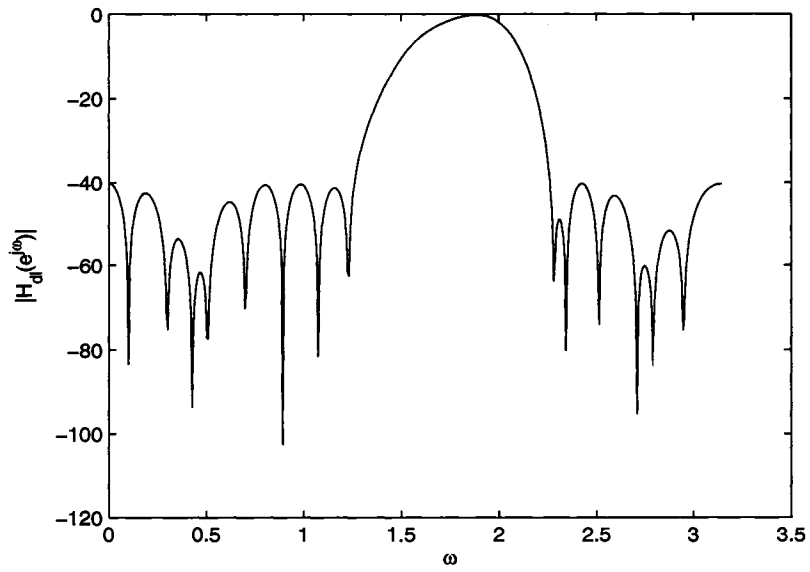


Figure 4.9: Magnitude response of masking digital sub-filter $H_{d1}(z)$ for lowpass FRM FIR digital filter case.

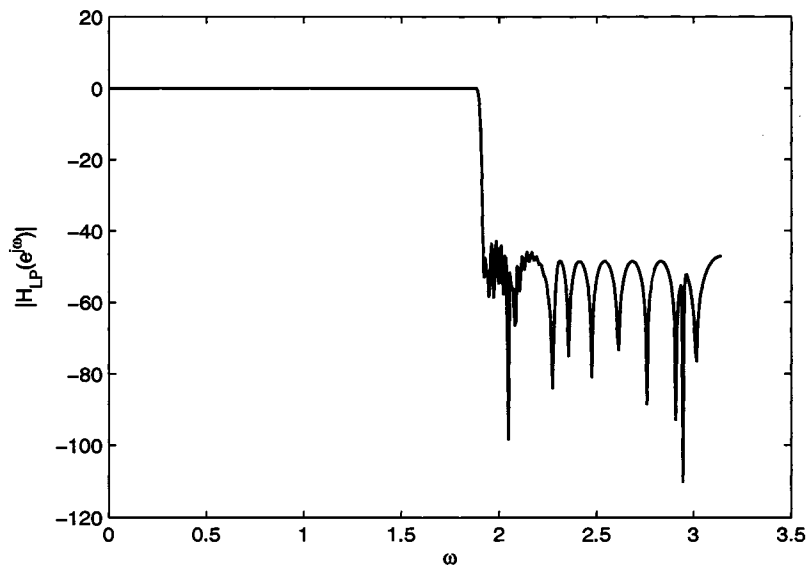


Figure 4.10: Infinite-precision lowpass FRM FIR digital filter.

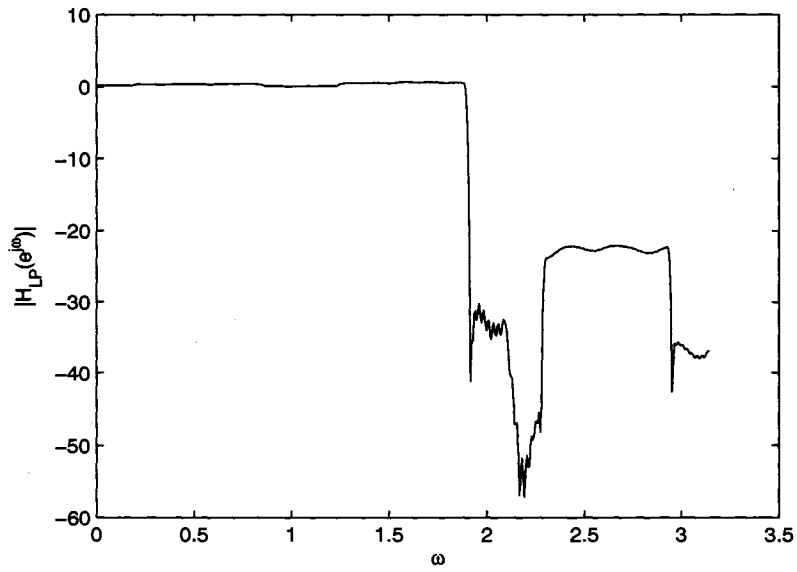


Figure 4.11: Lowpass CSD FRM FIR digital filter before DCGA optimization.

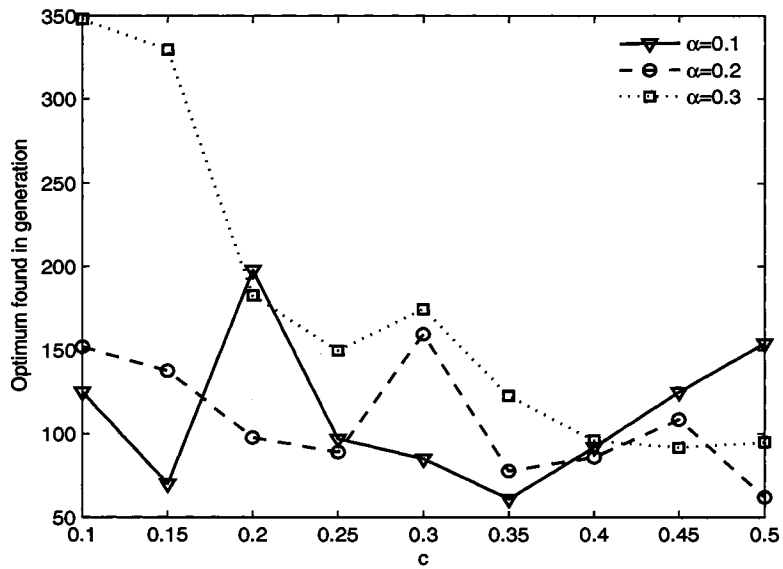


Figure 4.12: DCGA convergence speed for lowpass CSD FRM FIR digital filters for varying values of c and α .

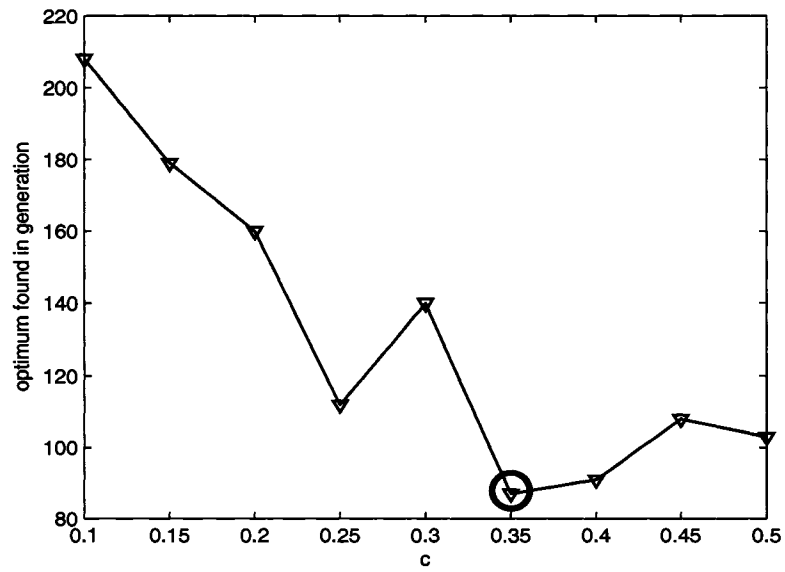


Figure 4.13: Average DCGA convergence speed for lowpass CSD FRM FIR digital filters for varying values of c .

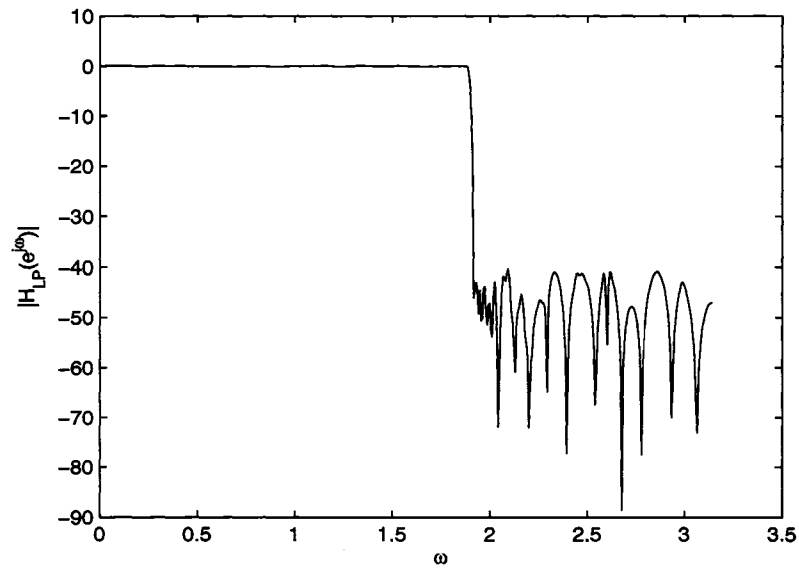


Figure 4.14: Lowpass CSD FRM FIR digital filter after DCGA optimization.

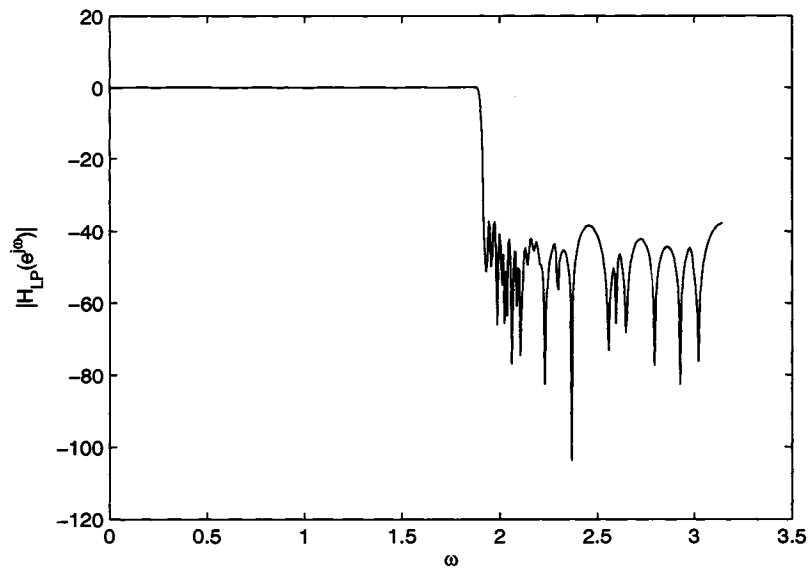


Figure 4.15: Lowpass DBNS FRM FIR digital filter before DCGA optimization.

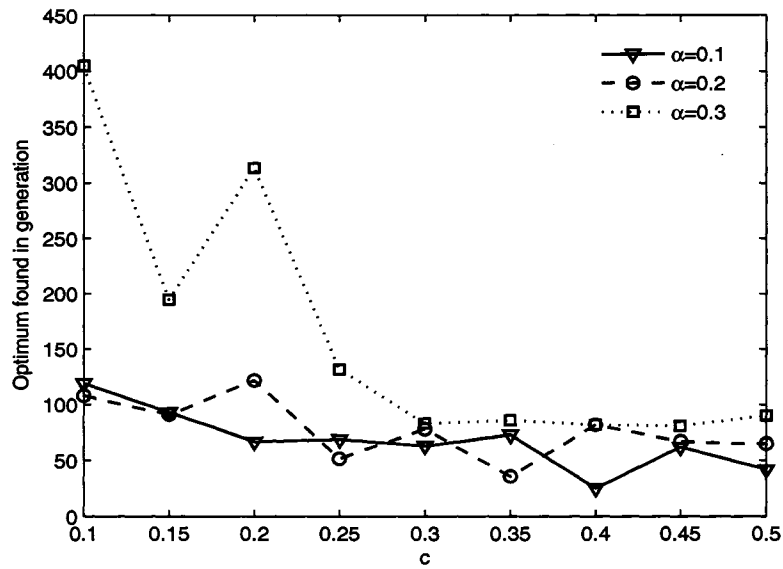


Figure 4.16: DCGA convergence speed for lowpass DBNS FRM FIR digital filters for varying values of c and α .

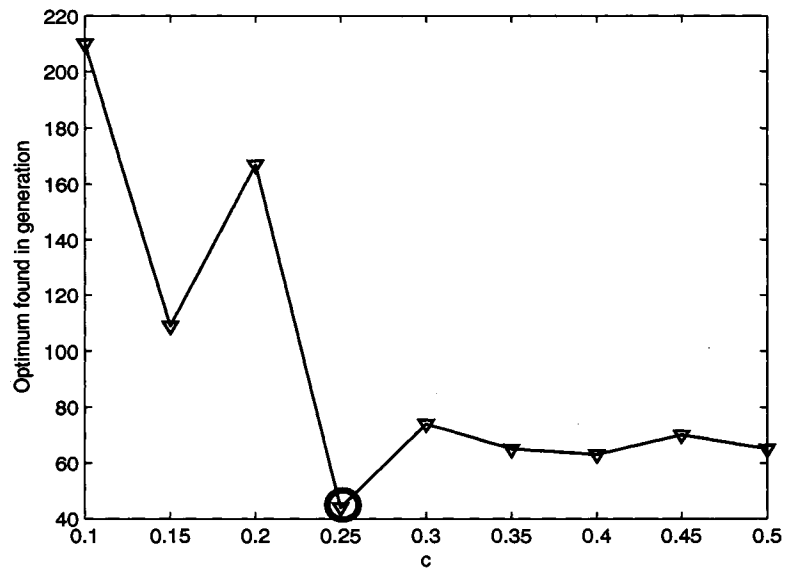


Figure 4.17: Average DCGA convergence speed for lowpass DBNS FRM FIR digital filters for varying values of c .

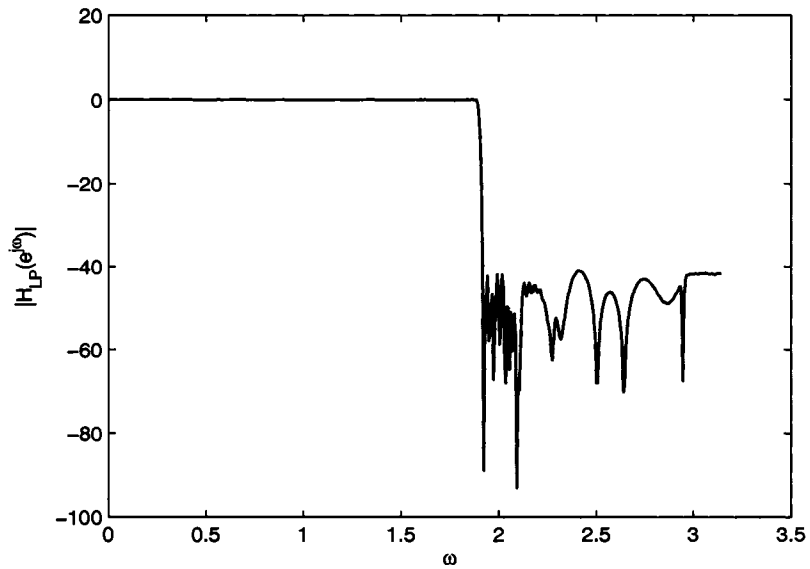


Figure 4.18: Lowpass DBNS FRM FIR digital filter after DCGA optimization.

4.4.2 Design of bandpass FRM FIR digital filters for the case $\Delta_l = \Delta_u$

Let us consider the design of a bandpass FRM FIR digital filter satisfying the following magnitude response specifications for implementation over the CSD/DBNS multiplier coefficient spaces.

Passband region	$0.21\pi \leq \omega \leq 0.6\pi$	
Lower stopband region	$0 \leq \omega \leq 0.2\pi$	
Upper stopband region	$0.61 \leq \omega \leq \pi$	(4.15)
Maximum passband ripple	± 0.1 dB	
Minimum stopband attenuation	40 dB.	

The above specifications can be easily recast into specifications for the constituent lowpass and highpass FRM FIR digital filters as shown in Eqns. 4.16 and 4.17.

CONSTITUENT LOWPASS FRM FIR DIGITAL FILTER DESIGN SPECIFICATIONS

Passband region	$0 \leq \omega \leq 0.6\pi$	
Stopband region	$0.61\pi \leq \omega \leq \pi$	(4.16)
Maximum passband ripple	± 0.1 dB	
Minimum stopband attenuation	40 dB,	

CONSTITUENT HIGHPASS FRM FIR DIGITAL FILTER DESIGN SPECIFICATIONS

Passband region	$0.21\pi \leq \omega \leq \pi$	
Stopband region	$0 \leq \omega \leq 0.2\pi$	(4.17)
Maximum pass-band ripple	± 0.1 dB	
Minimum stopband attenuation	40 dB.	

In this case, $M_{LP} = M_{HP} \equiv M$ because of equal lower and upper transition bandwidths Δ_l and Δ_u . By using Eqn. 2.13, the first approximation to the optimum value of the interpolation factor M is obtained as 7. Table 4.8 shows the overall bandpass FRM FIR digital filter length as a function of M in the vicinity of the first approximation. Through inspection of Table 4.8, the optimum value of M is found to be 6, yielding digital sub-filters $H_{al}(z)$, $H_{mal}(z)$, $H_{mb1}(z)$, $H_{ah}(z)$, $H_{mah}(z)$ and $H_{mbh}(z)$ of lengths 84, 24, 42, 78, 18 and 62.

The bandedge specifications of the above digital sub-filters are as summarized in Table 4.9. Moreover, the corresponding maximum passband ripple and minimum stopband attenuations are set as given in Table 4.10. By using the Parks-McClellan approach together with the design specifications in Tables 4.9 and 4.10, the initial infinite-precision digital sub-filters $H_{al}(z)$, $H_{mal}(z)$, $H_{mbl}(z)$, $H_{ah}(z)$, $H_{mah}(z)$ and $H_{mbh}(z)$ are designed to have the magnitude frequency responses as shown in Figs. 4.19 to 4.28. The magnitude frequency response of the infinite-precision bandpass FRM FIR digital filter is as shown in Fig. 4.29.

Table 4.8: Filter Lengths for a Bandpass FRM FIR Digital Filter with $\Delta_l = \Delta_u$ for Various Values of M

M	H_{al}	H_{mal}	H_{mbl}	H_{ah}	H_{mah}	H_{mbh}	Total Length
2	254	24	2	234	10	6	530
3	168	8	42	156	10	18	402
4	126	16	24	118	10	52	346
5	102	506	12	94	10	468	1192
6	84	24	42	78	18	62	308
7	72	22	86	68	30	38	316

Table 4.9: Bandedge Frequencies for Associated with $H_{al(h)}(z)$, $H_{mal(h)}(z)$ and $H_{mbl(h)}(z)$ Digital Sub-Filters for the Bandpass FRM FIR Digital Filter Case with $\Delta_l = \Delta_u$

Sub-filter	Passband Edge Frequencies	Stopband Edge Frequencies
$H_{al}(e^{j\omega})$	0.34π	0.4π
$H_{mal}(e^{j\omega})$	0.4π	0.61π
$H_{mbl}(e^{j\omega})$	0.6π	0.72π
$H_{ah}(e^{j\omega})$	0.8π	0.74π
$H_{mah}(e^{j\omega})$	0.46π	0.2π
$H_{mbh}(e^{j\omega})$	0.21π	0.13π

4.4.2.1 DCGA optimization of bandpass CSD FRM FIR digital filters for the case $\Delta_l = \Delta_u$

The parameters for the proposed DCGA optimization of the bandpass FRM FIR digital filter are as summarized in Table 4.11. By quantizing the constituent infinite-precision multiplier coefficients to their nearest counterparts in the CSD LUT, one can obtain a seed bandpass CSD FRM FIR digital filter having a magnitude fre-

Table 4.10: Passband Ripples and Stopband Attenuations for Associated with $H_{al(h)}(z)$, $H_{mal(h)}(z)$ and $H_{mbl(h)}(z)$ Digital Sub-Filters for the Bandpass FRM FIR Digital Filter Case with $\Delta_l = \Delta_u$

Sub-filter	Passband Ripple	Stopband Attenuation
$H_{al}(e^{j\omega})$	0.085 dB	-46 dB
$H_{mal}(e^{j\omega})$	0.085 dB	-46 dB
$H_{mbl}(e^{j\omega})$	0.085 dB	-46 dB
$H_{ah}(e^{j\omega})$	0.085 dB	-46 dB
$H_{mah}(e^{j\omega})$	0.085 dB	-46 dB
$H_{mbh}(e^{j\omega})$	0.085 dB	-46 dB

quency response as shown in Fig. 4.30. This magnitude frequency response violates the design specifications in Eqn. 4.15 by almost 1 dB in the passband, and by almost 18 dB in the stopband region (c.f. Table 4.12).

Fig. 4.31 shows the convergence speed of the DCGA optimization for the parameter c ranging from 0.1 to 0.5, and for the parameter α ranging from 0.1 to 0.3. In this way, the fastest convergence speed is obtained for $c = 0.5$ and $\alpha = 0.2$. Fig. 4.32 shows the convergence speed for varying values of the parameter c averaged over the parameter α . Consequently, on average, one can obtain high convergence speeds for c ranging from 0.3 to 0.5.

For $c = 0.5$ and $\alpha = 0.2$, the DCGA optimization converges to the optimal bandpass FRM FIR digital filter after 144 generations, resulting in a magnitude frequency response as shown in Fig. 4.33.

Table 4.11: Design Parameters for DCGA Optimization of Bandpass CSD FRM FIR Digital Filter for the Case $\Delta_l = \Delta_u$

Design Step	Design Parameters
1	$M = 6, N_{al} = 84, N_{mal} = 24, N_{mbl} = 42, N_{ah} = 78, N_{mah} = 18, N_{mbh} = 62$
2	$w = 3 \text{ bits}, W_I = 3 \text{ bits}, W_F = 14 \text{ bits}, B = 12 \text{ bits}$
3	$p_F = 0.8, N = 500$
4	$C = 30, W_p = 1.15, W_s = 0.85, \beta = 100, T_u = 0.0005, T_l = 0.008$
5	$L = 3696$

Table 4.12: Bandpass CSD FRM FIR Digital Filter Magnitude Responses for the case $\Delta_l = \Delta_u$ before and after DCGA Optimization

Multiplier Coefficient Representation	Passband Ripple	Lower Stopband Attenuation	Upper Stopband Attenuation
Infinite-Precision	0.075 dB	-41 dB	-42.8 dB
CSD before DCGA optimization	1.12 dB	-22.3 dB	-24.15 dB
CSD after DCGA Optimization	0.1 dB	-42.2 dB	-41.9 dB

4.4.2.2 DCGA optimization of bandpass DBNS FRM FIR digital filters for the case $\Delta_l = \Delta_u$

Table 4.13 shows the design parameters for the DCGA optimization of the DBNS bandpass FRM digital filter. The corresponding seed DBNS FRM FIR digital filter is obtained to have a magnitude frequency response as shown in Fig. 4.34, violating the magnitude response specifications by almost 0.05 dB in the passband, and by almost 3 dB in the stopband region (c.f. Table 4.14).

Fig. 4.35 shows the convergence speed of the DCGA optimization for the parameter c ranging from 0.1 to 0.5, and for the parameter α ranging from 0.1 to 0.3. The fastest convergence speed is obtained for $c = 0.4$ and $\alpha = 0.1$. Fig. 4.36 shows the convergence speed for varying values of the parameter c averaged over the value of the parameter α . It can be observed that for c ranging from 0.3 to 0.5 one can obtain higher speeds of convergence to the desired optimal bandpass DBNS FRM FIR digital filter.

For $c = 0.4$ and $\alpha = 0.1$, the DCGA optimization converges to the optimal bandpass DBNS FRM FIR digital filter after 45 generations, resulting in a magnitude frequency response as shown in Fig. 4.37.

Table 4.13: Design Parameters for DCGA Optimization of Bandpass DBNS FRM FIR Digital Filter for the Case $\Delta_l = \Delta_u$

Design Step	Design Parameters
1	$M = 6, N_{al} = 84, N_{mal} = 24, N_{mbl} = 42, N_{ah} = 78, N_{mah} = 18, N_{mbh} = 62$
2	$n = 96, m = 69, B = 12 \text{ bits}$
3	$p_F = 0.8, N = 500$
4	$C = 30, W_p = 1.15, W_s = 0.85, \beta = 100, T_u = 0.0005, T_l = 0.008$
5	$L = 3696$

Table 4.14: DBNS FRM FIR Bandpass Digital Filter Magnitude Responses before and after GA Optimization

Multiplier Coefficient Representation	Passband Ripple	Lower Stopband Attenuation	Upper Stopband Attenuation
Infinite-Precision	0.075 dB	-41 dB	-42.8 dB
DBNS before GA optimization	0.15 dB	-36.97 dB	-37.5 dB
DBNS after GA Optimization	0.09 dB	-42.2 dB	-40.5 dB

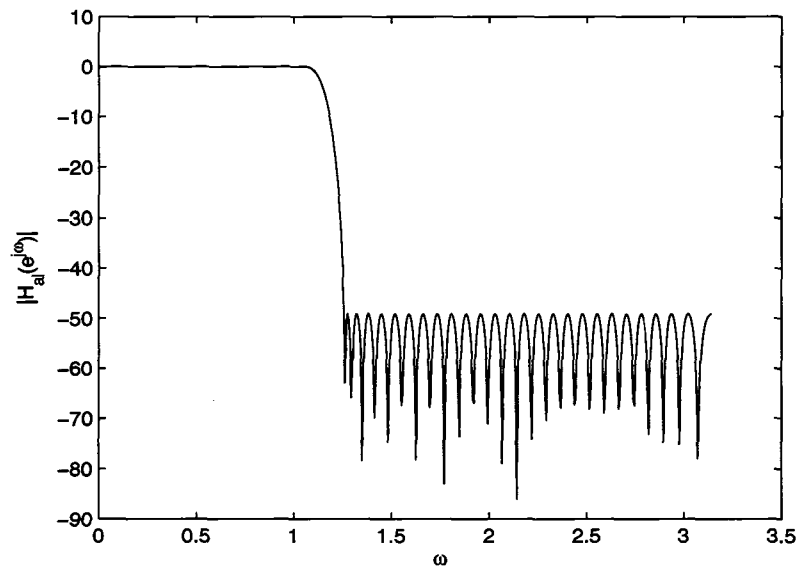


Figure 4.19: Magnitude response of digital sub-filter $H_{al}(z)$ for the bandpass FRM FIR digital filter case with $\Delta_l = \Delta_u$.

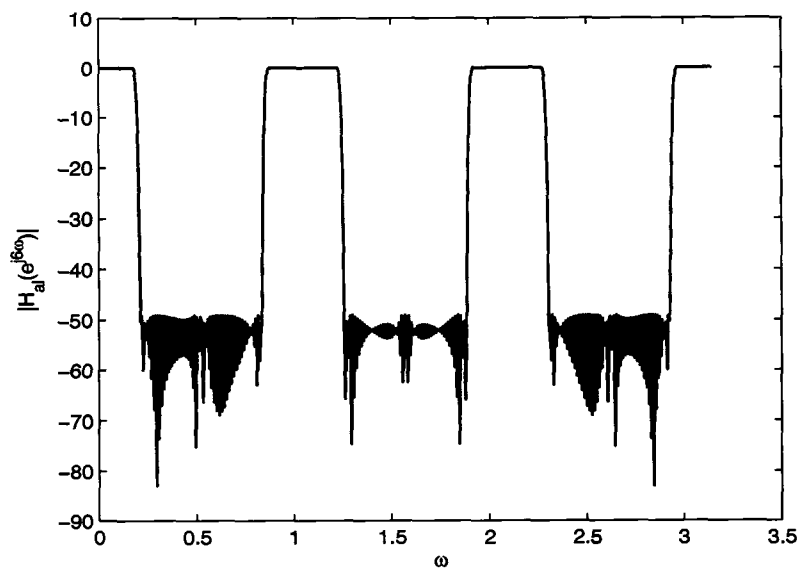


Figure 4.20: Magnitude response of M_{LP} -interpolated version of digital sub-filter $H_{d1}(z)$ for the bandpass FRM FIR digital filter case with $\Delta_l = \Delta_u$.

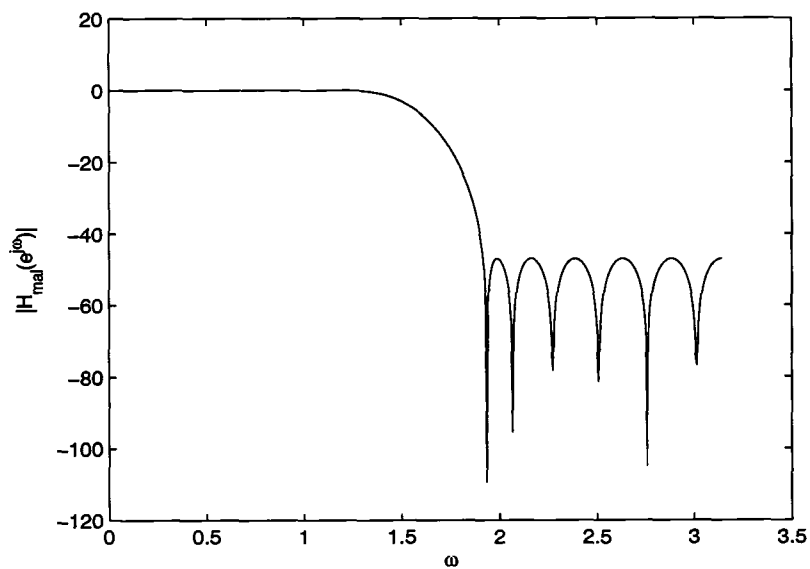


Figure 4.21: Magnitude response of masking digital sub-filter $H_{mal}(z)$ for the bandpass FRM FIR digital filter case with $\Delta_l = \Delta_u$.

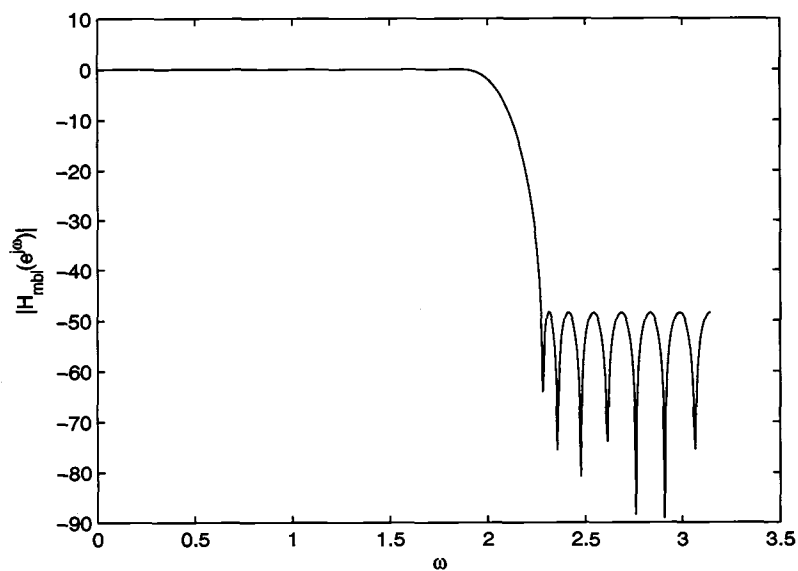


Figure 4.22: Magnitude response of masking digital sub-filter $H_{mb1}(z)$ for the band-pass FRM FIR digital filter case with $\Delta_l = \Delta_u$.

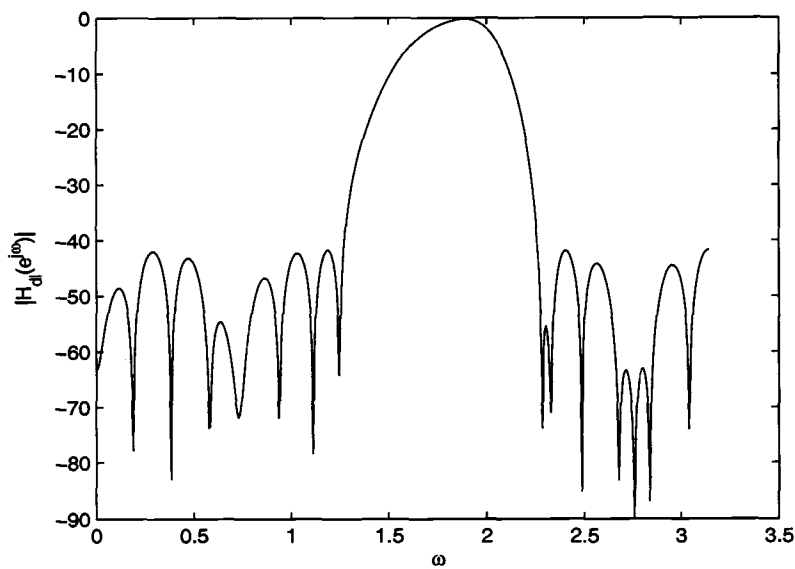


Figure 4.23: Magnitude response of masking digital sub-filter $H_{dl}(z)$ for the band-pass FRM FIR digital filter case with $\Delta_l = \Delta_u$.

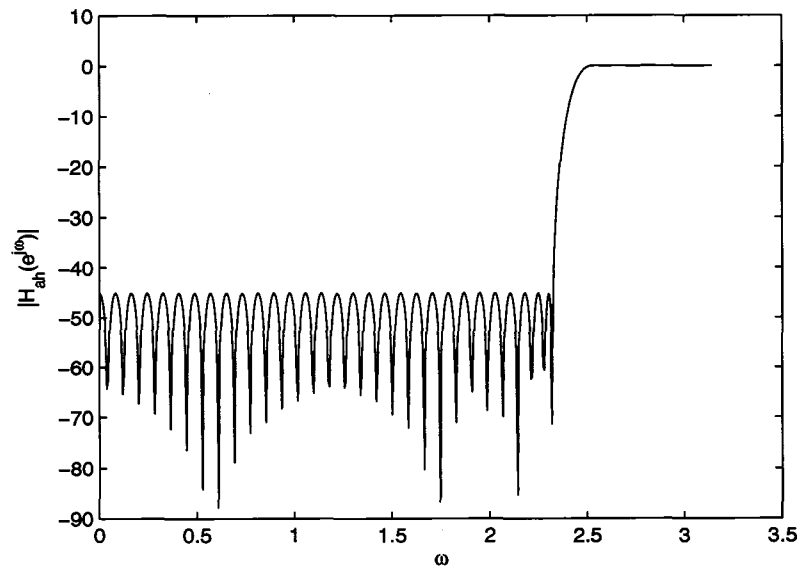


Figure 4.24: Magnitude response of digital sub-filter $H_{ah}(z)$ for the bandpass FRM FIR digital filter case with $\Delta_l = \Delta_u$.

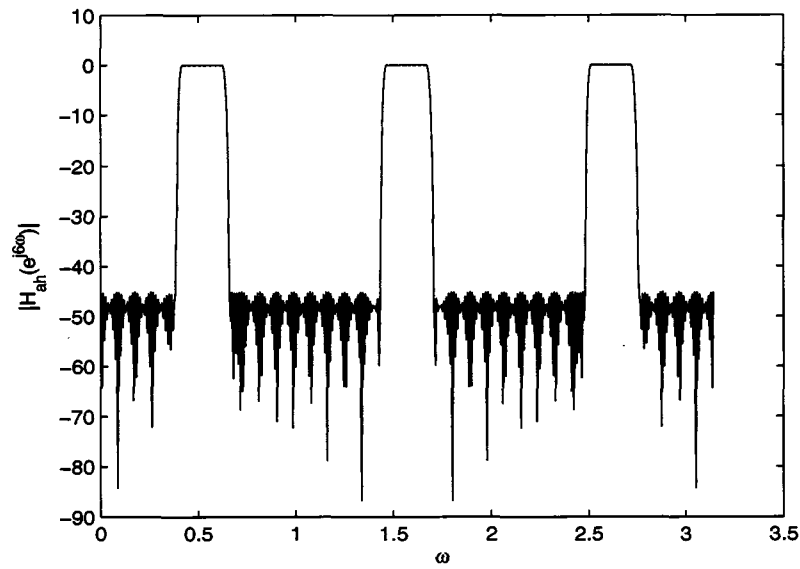


Figure 4.25: Magnitude response of M_{HP} -interpolated version of digital sub-filter $H_{ah}(z)$ for the bandpass FRM FIR digital filter case with $\Delta_l = \Delta_u$.

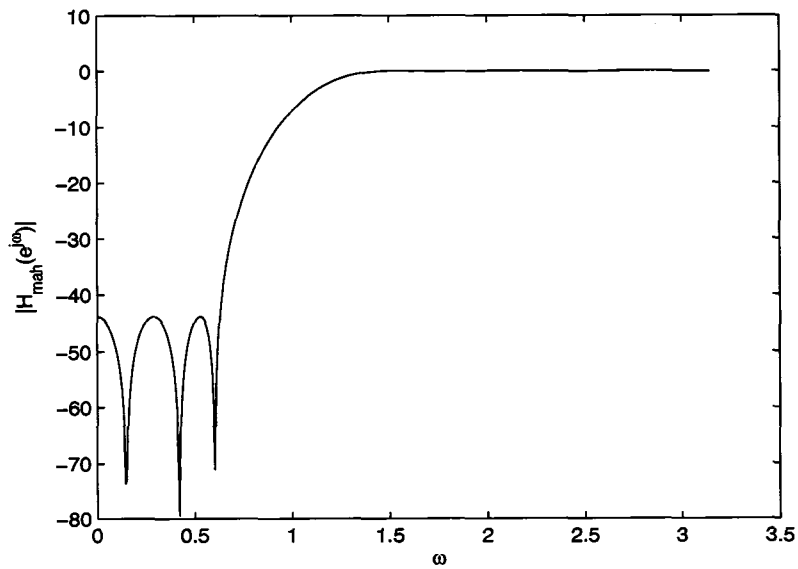


Figure 4.26: Magnitude response of masking digital sub-filter $H_{mah}(z)$ for the band-pass FRM FIR digital filter case with $\Delta_l = \Delta_u$.

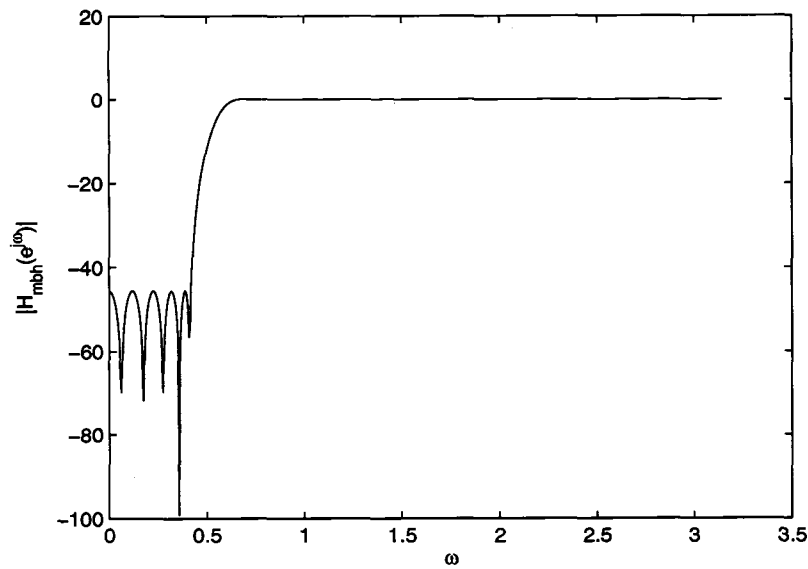


Figure 4.27: Magnitude response of masking digital sub-filter $H_{mbh}(z)$ for the band-pass FRM FIR digital filter case with $\Delta_l = \Delta_u$.

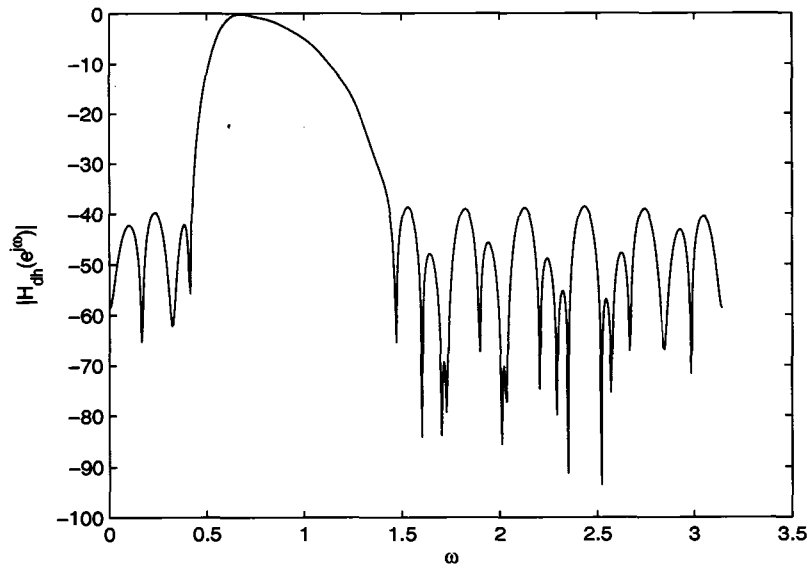


Figure 4.28: Magnitude response of masking digital sub-filter $H_{dh}(z)$ for the bandpass FRM FIR digital filter case with $\Delta_l = \Delta_u$.

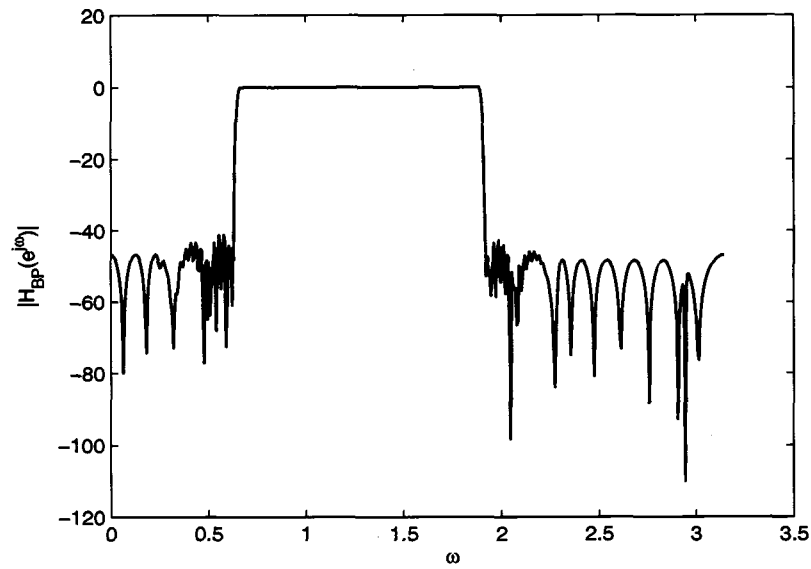


Figure 4.29: Infinite-precision bandpass FRM FIR digital filter with $\Delta_l = \Delta_u$.

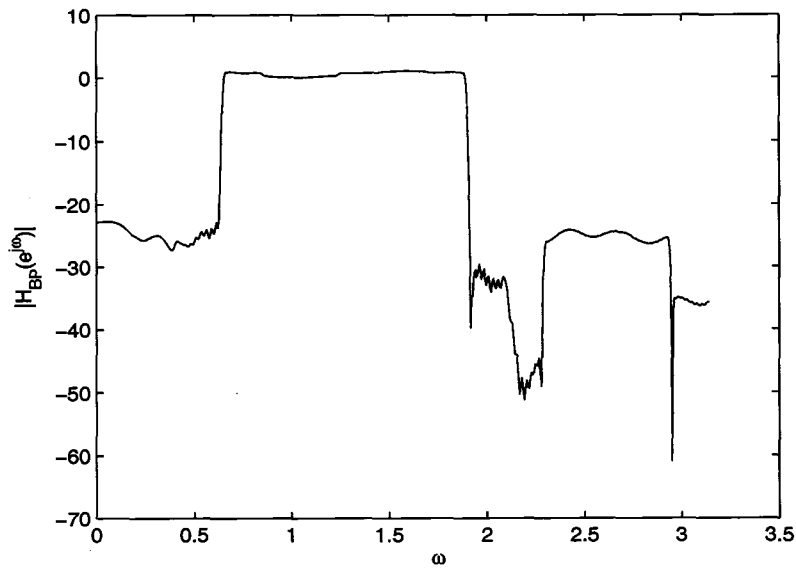


Figure 4.30: Bandpass CSD FRM FIR digital filter with $\Delta_l = \Delta_u$ before DCGA optimization.

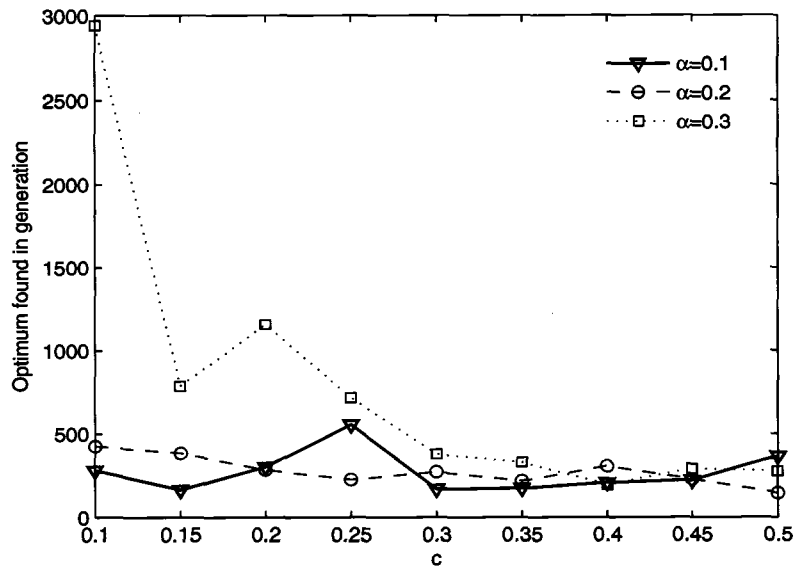


Figure 4.31: DCGA convergence speed for bandpass FRM FIR digital filters for varying values of c and α .

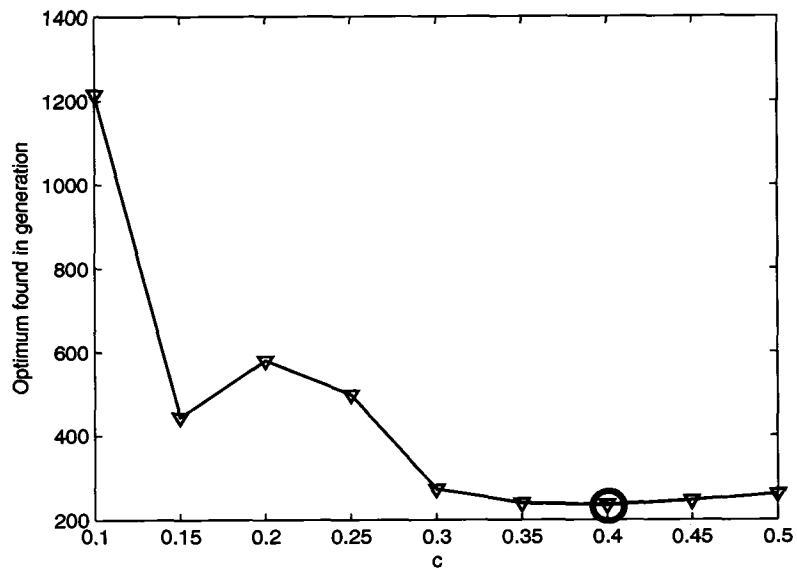


Figure 4.32: Average DCGA convergence speed for bandpass FRM FIR digital filters for varying values of c .

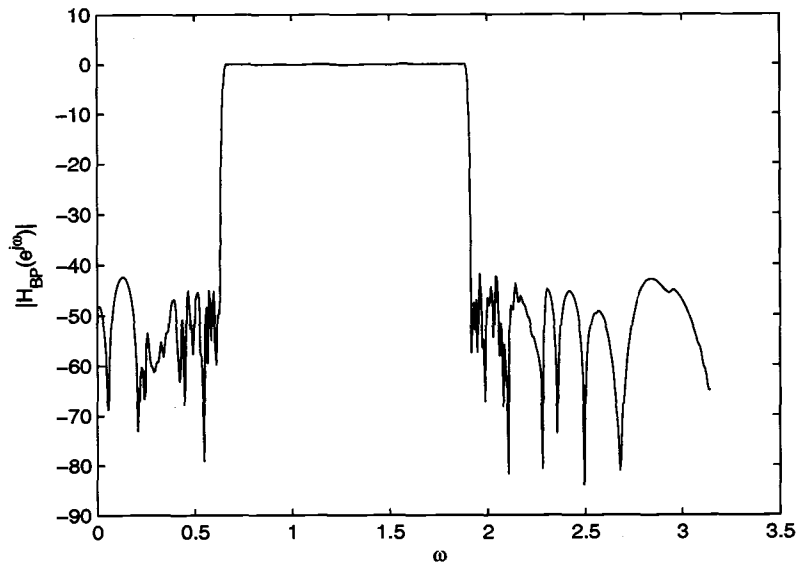


Figure 4.33: Bandpass CSD FRM FIR digital filter with $\Delta_l = \Delta_u$ after DCGA Optimization.

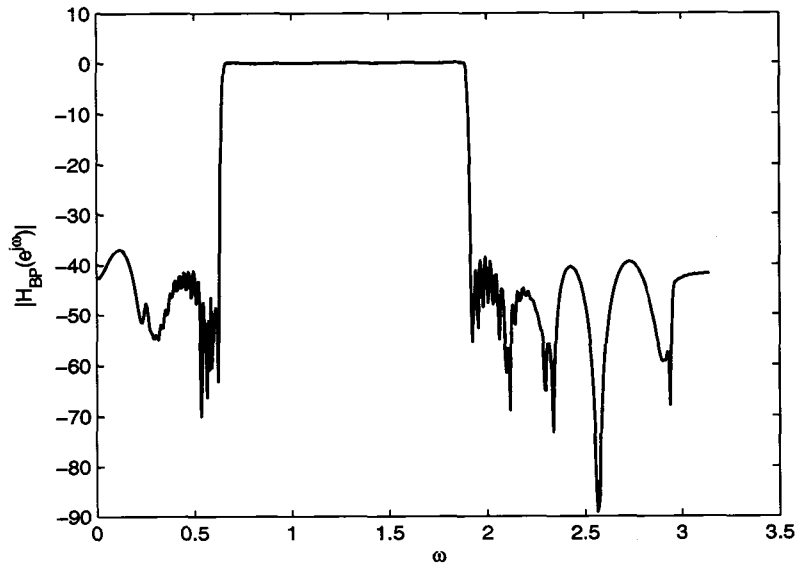


Figure 4.34: Bandpass DBNS FRM FIR Digital Filter with $\Delta_l = \Delta_u$ before DCGA optimization.

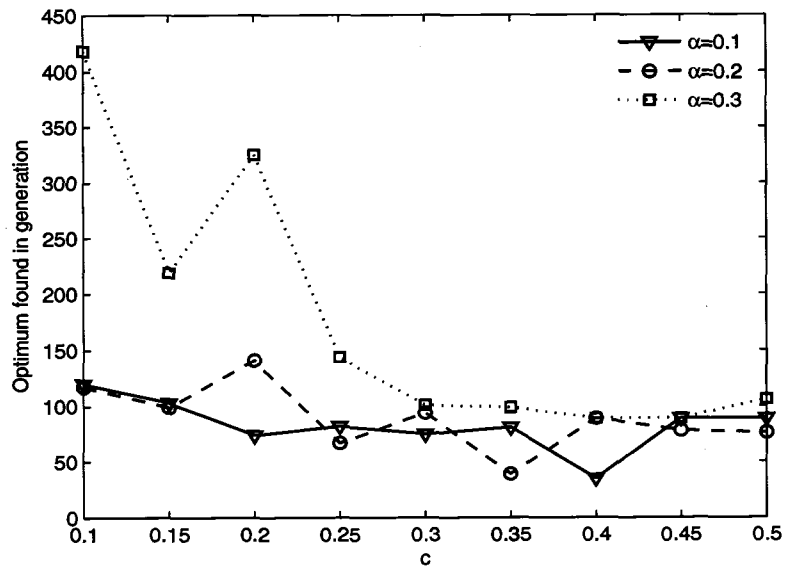


Figure 4.35: DCGA convergence speed for bandpass DBNS FRM FIR digital filters for varying values of c and α .

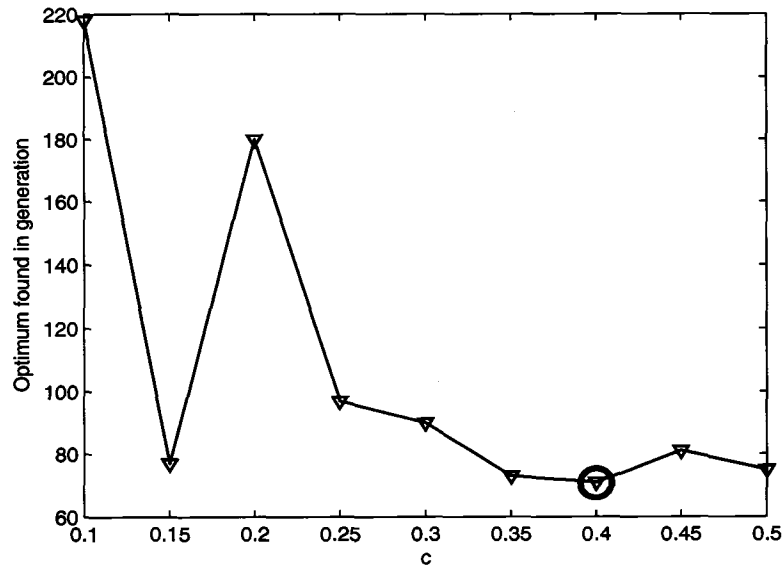


Figure 4.36: Average DCGA convergence speed for bandpass DBNS FRM FIR digital filters for varying values c .

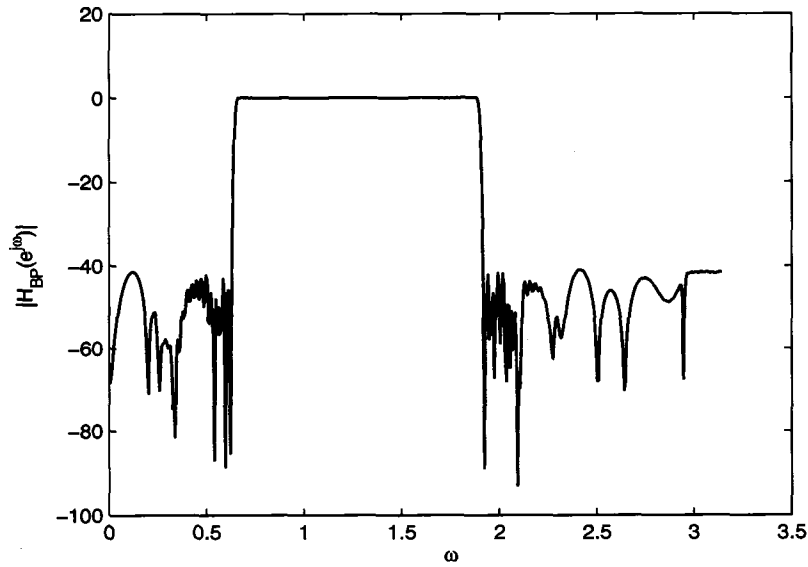


Figure 4.37: Bandpass DBNS FRM FIR digital filter $\Delta_l = \Delta_u$ after DCGA Optimization.

4.4.3 Design of bandpass FRM FIR digital filters for the case $\Delta_l \neq \Delta_u$

Let us consider the design of a bandpass FRM FIR digital filter with unequal transition bandwidths, satisfying the following magnitude response specifications over the CSD/DBNS multiplier coefficient spaces.

Passband region	$0.33\pi \leq \omega \leq 0.6\pi$	
Lower stopband region	$0 \leq \omega \leq 0.3\pi$	
Upper stopband region	$0.61 \leq \omega \leq \pi$	(4.18)
Maximum passband ripple	± 0.1 dB	
Minimum stopband attenuation	40 dB.	

The above specifications can be recast into corresponding specifications for the constituent lowpass and highpass FRM FIR digital filter in much the same way as before. In this case, because of unequal lower and upper transition bandwidths Δ_l and Δ_u , the first approximation to the optimum value of the interpolation factor M_{LP} is obtained as 7 while the first approximation to the interpolation factor M_{HP} is found as 4, respectively. Table 4.15 shows the lowpass FRM FIR digital filter length as a function of M_{LP} in the vicinity of its first approximation while Table 4.16 shows the highpass FRM FIR digital filter length as a function of M_{HP} in the vicinity of its first approximation. Through inspection of Tables 4.15 and 4.16, the optimum values of M_{LP} and M_{HP} are found to be 6 and 5 respectively, yielding FRM FIR digital sub-filters $H_{al}(z)$, $H_{mal}(z)$, $H_{mbl}(z)$, $H_{ah}(z)$, $H_{mah}(z)$ and $H_{mbh}(z)$ of lengths 84, 24, 42, 34, 30 and 22.

Table 4.17 shows the bandedge specifications for the above constituent digital sub-filters. In addition, the corresponding passband ripples and stopband attenuations are shown in Table 4.18. Using the design specifications in Tables 4.17 and 4.18, the Parks-McClellan approach is used to obtain the constituent digital sub-filters where Fig. 4.48 shows the magnitude frequency response of the overall infinite-precision bandpass FRM FIR digital filter $H_{BP}(z)$ having $\Delta_l \neq \Delta_u$.

Table 4.15: Filter Lengths for the Constituent Lowpass FRM FIR Digital Filter for Various Values of M_{LP}

M	H_{al}	H_{mal}	H_{mb1}	Total Length
2	254	24	2	280
3	168	8	42	218
4	126	16	24	166
5	102	506	12	620
6	84	24	42	150
7	72	22	76	170

Table 4.16: Filter Lengths for the Constituent Highpass FRM FIR Digital Filter for Various Values of M_{HP}

M	H_{ah}	H_{mah}	H_{mbh}	Total Length
2	84	6	12	102
3	56	6	138	200
4	42	12	40	94
5	34	30	22	86
6	28	138	16	182
7	24	86	22	132
8	20	40	42	102

4.4.3.1 DCGA optimization of bandpass CSD FRM FIR digital filters for the case $\Delta_l \neq \Delta_u$

Table 4.19 shows the design parameters of the proposed DCGA algorithm used for the optimization of the seed bandpass CSD FRM FIR digital filter with unequal lower and upper transition bandwidths. Fig. 4.49 shows the magnitude response of the seed bandpass CSD FRM FIR digital filter after the infinite-precision coefficients have been approximated to the nearest CSD counterparts. As can be observed, the magnitude response violates the design specifications in Eqn. 4.18 by almost 0.9 dB in the pass-band, and by around 20 dB in the stop-band region (c.f. Table 4.20).

Again, convergence speed of the DCGA optimization were plotted against varying values of parameter c and parameter α . From Fig. 4.50, the quickest convergence to an optimum was observed at $c = 0.5$ and $\alpha = 0.2$. Moreover, it can be observed from Fig. 4.51 that, on average, high convergence speeds were obtained for values of parameter c ranging from 0.3 to 0.5.

Table 4.17: Bandedge Frequencies Associated with $H_{al(h)}(z)$, $H_{mal(h)}(z)$ and $H_{mbl(h)}(z)$ Digital Sub-Filters for the Bandpass FRM FIR Digital Filter Case with $\Delta_l \neq \Delta_u$

Sub-filter	Passband Edge Frequencies	Stopband Edge Frequencies
$H_{al}(e^{j\omega})$	0.34π	0.4π
$H_{mal}(e^{j\omega})$	0.4π	0.61π
$H_{mbl}(e^{j\omega})$	0.6π	0.72π
$H_{ah}(e^{j\omega})$	0.5π	0.35π
$H_{mah}(e^{j\omega})$	0.47π	0.3π
$H_{mbh}(e^{j\omega})$	0.33π	0.1π

Table 4.18: Passband Ripples and Stopband Attenuations Associated with $H_{al(h)}(z)$, $H_{mal(h)}(z)$ and $H_{mbl(h)}(z)$ Digital Sub-Filters for the Bandpass FRM FIR Digital Filter case with $\Delta_l \neq \Delta_u$

Sub-filter	Passband Ripple	Stopband Attenuation
$H_{al}(e^{j\omega})$	0.085 dB	-46 dB
$H_{mal}(e^{j\omega})$	0.085 dB	-46 dB
$H_{mbl}(e^{j\omega})$	0.085 dB	-46 dB
$H_{ah}(e^{j\omega})$	0.085 dB	-46 dB
$H_{mah}(e^{j\omega})$	0.085 dB	-46 dB
$H_{mbh}(e^{j\omega})$	0.085 dB	-46 dB

Fig. 4.52, shows the optimal bandpass FRM FIR digital filter having $\Delta_l \neq \Delta_u$, obtained after 109 generations for $c = 0.5$ and $\alpha = 0.2$.

Table 4.19: Design Parameters for DCGA Optimization of Bandpass CSD FRM FIR Digital Filter for the Case $\Delta_l \neq \Delta_u$

Design Step	Design Parameters
1	$M_{LP} = 6, N_{al} = 84, N_{mal} = 24, N_{mbl} = 42,$ $M_{HP} = 5, N_{ah} = 34, N_{mah} = 20, N_{mbh} = 22$
2	$w = 3 \text{ bits}, W_I = 3 \text{ bits}, W_F = 14 \text{ bits}, B = 12 \text{ bits}$
3	$p_F = 0.8, N = 500$
4	$C = 30, W_p = 1.15, W_s = 0.85, \beta = 100, T_u = 0.0005, T_l = 0.008$
5	$L = 2712$

4.4.3.2 DCGA optimization of bandpass DBNS FRM FIR digital filters for the case $\Delta_l \neq \Delta_u$

Table 4.21 shows the design parameters for the DCGA optimization of the bandpass DBNS FRM digital filter. The corresponding DBNS FRM FIR seed digital filter is

Table 4.20: Bandpass CSD FRM FIR Digital Filter Magnitude Responses for the case $\Delta_l \neq \Delta_u$ before and after DCGA Optimization

Multiplier Coefficient Representation	Passband Ripple	Lower Stopband Attenuation	Upper Stopband Attenuation
Infinite-Precision	0.093 dB	-43 dB	-42.8 dB
CSD before DCGA optimization	0.98 dB	-20 dB	-24 dB
CSD after DCGA Optimization	0.1 dB	-43 dB	-42.3 dB

obtained to have a magnitude frequency response as shown in Fig. 4.53, violating the magnitude response specifications by almost 0.16 dB in the passband, and by almost 9.5 dB in the stopband region (c.f. Table 4.22).

The speed of convergence for the DCGA optimization for values of parameter c ranging from 0.1 to 0.5, and for the parameter α ranging from 0.1 to 0.3 is as shown Fig. 4.54. The fastest convergence speed is obtained for $c = 0.4$ and $\alpha = 0.1$. From Fig. 4.55 it can be observed that, on an average, higher convergence speeds to the desired bandpass DBNS FRM FIR digital filter with $\Delta_l \neq \Delta_u$ can be obtained for c ranging from 0.3 to 0.5.

For $c = 0.4$ and $\alpha = 0.1$, the DCGA optimization converges to the optimal bandpass DBNS FRM FIR digital filter with $\Delta_l \neq \Delta_u$ after 53 generations, resulting in a magnitude frequency response as shown in Fig. 4.56.

Table 4.21: Design Parameters for DCCA Optimization of Bandpass DBNS FRM FIR Digital Filter for the Case $\Delta_l \neq \Delta_u$

Design Step	Design Parameters
1	$M = 6, N_{al} = 84, N_{mal} = 24, N_{mbl} = 42, N_{ah} = 78, N_{mah} = 18, N_{mbh} = 62$
2	$n = 96, m = 69, B = 12 \text{ bits}$
3	$p_F = 0.8, N = 500$
4	$C = 30, W_p = 1.15, W_s = 0.85, \beta = 100, T_u = 0.0005, T_l = 0.008$
5	$L = 3696$

Table 4.22: Bandpass DBNS FRM FIR Digital Filter Magnitude Responses for the Case $\Delta_l \neq \Delta_u$ before and after DCGA Optimization

Multiplier Coefficient Representation	Passband Ripple	Lower Stopband Attenuation	Upper Stopband Attenuation
Infinite-Precision	0.075 dB	-41 dB	-42.8 dB
DBNS before GA optimization	0.26 dB	-30.6 dB	-38.5 dB
DBNS after GA Optimization	0.97 dB	-41.45 dB	-41 dB

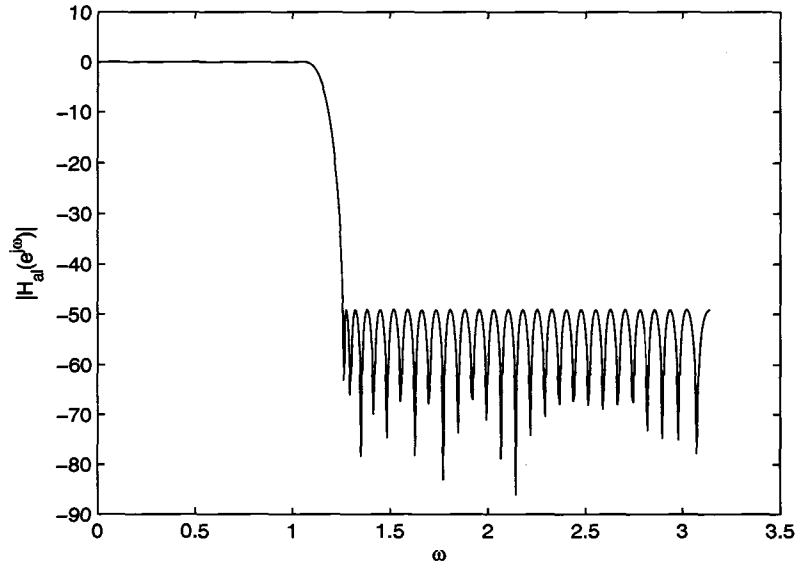


Figure 4.38: Magnitude response of digital sub-filter $H_{al}(z)$ for the bandpass FRM FIR digital filter case with $\Delta_l \neq \Delta_u$.

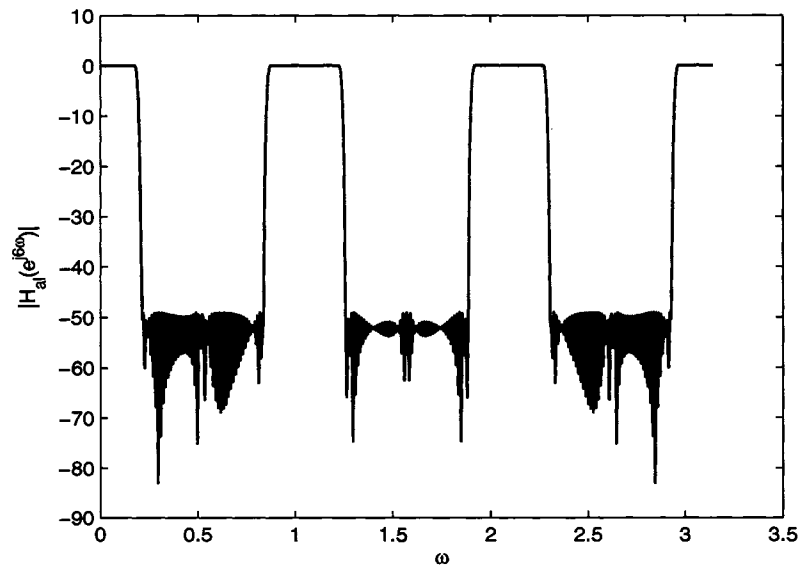


Figure 4.39: Magnitude response of M_{LP} -interpolated version of digital sub-filter $H_{al}(z)$ for the bandpass FRM FIR digital filter case with $\Delta_l \neq \Delta_u$.

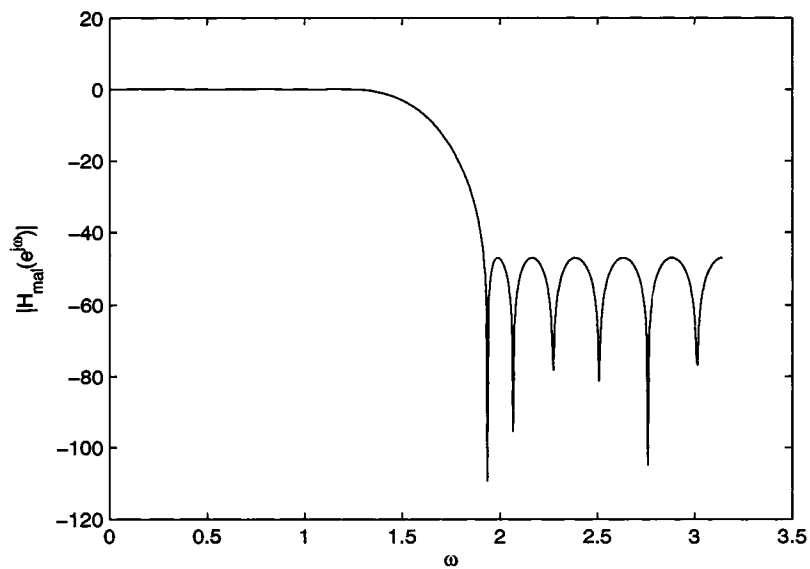


Figure 4.40: Magnitude response of masking digital sub-filter $H_{mal}(z)$ for the bandpass FRM FIR digital filter case with $\Delta_l \neq \Delta_u$.

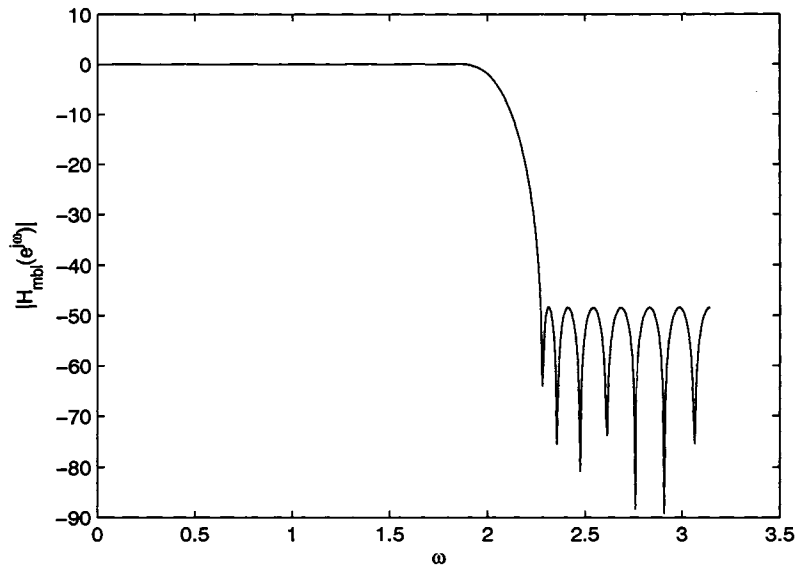


Figure 4.41: Magnitude response of masking digital sub-filter $H_{mbl}(z)$ for the band-pass FRM FIR digital filter case with $\Delta_l \neq \Delta_u$.

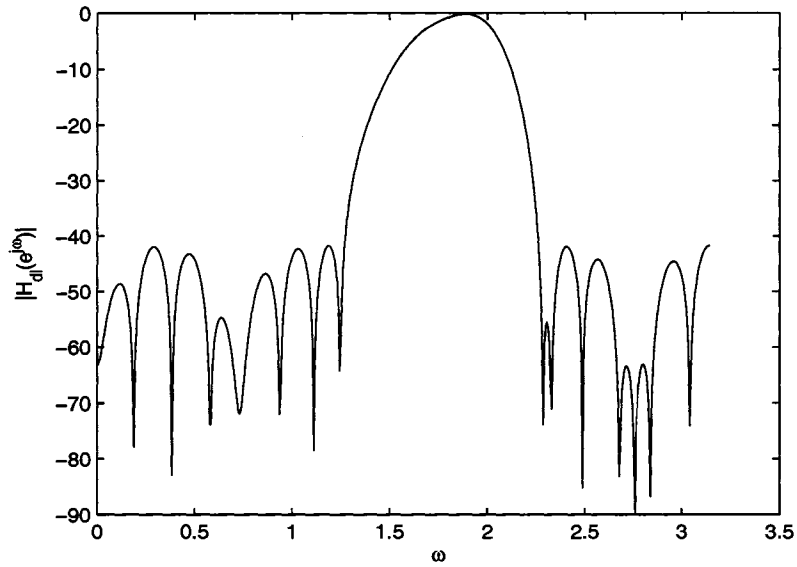


Figure 4.42: Magnitude response of masking digital sub-filter $H_{dl}(z)$ for the band-pass FRM FIR digital filter case with $\Delta_l \neq \Delta_u$.

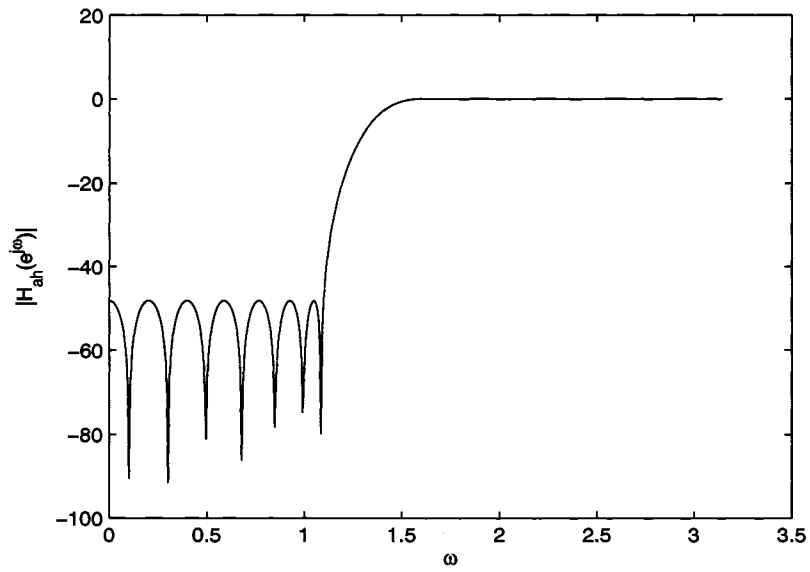


Figure 4.43: Magnitude response of digital sub-filter $H_{ah}(z)$ for the bandpass FRM FIR digital filter case with $\Delta_l \neq \Delta_u$.

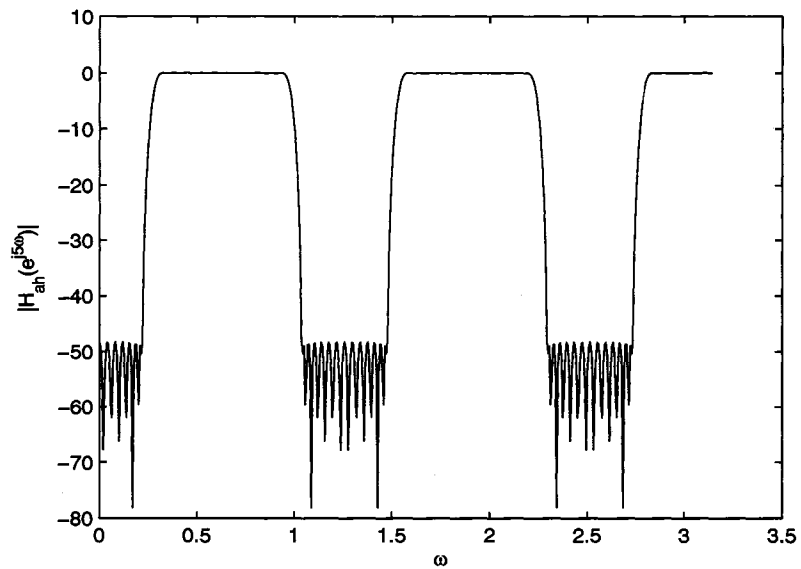


Figure 4.44: Magnitude response of M_{HP} -interpolated version of digital sub-filter $H_{ah}(z)$ for the bandpass FRM FIR digital filter case with $\Delta_l \neq \Delta_u$.

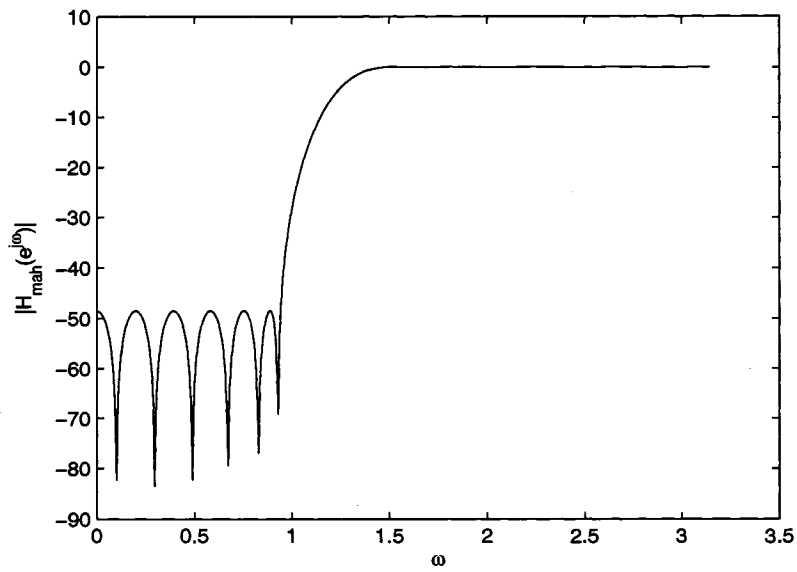


Figure 4.45: Magnitude response of masking digital sub-filter $H_{mah}(z)$ for the band-pass FRM FIR digital filter case with $\Delta_l \neq \Delta_u$.

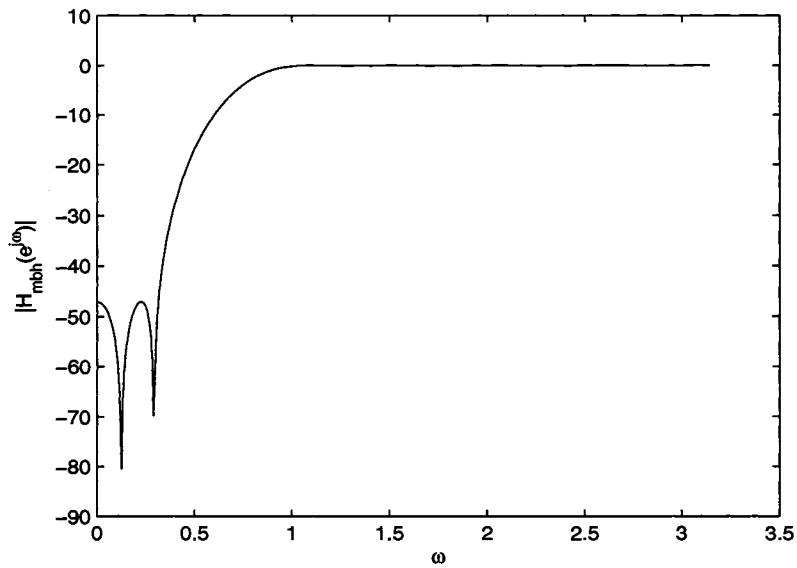


Figure 4.46: Magnitude response of masking digital sub-filter $H_{mbh}(z)$ for the band-pass FRM FIR digital filter case with $\Delta_l \neq \Delta_u$.

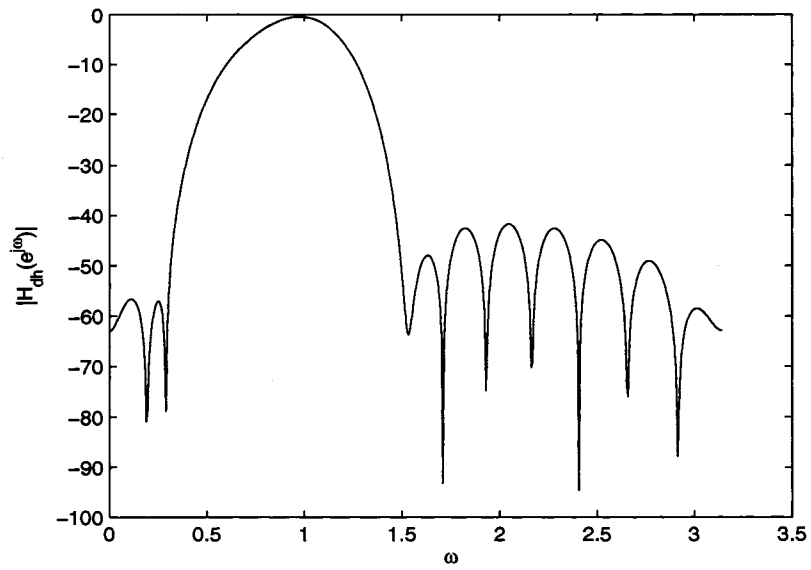


Figure 4.47: Magnitude response of masking digital sub-filter $H_{dh}(z)$ for the bandpass FRM FIR digital filter case with $\Delta_l \neq \Delta_u$.

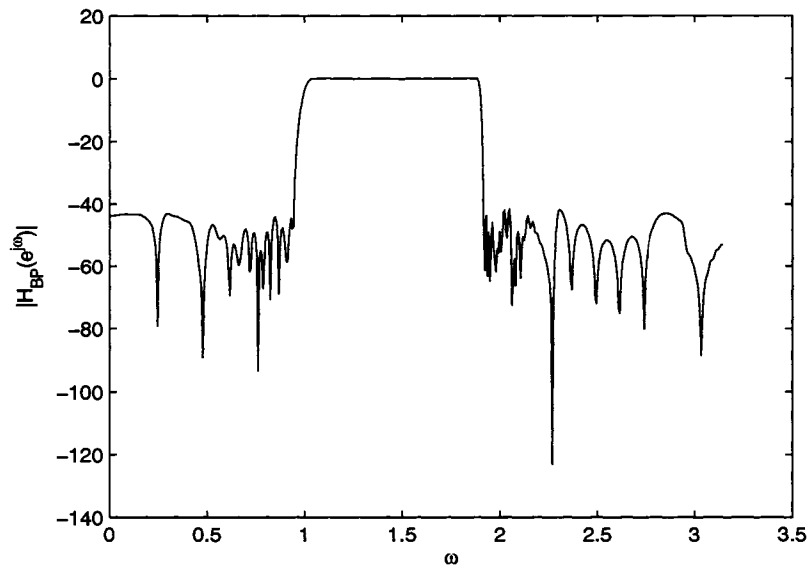


Figure 4.48: Infinite-precision bandpass FRM FIR digital filter with $\Delta_l \neq \Delta_u$.

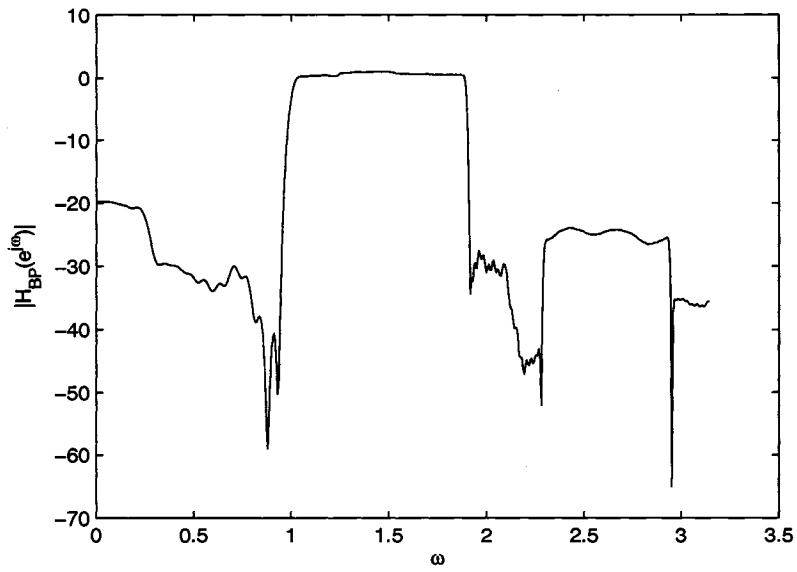


Figure 4.49: Bandpass CSD FRM FIR digital filter before DCGA optimization.

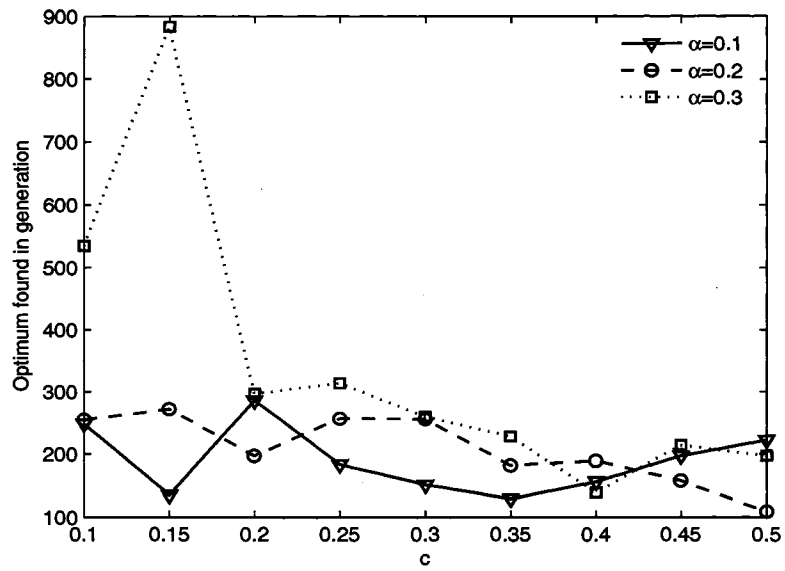


Figure 4.50: DCGA convergence speed for bandpass CSD FRM FIR digital filters for varying values of c and α .

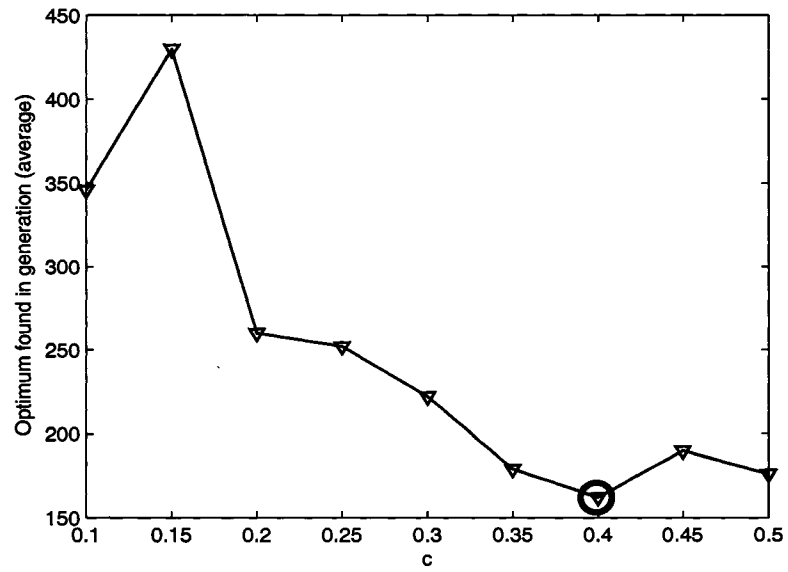


Figure 4.51: Average DCGA convergence speed for bandpass FRM FIR digital filters for varying values of c .

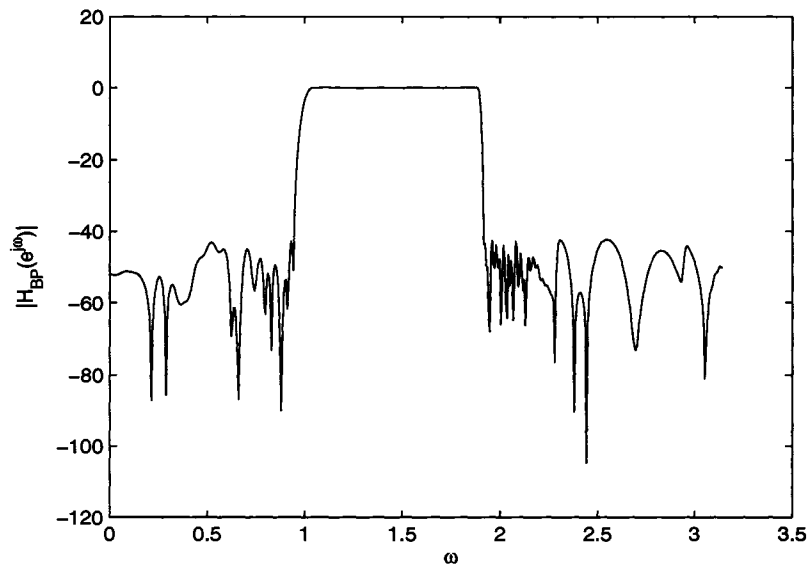


Figure 4.52: Bandpass CSD FRM FIR digital filter after DCGA optimization.

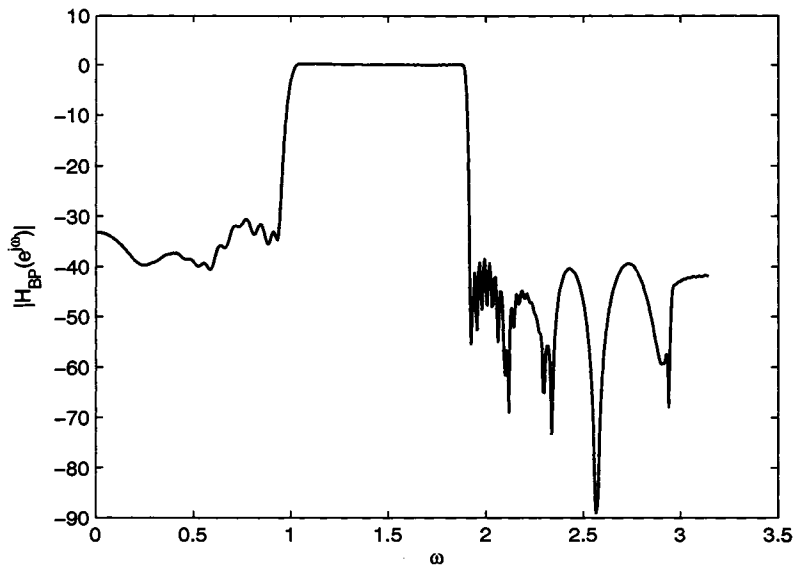


Figure 4.53: Bandpass DBNS FRM FIR digital filter with $\Delta_l \neq \Delta_u$ before DCGA optimization.

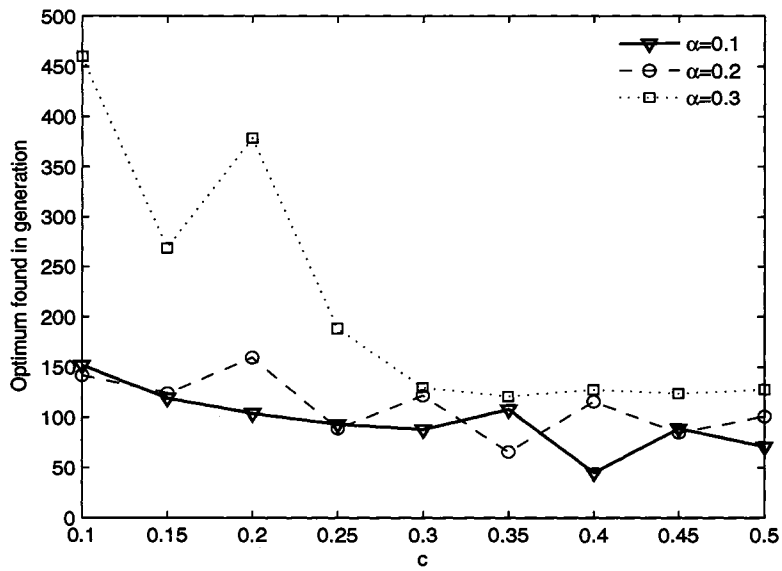


Figure 4.54: DCGA convergence speed for bandpass DBNS FRM FIR digital filters for varying values of c and α .

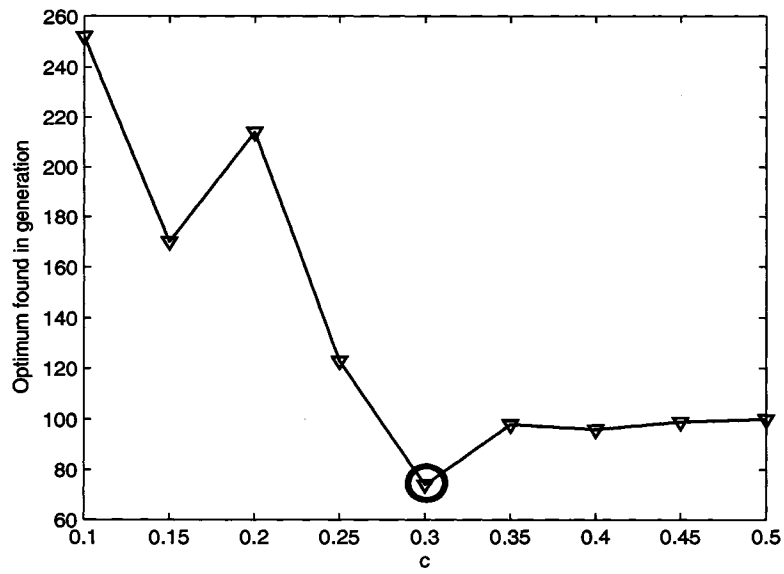


Figure 4.55: Average DCGA convergence speed for bandpass DBNS FRM FIR digital filters for varying values of c .

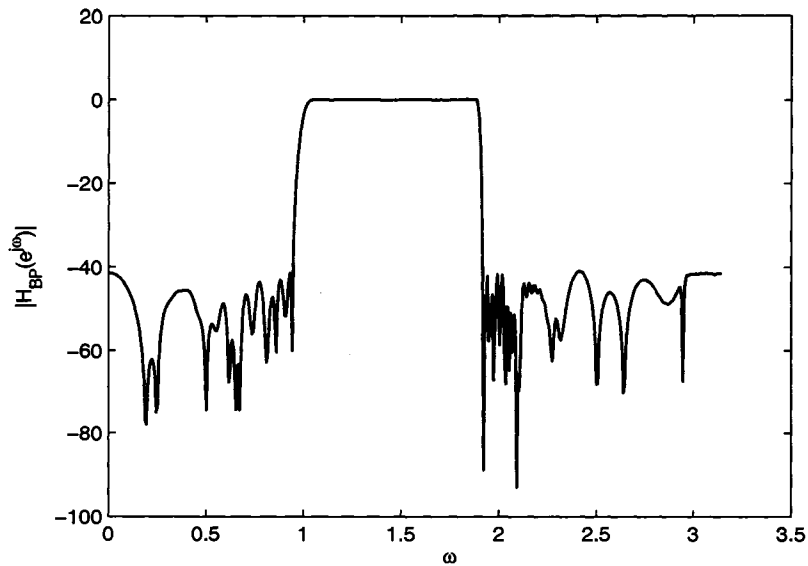


Figure 4.56: Bandpass DBNS FRM FIR digital filter after DCGA optimization.

Before concluding this chapter, it should be emphasized that in the above three cases, it was empirically shown that the desired population diversity for rapid con-

vergence can be obtained for appropriate values of parameters c and α . In the case of lowpass CSD FRM FIR digital filter this value of c ranges from 0.35 to 0.5 and in the DBNS case it ranges from 0.25 to 5. For bandpass CSD/DBNS FRM FIR digital filters with both equal and unequal lower and upper transition bandwidths, the appropriate values c lies in the range 0.3 to 0.5. For all three cases, the most appropriate value of α is found to be 0.2 in the CSD case and 0.1 in the DBNS case. By using these empirical values, the speed of convergence to the desired optimal FRM FIR digital filter increased by an order-of-magnitude as compared to that of the conventional GAs as shown in chapter 3 [18, 7, 14, 15].

Appendix C provides a table of CPU processing times for the design and optimization of FRM FIR digital filters using GA and DCGA. It can be clearly seen that DCGA provides a major convergence speed advantage over the conventional GAs.

Chapter 5

Concluding Remarks

This thesis has been concerned with the design and discrete optimization of FRM FIR digital filters using a novel LUT-based genetic algorithm (GA), over the CSD and DBNS multiplier coefficient spaces. The LUTs consist of permissible indexed CSD/DBNS numbers having pre-specified wordlengths and pre-specified number of non-zero bits, such that the indices form a *closed set* under the GA operations of crossover and mutation. The salient feature of the proposed GA is that it automatically leads to legitimate multiplier coefficients without any recourse to gene repair. The GA is employed to optimize a benchmark lowpass FRM FIR digital filter and a bandpass FRM FIR digital filter where the desired optimal solutions are obtained after approximately 1000 generations. The slow convergence speed of the GA was attributed to the lack of mechanisms through which entrapment at local optima could be successfully avoided (premature convergence). In order to improve the speed of convergence, the conventional GA is modified to a LUT-based diversity controlled genetic algorithm (DCGA) in which a cross-generational probabilistic survival selection scheme is employed to form the next-generation population pool. The advantages of DCGA were illustrated through its application to the benchmark lowpass and bandpass FRM FIR digital filters. Empirical investigations were undertaken to determine the DCGA control parameters for which convergence speeds were about an order-of-magnitude higher than those of the conventional GAs. Although the proposed GA and DCGA have been developed in terms of a corresponding infinite-precision seed FRM FIR digital filter, they can be easily modified to begin with a finite-precision (CSD/DBNS) FRM FIR digital filter. In the latter

case, the number of generations before obtaining an optimal FRM FIR digital filter may increase.

Bibliography

- [1] F. Ashrafzadeh A. fuller, B. Nowrouzian. Optimization of fir digital filters over the canonical signed-digit coefficient space using genetic algorithms. *Midwest Symposium on Circuits and Systems*, pages 456–469, Aug. 1998.
- [2] Vassil S. Dimitrov and Graham A. Jullien. Loading the bases: A new number representation with applications. Technical Report 1540-7977, IEEE Circuits and Systems Magazine, 2003.
- [3] M.J. Carey D.J. Goodman. Nine digital filters for decimation and interpolation. *IEEE. Trans. Accoust. Speech, Signal processing*, ASSP-25:121–126, Apr., 1977.
- [4] David E. Goldberg. *Genetic Algorithms in Search, Optimization, and Maching Learning*. Addison-Wesley, Reading, MA, 1989.
- [5] Jr. J. W. Adams, A.N. Willson. Some efficient digital prefilter structures. *IEEE Trans. on Circuits and Systems*, CAS-31:260–266, March, 1984.
- [6] Jr. J. W. Adams, A.N. Willson. A new approach to fir digital filters with fewer multipliers and reduced sensitivity. *IEEE Trans. on Circuits and Systems*, CAS-30:277–283, May, 1983.
- [7] Sai Mohan Kilambi and Behrouz Nowrouzian. A novel diversity controlled genetic algorithm for rapid optimization of bandpass frm fir digital filters over csd multiplier coefficient space. *Journal of Circuits, Systems and Signal Processing (JCSSP)*, submitted, 2007.
- [8] S.M. Kilambi and B. Nowrouzian. A genetic algorithm employing correlative roulette selection for optimization of frm digital filters over csd multiplier coefficient space. *IEEE APCCAS*, in press, Apr 2006.
- [9] S.M. Kilambi and B. Nowrouzian. A novel genetic algorithm for optimization

of frm digital filters over dbns multiplier coefficient space based on correlative roulette selection. *IEEE International Symposium on Signal Processing and Information Technology*, pages 228–231, Aug 2006.

- [10] Yong Chin Lim. A digital filter bank for digital audio systems. *IEEE Transactions on circuits and systems*, 33-8:848 – 849, Aug. 1986.
- [11] Yong Ching Lim. Frequency-response masking approach for the synthesis of sharp linear phase digital filters. *IEEE Transactions on Circuits and Systems*, CAS-33:357–364, Apr 1986.
- [12] Wu-Sheng Lu and T. Hinamoto. Optimal design of frequency-response-masking filters using semidefinite programming. *IEEE Transactions on Circuits and Systems*, 5:557–568, Apr. 2003.
- [13] Wu-Sheng Lu and T. Hinamoto. Improved design of frequency-response-masking filters using enhanced sequential quadratic programming. *IEEE International Symposium on Circuits and Systems*, 5:528–531, May 2004.
- [14] P. Mercier and B. Nowrouzian. Design of frm digital filters over the csd multiplier coefficient space employing genetic algorithms. *Proceedings of the 2006 IEEE International Conference on Acoustics, Speech and Signal Processing*, 3:968–971, May 2006.
- [15] P. Mercier and B. Nowrouzian. A genetic algorithm for the design and optimization of frm digital filters over a canonical double base multiplier coefficient space. *Proceedings of 2006 IEEE ISCAS*, pages 3289–3292, May 2006.
- [16] G.P. Lepagnol M.G. Bellanger, J.L. Daguét. Interpolation, extrapolation, and reduction of computation speed in digital filters. *IEEE. Trans. Accoust. Speech, Signal processing*, ASSP-22:231–235, Aug., 1974.
- [17] Sanjit K. Mitra. *Digital Signal Processing - A Computer-Based Approach*. McGraw Hill, NY, NY, 2006.
- [18] Sai Mohan Kilambi Pat Mercier and Behrouz Nowrouzian. Optimization of frm fir digital filters over csd and dbns multiplier coefficient spaces employing a novel genetic algorithm. *Journal of Computing*, submitted, 2007.
- [19] L.R. Rabiner R.E. Crochiere. A novel implementation for narrow-band fir digital filters. *IEEE. Trans. Accoust. Speech, Signal processing*, ASSP-23:457–

464, Oct., 1975.

- [20] L.R. Rabiner R.E. Crochiere. Optimum fir digital filter implementation for decimation, interpolation and narrow-band filtering. *IEEE. Trans. Accoust. Speech, Signal processing*, ASSP-23:444–456, Oct, 1975.
- [21] Yong-Ching Lim Rui Yang and Sydney R. Parker. Design of sharp linear-phase fir bandstop filters using the frequency-response-masking technique. *Circuits Systems Signal Processing*, 17:1–27, 1998.
- [22] Hisashi Shimodaira. Dcga: a diversity control oriented genetic algorithm. *Proceedings. on Ninth IEEE International Conference on Tools with Artificial Intelligence.*, pages 367 – 374, 3-8, Nov 1997.
- [23] Hisashi Shimodaira. A diversity-control-oriented genetic algorithm (dcga): Performance in function optimization. *Proceedings of the 2001 Congress on Evolutionary Computation*, 1:44–51, 27-30 May 2001.
- [24] R.R. Shively. On multistage finite impulse response (fir) filters with decimation. *IEEE. Trans. Accoust. Speech, Signal processing*, ASSP-23:353–357, Aug., 1975.
- [25] D. Suckley. Genetic algorithm in the design of fir filters. *IEEE Proceedings G.*, 138:234–238, April 1991.
- [26] S.K. Mitra Y. Neuvo, C.Y. Dong. Interpolated finite impulse response filters. *IEEE. Trans. Accoust. Speech, Signal processing*, ASSP-32:563–570, June, 1984.
- [27] Sydney R. Parker Yong Chin Lim and A.G. Constantinides. Finite word length fir filter design using integer programming over a discrete coefficient space. *IEEE Transactions on Acoustics, Speech and Signal Processing*, ASSP-30:661–664, Aug. 1982.
- [28] Dongning Li Yong Ching Lim, Rui Yang and Jianjian Song. Signed power-of-two term allocation scheme for the design of digital filters. *IEEE Transactions on Circuits and Systems - Analog and Digital Signal Processing*, II:577–584, May 1999.
- [29] Ya Jun Yu and Yong Ching Lim. Frm based fir filter design - the wls approach. *IEEE International Symposium on Circuits and Systems*, III:221–224, May

2002.

- [30] Ya Jun Yu and Yong Ching Lim. Genetic algorithm approach for the optimization of multiplierless sub-filters generated by the frequency response masking technique. *IEEE International Conference on Electronics, Circuits and Systems*, 3:1163–1166, Sept. 2002.
- [31] A.T. Fam Z. Jing. A new structure for narrow-transition band, lowpass digital filter design. *IEEE Trans. Accoust. Speech, Signal processing*, ASSP-32:362–370, Apr., 1984.

Appendix A

Author's Contributions

Refereed Journal Publications

- Pat Mercier, **S.Kilambi**, B.Nowrouzian, “Optimization of FRM FIR Digital Filters Over CSD and DBNS Multiplier Coefficient Spaces Employing a Novel Genetic Algorithm”, submitted to *Journal of Computers (JCP)*.
- **S.Kilambi**, B.Nowrouzian, “A Novel Diversity Controlled Genetic Algorithm for Rapid Optimization of Bandpass FRM FIR Digital Filters Over CSD Multiplier Coefficient Space”, submitted to *Journal of Circuits, Systems and Signal Processing (JCSSP)*.

Refereed Conference Publications

- **S.Kilambi**, B.Nowrouzian, “A Diversity Controlled Genetic Algorithm for Optimization of FRM Digital Filters over DBNS Multiplier Coefficient Space”, submitted to *2007 IEEE International Symposium on Circuits and Systems (ISCAS)* to be held May 27-30, at New Orleans, US.
- **S.Kilambi**, B.Nowrouzian, “Rapid Optimization of FRM digital filters over CSD multiplier coefficient space using a Diversity Controlled Genetic Algorithm (DCGA)”, submitted to *2007 International Conference on Acoustics, Speech, and Signal Processing (ICASSP)* to be held Apr 15-20, at Honolulu, Hawaii, US.
- **S.Kilambi**, B. Nowrouzian, “A Genetic Algorithm Employing Correlative Roulette Selection for Optimization of FRM Digital Filters over CSD

Multiplier Coefficient Space”, to appear in the Proc. of *IEEE Asia Pacific Conference on Circuits and Systems (APCCAS)* Singapore, December, 2006.

- **S.Kilambi**, B. Nowrouzian, “A Novel Genetic Algorithm for Optimization of FRM Digital Filters over DBNS Multiplier Coefficient Space Based on Correlative Roulette Selection”, to appear in the Proc. of *IEEE Symposium on Signal Processing and Information Technology (ISSPIT)*, August 27-30, 2006 at Vancouver, Canada.

Non-refereed Conference Publications

- **S.Kilambi**, “A Genetic Algorithm Employing Correlative Roulette Selection for Optimization of FRM Digital Filters over CSD Multiplier Coefficient space”, *CAIMS-MITACS, 2006, Joint Annual Conference*, Oral Presentation.

Appendix B

Filter Length Estimation

Different formulas have been derived for the estimation of filter length for lowpass filters. The minimum filter length N is calculated based on the information given in the filter specifications i.e. normalized passband edge frequency ω_p , normalized stopband edge frequency ω_s , peak passband ripple δ_p , and peak stopband ripple δ_s . Three of these formulas have been enlisted below:

1. *Kaiser's Formula*: The filter order can be computed from the relation

$$N \approx \frac{-20 \log_{10} (\sqrt{\delta_p \delta_s}) - 13}{14.6 (\omega_s - \omega_p) / 2\pi}. \quad (\text{B.1})$$

2. *Bellanger's Formula*: Another formula given by Bellanger for calculating filter length is as follows,

$$N \approx -\frac{2 \log_{10} (10 \delta_p \delta_s)}{3 (\omega_s - \omega_p) / 2\pi} - 1. \quad (\text{B.2})$$

3. *Hermann's Formula*: The formula derived by Hermann gives a more accurate estimation of filter length and is given by

$$N \approx \frac{D_\infty (\delta_p, \delta_s) - F (\delta_p, \delta_s) [(\omega_s - \omega_p) / 2\pi]^2}{(\omega_s - \omega_p)}, \quad (\text{B.3})$$

where

$$D_\infty (\delta_p, \delta_s) = \left[a_1 (\log_{10} \delta_p)^2 + a_2 (\log_{10} \delta_p) + a_3 \right] \log_{10} \delta_s - \left[a_4 (\log_{10} \delta_p)^2 + a_5 (\log_{10} \delta_p) + a_6 \right], \quad (\text{B.4})$$

and

$$F(\delta_p, \delta_s) = b_1 + b_2 [\log_{10} \delta_p - \log_{10} \delta_s], \quad (\text{B.5})$$

with

$$\begin{aligned} a_1 &= 0.005309, & a_2 &= 0.07114, & a_3 &= -0.4761 & (\text{B.6}) \\ a_4 &= 0.00266, & a_5 &= 0.5941, & a_6 &= 0.4278 \\ b_1 &= 11.01217, & b_2 &= 0.51244. \end{aligned}$$

The formula given in Eqn. B.3 is valid for $\delta_p \geq \delta_s$. If $\delta_p < \delta_s$, then the filter length formula is modified by interchanging δ_p and δ_s in Eqns. B.4 and B.5.

For small values of δ_p and δ_s all the above three formulas give good estimates of filter length. However, for larger values, Hermann's formula gives more accurate results. It is possible that the filter orders calculated may not be enough for a given filter specification. In this case, it is best to gradually increase the filter length until the specifications are met. The filter length in all three formulas, is inversely proportional to the transition width $\Delta = (\omega_s - \omega_p)$. Thus, it can be concluded that for very sharp transition filters, the filter length will be very high. The formulas given above have been derived for lowpass filters. They can also be used for calculating orders for highpass, bandpass and bandstop filters. In the case of bandpass and bandstop filters, filter length depends on the sharper transition band.

Appendix C

CPU Processing Times for GA and DCGA

The algorithms were run on an Dell Opteron System with an Intel Pentium 4 processor with 2 GB RAM. The following are the processing times that took for the design and optimization of FRM FIR digital filters.

Table C.1: CPU Processing Time for GA and DCGA Optimization of FRM FIR Digital filters

Algorithm	Type of Filter	Number of generations	Processing time
GA	CSD Lowpass	953	10 hrs
GA	DBNS Lowpass	1000	11 hrs
GA	CSD Bandpass	1000	11 hrs
	with $\Delta_l = \Delta_h$		
GA	DBNS Bandpass	976	10 hrs
	with $\Delta_l = \Delta_h$		
DCGA	CSD Lowpass	61	15 mins
DCGA	DBNS Lowpass	42	10 mins
DCGA	CSD Bandpass	144	35 mins
	with $\Delta_l = \Delta_h$		
DCGA	CSD Bandpass	45	10 mins
	with $\Delta_l = \Delta_h$		
DCGA	DBNS Bandpass	109	25 mins
	with $\Delta_l \neq \Delta_h$		
DCGA	DBNS Bandpass	53	12 mins
	with $\Delta_l \neq \Delta_h$		